INVESTIGATING MULTIPHOTON PHENOMENA USING NONLINEAR DYNAMICS

A Thesis
Presented to
The Academic Faculty

by

Shu Huang

In Partial Fulfillment
of the Requirements for the Degree
Doctor of Philosophy in the
School of Physics

Georgia Institute of Technology
April 2008

INVESTIGATING MULTIPHOTON PHENOMENA USING NONLINEAR DYNAMICS

Approved by:

Professor Turgay Uzer, Advisor
School of Physics
Georgia Institute of Technology

Professor Michael Schatz
School of Physics
Georgia Institute of Technology

Professor Raymond M. Flannery
School of Physics
Georgia Institute of Technology

Professor Mustafa M. Aral
School of Civil Engineering
Georgia Institute of Technology

Professor Chandra Raman
School of Physics
Georgia Institute of Technology

Date Approved: 11th March 2008

Dedicated to my wife and my parents,

ACKNOWLEDGEMENTS

First and foremost, I would like to thank my advisor, Turgay Uzer, for introducing me into this field. I have benefited greatly from his guidance, his wealthy scientific culture and the interactive environment he provided through my graduate research. I am also very grateful to Cristel Chandre, without whom, this thesis would not be possible. Cristel patiently imparted me so much knowledge in this field. Our close collaboration aroused many interesting ideas that are reflected in this thesis. My warmest thanks go to Predrag Cvitanović for his support in my research. I would like to acknowledge all members of the thesis committee for their work and time. I also would like to thank Ji Il Choi for his help and encouragement. Finally I want to thank my family for their love, support and understandings.

TABLE OF CONTENTS

LIST OF TABLES

LIST OF FIGURES

SUMMARY

Many seemingly simple systems can display extraordinarily complex dynamics which has been studied and uncovered through nonlinear dynamical theory. The leitmotif of this thesis is changing phase-space structures and their (linear or nonlinear) stabilities by adding control functions (which act on the system as external perturbations) to the relevant Hamiltonians. These phase-space structures may be periodic orbits, invariant tori or their stable and unstable manifolds. One-electron systems and diatomic molecules are fundamental and important staging ground for new discoveries in nonlinear dynamics. In past years, increasing emphasis and effort has been put on the control or manipulation of these systems. Recent developments of nonlinear dynamical tools can provide efficient ways of doing so. In the first subtopic of the thesis, we are adding a control function to restore tori at prescribed locations in phase space. In the remainder of the thesis, a control function with parameters is used to change the linear stability of the periodic orbits which govern the processes in question.

In this thesis, we report our theoretical analyses on multiphoton ionization of Rydberg atoms exposed to strong microwave fields and the dissociation of diatomic molecules exposed to bichromatic lasers using nonlinear dynamical tools. This thesis is composed of three subtopics. In the first subtopic, we employ local control theory to reduce the stochastic ionization of hydrogen atom in a strong microwave field by adding a relatively small control term to the original Hamiltonian. In the second subtopic, we perform periodic orbit analysis to investigate multiphoton ionization driven by a bichromatic microwave field. Our results show quantitative and qualitative agreement with previous studies, and hence identify the mechanism through

which short periodic orbits organize the dynamics in multiphoton ionization. In addition, we achieve substantial time savings with this approach. In the third subtopic we extend our periodic orbit analysis to the dissociation of diatomic molecules driven by a bichromatic laser. In this problem, our results based on periodic orbit analysis again show good agreement with previous work, and hence promise more potential applications of this approach in molecular physics.

CHAPTER I

INTRODUCTION

The leitmotif of this thesis is changing phase-space structures and their (linear or nonlinear) stabilities by adding control functions (which act on the system as external perturbations) to the relevant Hamiltonians. These phase-space structures may be periodic orbits, invariant tori or their stable and unstable manifolds. In this thesis, we report our theoretical analyses on multiphoton ionization of Rydberg atoms exposed to strong microwave fields and the dissociation of diatomic molecules driven by bichromatic lasers using nonlinear dynamics. In the first subtopic, we are adding a control function to restore tori at prescribed locations in phase space. In the remainder of the thesis, a control function with parameters is used to change the linear stability of the periodic orbits which govern the processes in question.

1.1 Background

In 1974, Bayfield and Koch [7], while experimentally studying multiphoton ionization of highly excited hydrogen atoms exposed to a strong microwave field, discovered that a high proportion of hydrogen atoms at principal quantum number $n \simeq 66$ (in Rydberg states) were unexpectedly ionized by absorption of about 80 photons of 9.9GHz frequency. They also performed additional experiments at lower microwave frequencies, for which a lot more photons were required to ionize hydrogen atoms, and again observed this striking phenomenon that a significant proportion of atoms were ionized. It should be pointed out that according to quantum perturbation theory, to compute multiphoton (for instance, 80 photons) ionization, one needs implement perturbation for many (for instance, 80) times. This theoretical approach to

Bayfield and Koch's experiment would produce an extremely small ionization probability resulting from the product of 80 small transition probability values, which is clearly in conflict with the experimental results. In other words, for highly excited hydrogen atoms, the actual microwave field strength required for ionization is much lower than that predicted by quantum perturbation theory. While early methods such as quantum perturbation theory failed to provide satisfactory explanations to the amazing multiphoton ionization, convincing illustrations of this experiment from the perspective of classical nonlinear dynamics (chaos) were presented by Meerson *et al* quantitatively [80]. The success of classical mechanics for this highly excited (high principal quantum number) hydrogen atoms experiment is not a surprise. Orbits with high principal quantum numbers are very closely-spaced and hence can be classically treated as continuous. A survey of the extensive research results can be found in review papers published by Casati *et al* [17], Jensen *et al* [60] and Koch and van Leeuwen [65]. Recently, more emphasis has been put on manipulating or controlling atomic or molecular systems, as elaborated by Rabitz [93], Shapiro and Brumer [103, 104], Gordon *et al* [46] and Charron *et al* [21]. Among control tools, bichromatic pulses are important because they provide many controlling parameters such as polarization, amplitudes and phases, as discussed by many references [6, 14, 21, 29, 36, 43, 46, 51, 52, 54, 57, 63, 66, 74, 89, 94, 103, 106–108]. However, most previous theoretical studies were based on time-consuming large-scale numerical simulations. There is still a great need for more efficient approaches to these systems governed by classical mechanisms. This thesis was written to address this need.

1.2 Brief Review

In this section, we will present a brief review on the application of classical mechanics to microwave-induced hydrogen (Rydberg) atom ionization.

The hydrogen atom problem is a very famous textbook example which may date

back to early twentieth century, when Bohr proposed his well-known model [12] which is considered a milestone of the history of quantum mechanics. With the development of microwaves and lasers, the interaction between atom/molecule and electromagnetic field has triggered many intensive studies since middle 1970's [65]. One of these topics is the hydrogen electron dynamics in the Coulomb potential driven by strong external microwave field. Meanwhile, this important problem has also been of great interest to nonlinear dynamicists since the microwave ionization behavior can be very well explained and understood through classical stochasticity [17, 60, 65], instead of quantum perturbation theory. From the perspective of microscopic systems, this typical quantum system exhibits chaotic dynamics and has been a good paradigm for the application of nonlinear dynamics for the past several decades. The quantum-classical correspondence is an attractive topic that has been investigated extensively to study the relationship between the classical domain and the quantum domain [17, 60, 65]. In quantum mechanics, the dynamical results depend on the numerical solutions of Schrödinger equation while in its classical counterpart, the numerical solutions of coupled Hamilton's equations of motion (linear differential equations) are the key. Specifically, in order to describe the dynamics of hydrogen atom exposed to an external linearly polarized microwave field, a commonly used one-dimensional model, namely surface-state-electrons (SSE) model in atomic units (a.u.) [17,33,58,59] reads

$$H(x,p,t) = \frac{p^2}{2} + \left\{ \begin{array}{ll} -\frac{1}{x}, & x > 0 \\ \infty, & x \leq 0 \end{array} \right\} + x\lambda \cos \omega t, \tag{1.2.1}$$

which has proven to be successful in illustrating the real three-dimensional experimental hydrogen atoms ionization thresholds in linearly polarized microwave field using the classical chaotic dynamics [17, 60, 65]. The striking success is due to the fact that the three-dimensional electronic states that are highly elongated along the field direction are the easiest to ionize, and those along other directions almost do not

make contributions to ionization [69]. As a result, the one-dimensional model (1.2.1) can actually simulate the process very accurately. Following the model (1.2.1), many classical investigations have been implemented and then compared to results based on quantum mechanics. Here we need to mention an important quantity, scaled frequency [17, 60, 65], which is defined as

$$\varpi = n^3\omega, \tag{1.2.2}$$

where n is the principal quantum number and ω is the frequency of the external microwave field in atomic units. Previous studies [64] have shown that for $0.1 \leq \varpi \leq 1.2$, the onset ionization threshold based on classical treatment agrees very well with quantum calculations and experimental results. The agreement in this regime results from the relatively high principal quantum numbers and correspondingly many closely-spaced states that can induce the transition from quantum to classical mechanics [17, 70, 71]. It should be pointed out that a large number of strongly and continuously coupled quantum states can make quantum simulations much more complicated than classical calculations [17, 60, 65]. Classical methods have proven to be very practically effective in this regime. When the scaled frequency ϖ rises above 1, quantum localization will start to take effect. This phenomenon was first explained using a theory presented by Casati *et al* [17]. They successfully analyzed the quantum suppression of classical diffusion that comes from quantum state interference. According to some studies [41, 77], this quantum localization effect appears significant only when the scaled frequency ϖ rises above 2. As a result, for the regime $1 \leq \varpi \leq 2$, classical calculations still agree with quantum treatment or experimental results [41], though not as well as for the regime $0.1 \leq \varpi \leq 1$. While for $\varpi > 2$, quantum localization effect dominates to make the onset ionization threshold a lot higher than what classical calculation indicates and hence disagreement between classical and quantum approaches grows sharply [17]. At the low end of the regime $0.1 \leq \varpi \leq 1.2$, some tiny bumps or peaks appear on the onset ionization curve due

to quantal resonance effect [10, 64, 97]. However this phenomenon does not affect the overall agreement between classical and quantum calculations. For the regime $0.07 < \varpi < 0.1$, classical-quantum correspondence is still close though quantum tunneling effect starts to rise. At $\varpi \leq 0.07$, the quantum tunneling effect reflected by the onset of ionization was observed in experiments [64]. In this regime ($\varpi < 0.07$), the multiphoton ionization occurs by quantum tunneling through a slowly oscillating barrier composed of the Coulomb potential and microwave fields [17,60,65], and hence some quantum theories such as Ammosov-Delone-Krainov (ADK) [1] and Keldysh-Faisal-Reiss (KFR) [37, 62, 96] methods should apply. Generally speaking, for the scaled frequency regime $0.1 \leq \varpi \leq 1.2$, classical calculations agree strikingly well with quantum simulations. For the regime $1.2 < \varpi \leq 2$ and $0.07 < \varpi < 0.1$, classical-quantum correspondence is still close. In this thesis, all hydrogen atom-related problems are discussed within the regime $0.095 \leq \varpi \leq 1.49$ where the classical-quantum correspondence is close enough for us to implement classical approach.

From a chaos point of view, the stochastic ionization of hydrogen atoms in external field is a process of classical chaotic diffusion, which can be well described by classical Hamilton's equations of motion under small perturbations [17,60,65,70,71] using the Chirikov resonance overlap criterion [23] in phase space. The Chirikov criterion has been traditionally used to determine the chaos border. According to the Chirikov criterion, the overlap of resonant zones in phase space results in large-scale chaos [23]. The linearly polarized field in (1.2.1) is the perturbation for the originally unperturbed hydrogen Hamiltonian. With this small perturbation, the Hamiltonian of hydrogen atom becomes nearly integrable. Usually, the one-dimensional model (1.2.1) is written in terms of action-angle variables in order to make the analysis much easier because only action variable survives in unperturbed Hamiltonian [3]. In general, the equations of motion for an integrable Hamiltonian (unperturbed) $H_0(\mathbf{A})$ with L degrees

of freedom are written as

$$\begin{bmatrix} \frac{d\mathbf{A}}{dt} = \mathbf{0} \\ \frac{d\boldsymbol{\phi}}{dt} = \frac{\partial H_0}{\partial \mathbf{A}} = \boldsymbol{\omega}_{\mathbf{0}}(\mathbf{A}) \end{bmatrix}, \tag{1.2.3}$$

where action-angle variables $(\mathbf{A}, \boldsymbol{\phi}) \in \mathbb{R}^L \times \mathbb{T}^L$, $\mathbb{T}$ being an angle space typically within $[0, 2\pi[$. $\boldsymbol{\omega}_{\mathbf{0}}$ are frequency vectors of invariant tori. For the particular one-dimensional hydrogen atom problem, the unperturbed Hamiltonian in terms of action-angle variables reads

$$H_0(J) = -\frac{1}{2J^2}. \tag{1.2.4}$$

The action variable J directly corresponds to the principal quantum number. The angle variable does not appear because (1.2.4) is integrable. However, for perturbed (non-integrable) Hamiltonian $H(\mathbf{A}, \boldsymbol{\phi})$, the equations of motion (1.2.3) should be replaced by

$$\begin{bmatrix} \frac{d\mathbf{A}}{dt} = -\frac{\partial H}{\partial \boldsymbol{\phi}} \neq \mathbf{0} \\ \frac{d\boldsymbol{\phi}}{dt} = \frac{\partial H}{\partial \mathbf{A}} \end{bmatrix}. \tag{1.2.5}$$

The system then behaves chaotically. Following (1.2.5), we construct Hamilton's equations of motion for hydrogen atom in a linearly polarized microwave field, which will be discussed in detail in Chapter III. The Kolmogorov-Arnold-Moser theorem (KAM theorem) [2, 67, 84] provides a systematic theory illustrating the survival or breakup of periodic orbits or invariant tori in phase space for Hamiltonian systems under small perturbations. The KAM theorem states that with small perturbations, those tori with rational frequency vectors (commensurate) are destroyed while those with "sufficiently irrational" (incommensurate) frequency vectors are only slightly deformed but still survive [2, 67, 84]. For the hydrogen atom ionization problem, with small perturbations of an external microwave field, some originally invariant tori are broken and chaotic diffusion appears. This is the mechanism of the onset of multiphoton ionization according to chaotic theory [95]. In addition to the ionization thresholds of hydrogen atom in linearly polarized microwave field, many other

interesting results have also been obtained using classical chaotic theory, such as ionization of Rydberg atoms in circularly polarized microwave field [39, 55, 81, 85, 98] and in elliptically polarized microwave field [48, 105]. In recent years, with better understanding of these perturbed atomic or molecular systems experimentally and theoretically, more attention has been focused on manipulating them by some control parameters [21, 46, 93, 103, 104]. This work was thus initiated to analyze and identify the functions of control parameters for some multiphoton phenomena in atomic or molecular systems through the classical approach.

1.3 Motivation and Contribution of the Thesis

In this thesis, we perform theoretical analyses on the ionization of hydrogen atoms exposed to microwave fields based on classical dynamical tools such as local control theory and stability analysis of periodic orbits, and then extend the classical investigation to the dissociation of diatomic molecules driven by a laser field. The motivation to perform these studies lies in manipulating these atomic or molecular systems using control parameters through the understanding of the underlying classical mechanisms governing these systems. Our results have shown excellent agreement, either quantitatively or qualitatively, with experimental results, direct simulations of classical mechanics or quantum mechanical calculations in the regime where the quantum-classical correspondence is pretty close. In addition, our computations achieve substantial time savings compared to traditional large-scale numerical simulations. We also make predictions for various parameters based on our analyses. Our work has demonstrated that in some appropriate regimes, calculations based on our classical analyses yield very accurate results with very high efficiency. These outcomes heuristically pave the way of controlling and manipulating more complex systems or making significant predictions in a very efficient style through classical mechanics.

1.4 Organization of the Thesis

In this thesis we illustrate our investigation of multiphoton ionization of hydrogen atoms and dissociation of diatomic molecules exposed to external fields for one-dimensional model through classical approaches. Following a summary of local control method in Chapter II, we present a procedure in Chapter III to reduce the stochastic ionization of hydrogen atom in a strong microwave field. The way of ionization reduction lies in adding to the original Hamiltonian a comparatively small control term which might consist of an additional set of microwave fields. This modification restores select invariant tori in the dynamics and prevents ionization. The complete control term is derived based on local control theory [20]. We then simplify the complete control term using fast Fourier transformation. The approximate form of control term is obtained by modification of the simplified control term. We demonstrate the procedure on the one-dimensional model of microwave ionization. Numerical simulations give Poincaré sections and laminar plots showing the reduction of ionization. After a brief introduction on some key concepts of linear stability analysis in Chapter IV, we perform periodic orbit analysis in Chapter V to investigate the multiphoton ionization of hydrogen atom driven by strong bichromatic microwave fields. The Newton-Raphson multi-shooting algorithm [30] is employed to capture and monitor specific periodic orbits. The stability of picked periodic orbits is reflected by an indicator: Green's residue [47, 76]. Through the stability of periodic orbits we can match qualitatively the variation of experimental ionization rates with a control parameter, the relative phase between the two modes of the field. Moreover, we devise an empirical formula which reproduces quantum simulations [66] to a high degree of accuracy. This quantitative agreement shows how short periodic orbits organize the dynamics in multiphoton ionization. In Chapter VI, we extend the stability analysis of periodic orbits to the dissociation of hydrogen fluoride (HF) molecules exposed to a bichromatic laser. The results based on our periodic orbit analysis shows striking

agreement with direct simulations [29] on most parameter space. General conclusions are in Chapter VII.

CHAPTER II

LOCAL CONTROL METHOD ON CHAOTIC SYSTEM

For many complex dynamical systems, equations of motion based on the Hamiltonian show chaotic behavior due to sensitivity to external small perturbations [91]. In these systems, a slight deviation on the initial conditions may be amplified and then cause drastically different trajectories afterwards. In many fields ranging from physics to engineering, various efforts have been made to control these chaotic behaviors [13, 22, 35, 42, 61, 75, 90, 101]. In this chapter, we give a brief introduction on a local control method intensively reported by Ciraolo *et al* [25], Vittot *et al* [110] and Chandre *et al* [20] for near-integrable Hamiltonian system. With this control strategy, one can significantly reduce or even shut off Hamiltonian chaos. In Chapter III, we apply this technique to reduce multiphoton ionization of hydrogen atom in a linearly polarized microwave field.

2.1 Basic idea

A near-integrable Hamiltonian systems with L degrees of freedom can be written into action-angle variables $(\mathbf{A}, \boldsymbol{\phi})$ in the form

$$H(\mathbf{A}, \boldsymbol{\phi}) = H_0(\mathbf{A}) + \varepsilon V(\mathbf{A}, \boldsymbol{\phi}), \tag{2.1.1}$$

where $(\mathbf{A}, \boldsymbol{\phi}) \in \mathbb{R}^L \times \mathbb{T}^L$, $\mathbb{T}$ being an angle space typically within $[0, 2\pi[$. The $H_0(\mathbf{A})$ in Eq. (2.1.1) represents the integrable part of the Hamiltonian while $\varepsilon V(\mathbf{A}, \boldsymbol{\phi})$ is the small perturbation. The KAM theorem [2, 67, 84] presents complete analyses on stability of invariant tori. Between these tori exist chaotic regions. For nearly integrable Hamiltonians like Eq. (2.1.1), the increase of perturbation term εV leads to successive break-ups of invariant tori [75, 95]. As a consequence, the dynamical

system becomes more chaotic such that a large number of trajectories diffuse across the action-angle space.

The idea of the local control method is to devise a control term f such that when it is added to the nearly integrable Hamiltonian, it makes the trajectories of the controlled Hamiltonian $H_0 + \varepsilon V + f$ more regular. Meanwhile, other properties of the dynamical system in phase space should not be affected. The feasibility of this design is justified as long as the perturbed Hamiltonian is nearly integrable (ε is very small). Moreover, the desired control term f has to be small when compared with perturbation term εV for practical energy concerns. Therefore the acceptable control term has to be of the order of ε^2 or smaller.

Following Hamiltonian (2.1.1), the phase space in the integrable case ($\varepsilon = 0$) is foliated by invariant tori with frequency $\boldsymbol{\omega}(\mathbf{A}) = \partial H_0/\partial \mathbf{A}$. Now consider one of these invariant tori with frequency $\boldsymbol{\omega}$ and position $\mathbf{A}_0$. $\boldsymbol{\omega}$ is assumed non-resonant, i.e. there is no non-zero integer vector $\mathbf{k}$ such that $\boldsymbol{\omega} \cdot \mathbf{k} = 0$. This invariant torus is generally destroyed by the perturbation $V(\mathbf{A}, \boldsymbol{\phi})$ when the parameter ε is greater than a critical value ε_c. The idea of the control is to rebuild this invariant torus with frequency $\boldsymbol{\omega}$ for $\varepsilon > \varepsilon_c$ by adding a small control term f to the original Hamiltonian H. Thus the controlled Hamiltonian H_c can be constructed as

$$H_c(\mathbf{A}, \boldsymbol{\phi}) = H(\mathbf{A}, \boldsymbol{\phi}) + f(\boldsymbol{\phi}). \tag{2.1.2}$$

2.2 Brief description of the local control formula

With an appropriate expansion around a region near $\mathbf{A} = \mathbf{0}$, Hamiltonian (2.1.1) can be written in the form

$$H(\mathbf{A}, \boldsymbol{\phi}) = \boldsymbol{\omega} \cdot \mathbf{A} + \varepsilon p(\boldsymbol{\phi}) + w(\mathbf{A}, \boldsymbol{\phi}). \tag{2.2.1}$$

It should be pointed out that for $\varepsilon = 0$ the Hamiltonian (2.2.1) has an invariant torus at $\mathbf{A} = \mathbf{0}$ with frequency vector $\boldsymbol{\omega}$. As can be seen here, Hamiltonian (2.2.1)

is composed of three terms. The first term, $\boldsymbol{\omega} \cdot \mathbf{A}$, represents the integrable part of the Hamiltonian. The second term stands for a small perturbation. The third term is a higher order term in action-angle variables. The controlled Hamiltonian is hence desired in the form

$$H_c(\mathbf{A}, \boldsymbol{\phi}) = \boldsymbol{\omega} \cdot \mathbf{A} + \varepsilon p(\boldsymbol{\phi}) + w(\mathbf{A}, \boldsymbol{\phi}) + f(\boldsymbol{\phi}). \tag{2.2.2}$$

Hamiltonian (2.2.2) is exactly the same as (2.1.2). The control term $f(\boldsymbol{\phi})$ is given by

$$f(\boldsymbol{\phi}) = -w(-\varepsilon \Gamma \partial_{\boldsymbol{\phi}} p, \boldsymbol{\phi}), \tag{2.2.3}$$

where Γ is a linear operator defined as a pseudo-inverse of $\boldsymbol{\omega} \cdot \partial_{\boldsymbol{\theta}}$. Its explicit expression is

$$\Gamma p(\boldsymbol{\phi}) = \sum_{\boldsymbol{\omega} \cdot \mathbf{k} \neq 0} \frac{p_{\mathbf{k}}}{i \boldsymbol{\omega} \cdot \mathbf{k}} e^{i \mathbf{k} \cdot \boldsymbol{\phi}}. \tag{2.2.4}$$

The operators Γ and $\partial_{\boldsymbol{\phi}}$ do commute with each other. Consequently, the invariant torus for Hamiltonian (2.2.2) is located at

$$\mathbf{A} = -\varepsilon \Gamma \partial_{\boldsymbol{\phi}} p. \tag{2.2.5}$$

The detailed mathematical proof on control term (2.2.3) can be found in Refs. [20, 25, 110].

CHAPTER III

REDUCING MULTIPHOTON IONIZATION IN A LINEARLY POLARIZED MICROWAVE FIELD BY LOCAL CONTROL

With permission from American Physical Society, this chapter is modified from the paper originally published as:

S. Huang, C. Chandre and T. Uzer, "Reducing multiphoton ionization in a linearly polarized microwave field by local control", Phys. Rev. A **74**, 053408 (2006).

http://dx.doi.org/10.1103/PhysRevA.74.053408

3.1 Introduction

The multiphoton ionization of hydrogen Rydberg atoms [40] in a strong microwave field [7] is an experiment which revolutionized the way we view the physics of highly excited atoms [26]. Some previous thorough reviews have been completed by Koch and Leeuwen [65], Casati *et al* [17,19] and Jensen [60]. The interpretation of multiphoton ionization of Rydberg atoms remained a puzzle until its stochastic, diffusive nature was uncovered through the then-new theory of chaos by Casati *et al* [17,19], Meerson *et al* [80], Leopold and Percival [71] and Jensen [59]. Casati *et al* [17,19], Mackay and Meiss [77], Farrelly and Uzer [38], Howard [54,55] and Reichl [95] have pointed out that the multiphoton ionization occurs when the electrons diffuse to increasingly higher energies chaotically by taking advantage of the breakups of local invariant tori in phase space. Classical theory can be applied to the ionization of hydrogen in the parameter regime where the microwave and Kepler frequencies are nearly equal [60,77]. Because

the classical dynamics of this system is chaotic, Blümel and Reinhardt [9], Buchleitner *et al* [14] and Krug and Buchleitner [68] used the Rydberg states of hydrogen as an excellent testbed for investigating the quantal manifestations of classical chaos, i.e., the field of "quantum chaology" as introduced by Casati *et al* [17,19], Reichl [95] and Berry [8]. Indeed, the literature on the correspondence between classical and quantum behavior in the ionization of Rydberg atoms is extensive [8, 9, 11, 14, 17, 19, 32, 38, 54, 55, 59, 60, 68, 71–73, 77, 80, 88, 95]. We perform our purely classical calculations in the regime where the quantum-classical correspondence is particularly close [60].

Recently, the research focus in this field has shifted from understanding to manipulating the ionization process [63, 66, 78, 79, 106, 107]. Since microwave ionization of Rydberg states is a paradigm for time-dependent nonintegrable systems, learning to manipulate stochastic ionization is expected to pave the way of controlling other, more involved systems. The control of stochastic ionization has been investigated using both quantum and classical approaches in the past few years [66, 78, 92, 106, 107]. Here, we return to the basic dynamics of the stochastic ionization process to answer the most elementary manipulation question: If the multiphoton ionization is made possible by broken invariant tori, can ionization be reduced (or even stopped) by restoring invariant tori at carefully chosen locations in phase space?

In this chapter, we will show how to reduce or shut off the ionization of Rydberg atoms using a "local" control strategy which originates in plasma physics [20]. The premise of the procedure is to reduce the chaos (and thus ionization) in a selected parameter range through a small perturbation which regularizes the dynamics in that narrow area but does not affect the dynamics elsewhere. Technically, local control achieves this by creating an invariant torus in a selected region of phase space without significantly changing other parts of phase space.

The problem of finding such a modification of the original Hamiltonian system is, a priori, nontrivial : A generic modification term would lead to the enhancement

of the chaotic behavior (following the intuition given by Chirikov's criterion [23]). Modification terms with a regularizing effect are, of course, rare. However, there is a general strategy and an explicit algorithm to design such modifications which indeed drastically reduce chaos and its attendant diffusion by building barriers in phase space [20,24], as we will show on the one-dimensional hydrogen Rydberg atom in a strong microwave field.

One-dimensional models of microwave ionization in linearly polarized microwave fields have proven perfectly adequate to explain most experimental observations [17, 19,60,65] since many of the experiments considered extended, quasi-one-dimensional hydrogen atoms [7,60,65,95] in which the angular momentum of the Rydberg electrons is much smaller than their principal quantum number. As a result, the atoms resemble needles in which the electron bombards the core with zero angular momentum. The one-dimensional Hamiltonian model in atomic units reads

$$H(p,x,t) = \frac{p^2}{2} - \frac{1}{x} + \lambda x \cos \omega t, \tag{3.1.1}$$

where λ is the amplitude of the external field and $x > 0$.

The desired Hamiltonian with the control field reads

$$H(p,x,t) = \frac{p^2}{2} - \frac{1}{x} + \lambda x \cos \omega t + x g(t), \tag{3.1.2}$$

where $x > 0$. For practical purposes, we expect that the control field $g(t)$ has the same form as the perturbation field but with relatively small amplitude. Despite the fact that g introduces an additional set of resonances, its effect, if it is appropriately chosen, is to restore specific invariant tori.

This chapter is organized as follows: In Sec. 3.2, we implement the local control method on a one-dimensional hydrogen atom driven by a linearly polarized microwave field. In Sec. 3.3, we present the numerics of the control term and show its efficiency by using Poincaré sections, laminar plots and diffusion curves. In order to be relevant

and feasible for physical implementations, the control term has to be robust, i.e., sufficiently good approximations to it should reduce chaos effectively, too. We pay particular attention to this point and show numerically that reasonable approximations to our control terms are effective in reducing chaos also. Conclusions are in Sec. 3.4.

3.2 Computation of the control term

In order to apply this method [20,25,110] to a one-dimensional hydrogen atom driven by a microwave field, we first need to map Hamiltonian (3.1.1) into action-angle variables of the unperturbed system ($\lambda = 0$). Its action-angle variables (J, θ) are [72]

$$x = 2J^2 \sin^2 \varphi,$$
$$p = \frac{1}{J} \cot \varphi,$$

with

$$\theta = 2\varphi - \sin 2\varphi.$$

After rescaling energy, time, position and momentum as $H' = \omega^{-2/3} H, t' = \omega t, x' = \omega^{2/3} x, p' = \omega^{-1/3} p$, we obtain the rescaled field amplitude $\lambda' = \omega^{-4/3}\lambda$. The rescaled Hamiltonian (dimensionless) still satisfies the equations of motion, and we assume $\omega = 1$ without loss of generality in Eq. (3.1.1). The scaled frequency, or say, winding ratio in the rescaled system is thus defined as $\varpi \equiv J^3\omega = J^3$. Expanding x', we rewrite Hamiltonian (3.1.1) [17]

$$H = -\frac{1}{2J^2} + 2J^2\lambda(\frac{a_0}{2} + \sum_{n=1}^{\infty} a_n \cos n\theta) \cos t, \tag{3.2.1}$$

where

$$a_n = \frac{J_n(n) - J_{n-1}(n)}{n},$$

J_n's are Bessel functions of the first kind and $a_0 = 1.5$. We abbreviate the Hamiltonian (3.2.1) as

$$H = -\frac{1}{2J^2} + \lambda J^2 v(\theta, t).$$

where

$$v(\theta, t) = a_0 \cos t + \sum_{n=1}^{\infty} a_n[\cos(n\theta + t) + \cos(n\theta - t)]. \tag{3.2.2}$$

The Hamiltonian (3.2.1) displays a set of primary resonances approximately located at $J_n = n^{1/3}$. The overlap of these resonances [23] leads to large-scale chaos and hence ionization. We expect the lower action region to be more regular, and it is chaotic for sufficiently large λ by resonance overlap. The idea is, given a value of n, to restore an invariant torus in between the resonances approximately located at J_n and J_{n+1}. For $\lambda = 0$, this invariant torus with (Kepler) frequency ω_0 is located at $J_0 = \omega_0^{-1/3}$. In order to do this, we need to compute the control term.

The step of the control algorithm is to map the time-dependent Hamiltonian into an autonomous one. We consider that t (modulus 2π) is an additional angle variable and we call its corresponding action variable E. The autonomous Hamiltonian becomes $H(J, \theta, t) + E$. The action-angle variables are $\mathbf{A} = (J, E)$ and $\boldsymbol{\phi} = (\theta, t)$. The frequency vector of the torus is $\boldsymbol{\omega} = (\omega_0, 1)$. In particular, the detailed derivation of the control term $f(\theta, t)$ is as follows:

We have Hamiltonian Eqn. (3.2.1)

$$H = -\frac{1}{2J^2} + 2J^2\lambda(\frac{a_0}{2} + \sum_{n=1}^{\infty} a_n \cos n\theta) \cos t,$$

where

$$a_n = \frac{J_n(n) - J_{n-1}(n)}{n},$$

which leads to

$$H = -\frac{1}{2J^2} + \lambda J^2(a_0 \cos t + \sum_{n=1}^{\infty} a_n[\cos(n\theta + t) + \cos(n\theta - t)]).$$

After shifting the action J such that the torus is located at $J = 0$, we have

$$H = -\frac{1}{2(J + \omega_0^{-\frac{1}{3}})^2} + \lambda(J + \omega_0^{-\frac{1}{3}})^2(a_0 \cos t + \sum_{n=1}^{\infty} a_n[\cos(n\theta + t) + \cos(n\theta - t)]).$$

Implementing Taylor expansion on the first term of right hand side with respect to $J = 0$ leads to

$$H = -\frac{1}{2\omega_0^{-\frac{2}{3}}} + \omega_0 J + \sum_{k=2}^{\infty} C_k J^k + \lambda(J^2 + 2\omega_0^{-\frac{1}{3}} J + \omega_0^{-\frac{2}{3}})(a_0 \cos t + \sum_{n=1}^{\infty} a_n[\cos(n\theta + t) + \cos(n\theta - t)]), \tag{3.2.3}$$

where

$$C_k = (-1)^{k+1} \frac{k+1}{2} \omega_0^{\frac{k+2}{3}}.$$

Here we drop the first term of the Hamiltonian (3.2.3) since it is a constant and does not affect the dynamics of this system. In order to make the Hamiltonian time-independent, we add an additional term E to this Hamiltonian as the second action variable which is canonically conjugate to time. Then the autonomous Hamiltonian becomes

$$H = E + \omega_0 J + \sum_{k=2}^{\infty} C_k J^k + \lambda(J^2 + 2\omega_0^{-\frac{1}{3}} J + \omega_0^{-\frac{2}{3}})(a_0 \cos t + \sum_{n=1}^{\infty} a_n[\cos(n\theta + t) + \cos(n\theta - t)]). \tag{3.2.4}$$

Note this Hamiltonian is the expansion of the original Hamiltonian (3.2.1) around $\mathbf{A}_0 = \mathbf{0}$.

Following the local control method introduced in Chapter II, we identify that in Hamiltonian (3.2.4),

$$E + \omega_0 J = \boldsymbol{\omega} \cdot \mathbf{A},$$

$$\lambda \omega_0^{-\frac{2}{3}} (a_0 \cos t + \sum_{n=1}^{\infty} a_n[\cos(n\theta + t) + \cos(n\theta - t)] = \varepsilon p(\boldsymbol{\phi})$$

and

$$\sum_{k=2}^{\infty} C_k J^k + \lambda(J^2 + 2\omega_0^{-\frac{1}{3}} J)(a_0 \cos t + \sum_{n=1}^{\infty} a_n[\cos(n\theta + t) + \cos(n\theta - t)]) = w(\mathbf{A}, \boldsymbol{\phi})$$

in Eqn. (2.2.1) respectively. For this problem, the control term (2.2.3) can be rewritten

in an alternative way more clearly as

$$f(\boldsymbol{\phi}) = -H(\mathbf{A}_0 - \partial_{\boldsymbol{\phi}}\Gamma b(\boldsymbol{\phi}), \boldsymbol{\phi}), \tag{3.2.5}$$

where $b(\boldsymbol{\phi}) = H(\mathbf{A}_0, \boldsymbol{\phi})$ and $\mathbf{A}_0 = \mathbf{0}$ (Note here $\mathbf{A}_0 = \mathbf{0}$ because we have shifted the original Hamiltonian (3.2.1) by $\omega_0^{-\frac{1}{3}}$ in order to make the targeted invariant torus at $J = 0$. If there were no such shift, $\mathbf{A}_0$ should be equal to $(\omega_0^{-\frac{1}{3}}, 0)$). Γ is a linear operator defined as a pseudo-inverse of $\boldsymbol{\omega} \cdot \partial_{\boldsymbol{\phi}}$. Its explicit expression is

$$\Gamma b(\boldsymbol{\phi}) = \sum_{\boldsymbol{\omega}\cdot\mathbf{k}\neq 0} \frac{b_{\mathbf{k}}}{i\boldsymbol{\omega}\cdot\mathbf{k}} e^{i\mathbf{k}\cdot\boldsymbol{\phi}}. \tag{3.2.6}$$

for $b(\boldsymbol{\phi}) = \sum_{\mathbf{k}\in\mathbb{Z}^L} b_{\mathbf{k}} e^{i\mathbf{k}\cdot\boldsymbol{\phi}}$. The restored invariant torus of the controlled Hamiltonian H_c has the equation :

$$\mathbf{A} = \mathbf{A}_0 - \Gamma\partial_{\boldsymbol{\phi}} H(\mathbf{A}_0, \boldsymbol{\phi}), \tag{3.2.7}$$

which is equivalent to Eqn. (2.2.5). Here $\mathbf{A}_0 = \mathbf{0}$ for the shifted Hamiltonian. Such an invariant torus acts as a barrier to diffusion for Hamiltonian systems with two degrees of freedom. The frequency vector is $(\omega_0, 1)$. The action variables is $\mathbf{A} = (J, E)$ and the angle variables is $\boldsymbol{\phi} = (\theta, t)$. Following the Eqn. (3.2.5) and (3.2.6), $b(\boldsymbol{\phi}) = H(\mathbf{A}_0, \boldsymbol{\phi}) = H((J = 0, E = 0), (\theta, t))$. Therefore,

$$b(\boldsymbol{\phi}) = H(\mathbf{A}_0, \boldsymbol{\phi}) = \lambda\omega_0^{-\frac{2}{3}}(a_0 \cos t + \sum_{n=1}^{\infty} a_n[\cos(n\theta + t) + \cos(n\theta - t)]). \tag{3.2.8}$$

Then

$$\partial_{\boldsymbol{\phi}}\Gamma H(\mathbf{A}_0, \boldsymbol{\phi}) = (\partial_\theta \Gamma H(\mathbf{A}_0, \boldsymbol{\phi}), \partial_t \Gamma H(\mathbf{A}_0, \boldsymbol{\phi})), \tag{3.2.9}$$

where

$$\partial_\theta \Gamma H(\mathbf{A}_0, \boldsymbol{\phi}) = \lambda\omega_0^{-\frac{2}{3}} \sum_{n=1}^{\infty} n a_n [\frac{\cos(n\theta + t)}{n\omega_0 + 1} + \frac{\cos(n\theta - t)}{n\omega_0 - 1}],$$

$$\partial_t \Gamma H(\mathbf{A}_0, \boldsymbol{\phi}) = \lambda\omega_0^{-\frac{2}{3}}(a_0 \cos t + \sum_{n=1}^{\infty} a_n [\frac{\cos(n\theta + t)}{n\omega_0 + 1} - \frac{\cos(n\theta - t)}{n\omega_0 - 1}]).$$

Since $\mathbf{A_0} = (\mathbf{0}, \mathbf{0})$ for the shifted Hamiltonian (3.2.4),

$$\mathbf{A}_0 - \partial_{\boldsymbol{\phi}}\Gamma H(\mathbf{A}_0, \boldsymbol{\phi}) = (-\partial_\theta \Gamma H(\mathbf{A}_0, \boldsymbol{\phi}), -\partial_t \Gamma H(\mathbf{A}_0, \boldsymbol{\phi})). \tag{3.2.10}$$

Recall the expression of control term Eqn. (3.2.5), we have

$$f(\boldsymbol{\phi}) = -H(\mathbf{A}_0 - \partial_{\boldsymbol{\phi}}\Gamma H(\mathbf{A}_0, \boldsymbol{\phi}), \boldsymbol{\phi}). \tag{3.2.11}$$

Therefore in Hamiltonian (3.2.4) we replace J with $-\partial_\theta \Gamma H(\mathbf{A}_0, \boldsymbol{\phi})$, replace E with $-\partial_t \Gamma H(\mathbf{A}_0, \boldsymbol{\phi})$) and then put a negative sign in front. Consequently, we obtain the control term

$$\begin{aligned} f(\theta, t) &= \sum_{k=2}^{\infty} \frac{k+1}{2} \lambda^k \omega_0^{\frac{2-k}{3}} (\Gamma \partial_\theta v)^k \\ &\quad + (2\lambda^2 \omega_0^{-1} \Gamma \partial_\theta v - \lambda^3 \omega_0^{-\frac{4}{3}} (\Gamma \partial_\theta v)^2) v, \end{aligned} \tag{3.2.12}$$

where

$$\Gamma \partial_\theta v = \sum_{n=1}^{\infty} n a_n \left[\frac{\cos(n\theta + t)}{n\omega_0 + 1} + \frac{\cos(n\theta - t)}{n\omega_0 - 1} \right].$$

For λ small, we approximate the control term f by its leading order in λ^2 which is given by

$$f_2(\theta, t) = \frac{3}{2} \lambda^2 (\Gamma \partial_\theta v)^2 + 2\lambda^2 \omega_0^{-1} v \Gamma \partial_\theta v. \tag{3.2.13}$$

Obviously, the location of the restored invariant torus depends on the choice of Kepler frequency ω_0 or equivalently of its location in the integrable case J_0. The theoretical torus curve for the shifted Hamiltonian is given by

$$J_{shifted} = -\lambda \omega_0^{-\frac{2}{3}} \Gamma \partial_\theta v(\theta, t).$$

After this torus is shifted back by $\omega_0^{-\frac{1}{3}}$, we obtain the torus for the controlled original Hamiltonian (Hamiltonian (3.2.1) plus control term (3.2.12)) located at

$$J = J(\theta, t) = \omega_0^{-\frac{1}{3}} - \lambda \omega_0^{-\frac{2}{3}} \Gamma \partial_\theta v(\theta, t). \tag{3.2.14}$$

This torus is λ-close to $J_0 = \omega_0^{-1/3}$. We notice that the control term as well as the invariant torus are 2π-periodic in θ and time t.

Remark : In the local control method, we have searched for control terms only dependent on $\boldsymbol{\phi}$. However, in order to be more consistent with the specific shape of

the control waves, it can be appropriate to search for controlled Hamiltonian of the form

$$H_c(\mathbf{A}, \boldsymbol{\phi}) = H(\mathbf{A}, \boldsymbol{\phi}) + (\boldsymbol{\Omega} \cdot \mathbf{A})^2 f(\boldsymbol{\phi}),$$

where $\boldsymbol{\Omega}$ is a fixed vector, e.g., $\boldsymbol{\Omega} = (1, 0)$ in that case. Following the same arguments as in Ref. [20], the formula of the control term is

$$f(\boldsymbol{\phi}) = -\frac{H(\mathbf{A}_0 - \partial_{\boldsymbol{\theta}} \Gamma b, \boldsymbol{\phi})}{(\boldsymbol{\Omega} \cdot \mathbf{A}_0 - \boldsymbol{\Omega} \cdot \partial_{\boldsymbol{\phi}} \Gamma b)^2}, \tag{3.2.15}$$

where $b(\boldsymbol{\phi}) = H(\mathbf{A}_0, \boldsymbol{\phi})$. We notice that the control term (3.2.15) is still of the same order as the one given by Eq. (3.2.12) and it is ε^3-close to the one given by Eq. (3.2.5) divided by $(\boldsymbol{\Omega} \cdot \mathbf{A}_0)^2$, since $\partial_{\boldsymbol{\phi}} b$ is of order ε.

3.3 Numerical analysis

In what follows, the series which give v and $\Gamma \partial_\theta v$ are truncated at $n = 30$ for numerical purposes, and the first series of f is truncated at $k = 20$. Also, we choose ω_0 in the interval $[\frac{1}{n_0+1}, \frac{1}{n_0}]$ which corresponds to a region in between two primary resonances, and n_0 is in general chosen equal to 1, 2, 3... (With a relatively big n_0, local control theory still holds though quantum suppression leads to a higher ionization threshold [18]).

3.3.1 Analysis of the control term

Figure 3.3.1 depicts a contour plot of f given by Eqn. (3.2.12) and f_2 given by Eqn. (3.2.13) for $\omega_0 = 0.6750$ (which corresponds to $n_0 = 1$) and $\lambda = 0.03$. In this case, the scaled frequency at the intended invariant torus for $\lambda = 0$ is $\varpi = J_0^3 = \omega_0^{-1} = 1.4815 < 2$ which justifies the application of classical theory to the regime we are interested [41, 77]. Since f and f_2 are 2π-periodic in t and θ, these contour plots are represented for $(t, \theta) \in [0, 2\pi]^2$. In order to compare the control term with the perturbation, Fig. 3.3.2 represents a contour plot of the perturbation at an action $J = J_0$ where the control acts. These figures show that for this value of λ the control

term is small (by a factor approximately equal to 10) compared with the value of the external field $\lambda J_0^2 v(\theta, t)$.

However, the control terms f and f_2 given by Eqs. (3.2.12) and (3.2.13) appear to have a much richer Fourier spectrum. We have represented in Fig. 3.3.3 their two-dimensional Fourier transforms. They have an infinite number of Fourier modes and therefore not practical for a numerical or experimental realization. However, it is seen on Fig. 3.3.3 that only few Fourier coefficients contribute significantly to the control terms. Therefore, it is feasible to truncate them since the method has been shown to be robust [24]. The tailored control term results in general from a trade-off between the ability to control chaos and restrictions on the desired shape for the specific problem at hand.

In order to identify the main Fourier modes, we introduce a parameter A defined as

$$A_{k_1,k_2} \equiv \frac{|f_{k_1,k_2}|}{|k_1\omega_0 + k_2|}, \tag{3.3.1}$$

where f_{k_1,k_2} is the Fourier coefficient with wavevector (k_1, k_2) of f or f_2. The dominant Fourier mode is supposed to have maximal A. We notice that this definition contains two effects : First a dominant Fourier mode has to have a significant amplitude, and second, its corresponding wavevector has to be close to a resonance with the frequency vector of the integrable motion (and hence close to a resonance). For $\omega_0 = 0.6750$ (which corresponds to $n_0 = 1$) and $\lambda = 0.03$, there is only one dominant Fourier mode in f or f_2 which has a frequency which is twice the microwave frequency. The truncated control term is given by

$$f_a(\theta, t) = f_{3,-2} \cos(3\theta - 2t), \tag{3.3.2}$$

where $f_{3,-2} \approx -9.772 \times 10^{-4}$ for control term f given by Eqn. (3.2.12) and $f_{3,-2} \approx -9.739 \times 10^{-4}$ for the approximate control term f_2 given by Eqn. (3.2.13). We notice that these two values are very close. For this mode, we have $A_{3,-2} \approx 3.90 \times 10^{-2}$

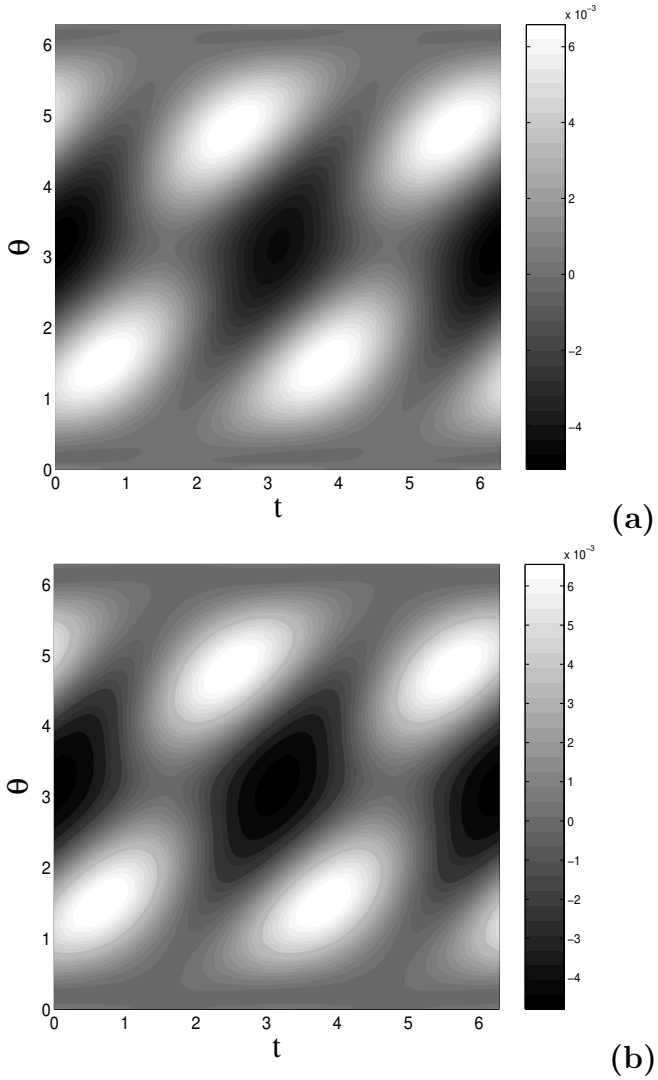

Figure 3.3.1: Contour plots of (a) f given by Eqn. (3.2.12) and (b) f_2 given by Eqn. (3.2.13) for $\lambda = 0.03$ and $\omega_0 = 0.6750$.

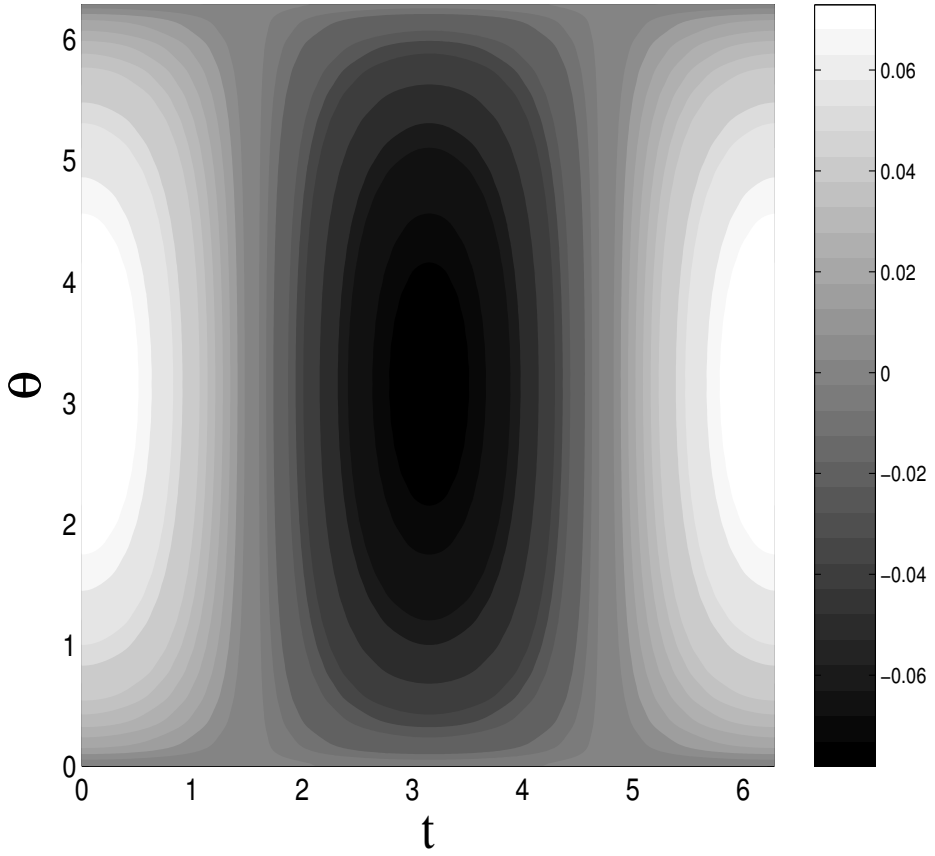

Figure 3.3.2: Contour plot of $\lambda J_0^2 v(\theta, t)$ where v is given by Eqn. (3.2.2) for $\lambda = 0.03$ and $\omega_0 = 0.6750$.

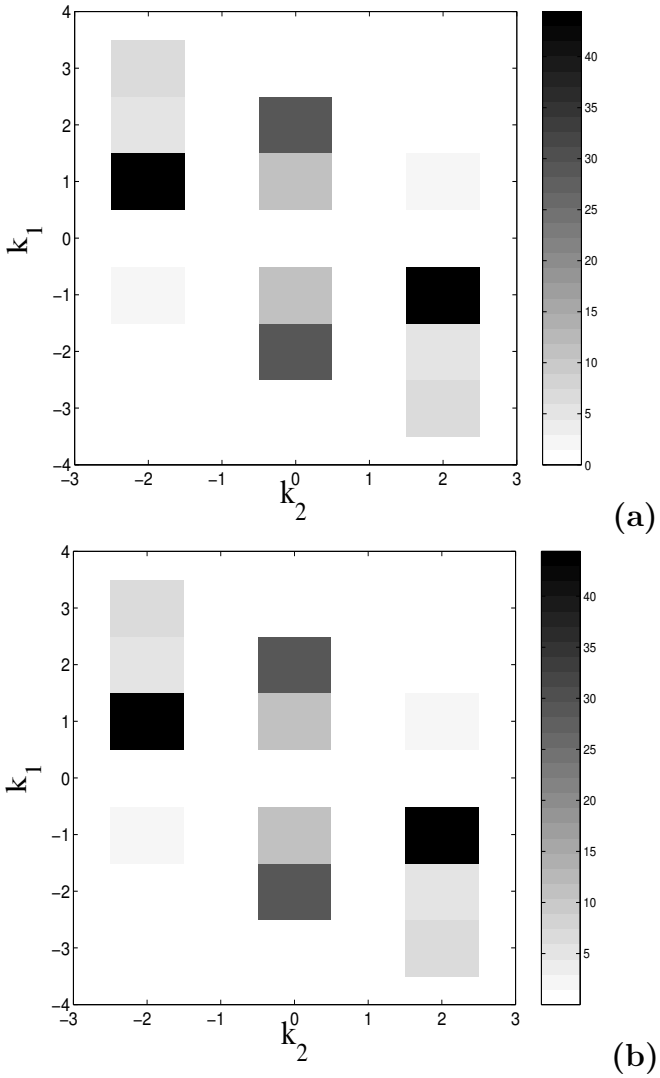

Figure 3.3.3: Two-dimensional Fourier transforms of (a) f given by Eqn. (3.2.12) and (b) f_2 given by Eqn. (3.2.13) for $\lambda = 0.03$ and $\omega_0 = 0.6750$.

which is more than ten times larger than the second largest one $A_{1,-2} \approx 1.90 \times 10^{-3}$. We notice that the continued fraction expansion of ω_0 is $[0, 1, 2, \ldots]$. One best approximant is $[0, 1, 2] = 2/3$ which is the frequency of the mode of f_a.

3.3.2 Poincaré sections

In order to test the efficiency of the control terms to restore invariant tori in phase space, we perform Poincaré sections of $H + f$, $H + f_2$ and $H + f_a$ and compare them to the Poincaré section of H given by Eqn. (3.2.1). Since all these Hamiltonians are periodic in time with period 2π, the natural Poincaré section is a stroboscopic plot with period 2π.

Figure 3.3.4 depicts Poincaré sections of Hamiltonian (3.2.1) in panel (a), Hamiltonian $H + f$ where f is given by Eqn. (3.2.12) in panel (b), Hamiltonian $H + f_2$ where f_2 is given by Eqn. (3.2.13) in panel (c) and Hamiltonian $H + f_a$ where f_a is given by Eqn. (3.3.2) in panel (d) for $\omega_0 = 0.6750$ and $\lambda = 0.03$. We notice that with the addition of the control terms, an invariant torus has been restored which prevent the diffusion from below to above the invariant torus. It is also worth noticing that all of these control terms are efficient although only f is expected to be, indicating that the presence of the control field f_2 contributes dominantly to a restoration of invariant tori at specific locations such that higher order resonances are eliminated which, in the Chirikov's approach [23], leads to less chaos and hence less stochastic ionization [16, 20] in our problem. It reinforces the robustness of the method and allows one to tailor a control term which is simpler to implement.

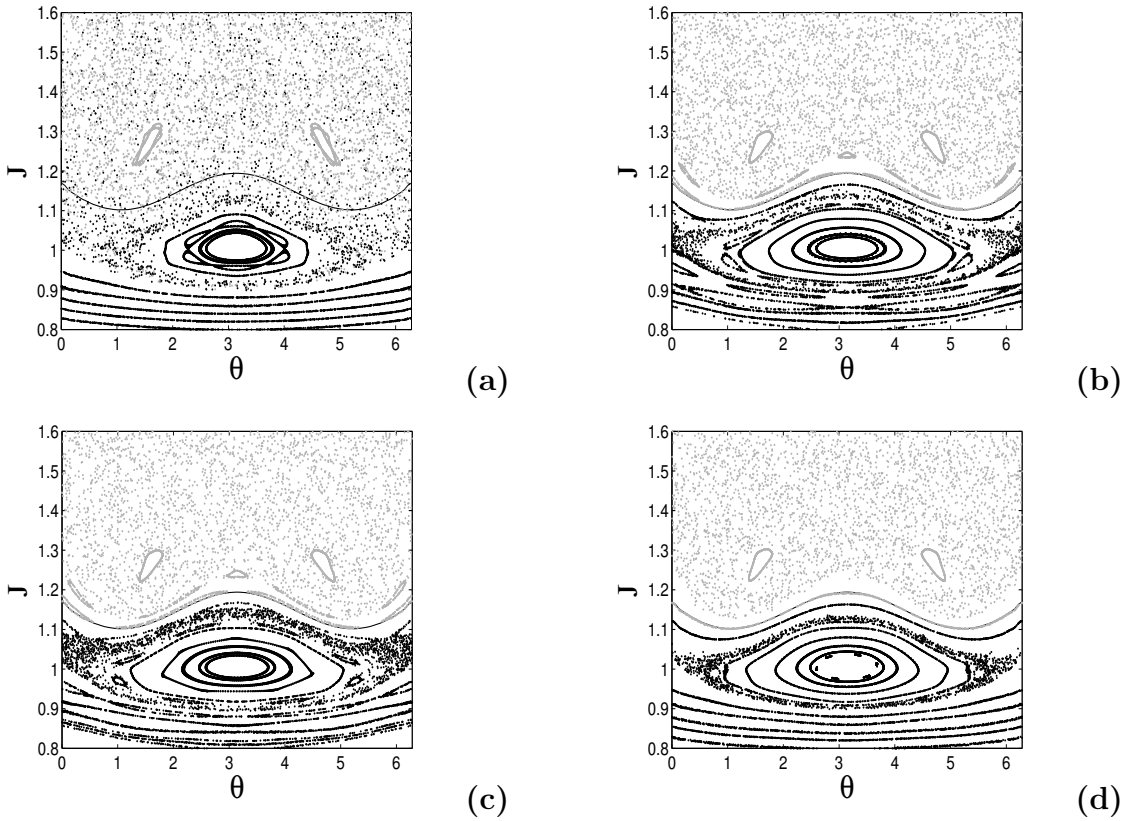

Figure 3.3.4: Poincaré sections of (a) The uncontrolled Hamiltonian H given by Eqn. (3.2.1), (b) The controlled Hamiltonian $H + f$ where f is given by Eqn. (3.2.12), (c) The controlled Hamiltonian $H + f_2$ where f_2 is given by Eqn. (3.2.13), and (d) The controlled Hamiltonian $H + f_a$ where f_a is given by Eqn. (3.3.2) for $\lambda = 0.03$ and $\omega_0 = 0.6750$. The thin wary curve indicates the location where the invariant torus is restored. The black dots are from trajectories launched below this curve, and gray dots are from trajectories launched above this curve. Note how they are interspersed in (a), as is expected of chaotic trajectories, and how the control restricts their movements in phase space through the invariant torus.

3.3.3 A control term as an additional wave

In Sec. 5.3.1, we show that the frequency of the control wave should be twice the one of the initial wave [1]. Therefore, a possible controlled Hamiltonian is

$$H = \frac{p^2}{2} - \frac{1}{x} + \lambda x \cos t + \mu x \cos 2t, \tag{3.3.3}$$

which corresponds to a control term $g(t) = \mu \cos 2t$ in Eqn. (3.1.2). In order to obtain the value of μ, we use the Fourier decomposition of the control term f obtained previously. First we map the controlled Hamiltonian into action-angle variables :

$$H = -\frac{1}{2J^2} + 2J^2 \left(\lambda \cos t + \mu \cos 2t\right) u(\theta), \tag{3.3.4}$$

where

$$u(\theta) = \frac{a_0}{2} + \sum_{n=1}^{\infty} a_n \cos n\theta.$$

If we give a value of the action J_0 where the invariant torus has to be restored, we have seen that the dominant Fourier mode is proportional to $\cos[(2n+1)\theta - 2t]$ where n is obtained using the continued fraction expansion of $\omega_0 = J_0^{-3}$. This mode is present in Eqn. (3.3.4) and has an amplitude given by $\mu J_0^2 a_{2n+1}$. If $f_{2n+1,-2}$ denotes the amplitude of the dominant Fourier mode in Eqn. (3.2.12) for the values of the parameters ω_0 and λ, then the amplitude of the control field is chosen to be

$$\mu = \frac{f_{2n+1,-2}}{J_0^2 a_{2n+1}}. \tag{3.3.5}$$

The real parameters taken for the external microwave field and control field are flexible for a set of rescaled amplitude of external field $\lambda = 0.03$ and frequency $\omega = 1$ as long as they satisfy rescaling relationships.

Figure 3.3.5 depicts the Poincaré section of the controlled Hamiltonian (3.3.4) with $\lambda = 0.03$ and $\mu = 0.0127$. Figure 3.3.5 does not show the restoration of an invariant

[1] Bichromatic microwave experiments are commonly used in manipulating microwave ionization [?, 63, 66, 107].

torus as in the previous cases and hence, the ionization reduction is not obvious. This comes from the fact that the additional wave is quite far from the control term (3.2.12) due to additional resonances which break-up the restored invariant torus.

However, the ionization process is still reduced, and this can be seen from the laminar plots. Such plots are obtained by looking at a grid of initial conditions and plotting the number of iterations it takes the action to exceed a certain threshold. Figure 3.3.6 depicts the laminar plots for Hamiltonian (3.2.1) and Hamiltonian (3.3.4) with $\lambda = 0.03$ and $\mu = 0.0127$. The action threshold is chosen to be $J_{th} = 1.30$. The maximum integration time is 600π. The darker the region is the smaller time it takes to have $J \geq J_{th}$. It is expected that the laminar plots with brighter regions are cases where there is less ionization.

In order to compare the diffusion time of trajectories for Hamiltonian (3.2.1) with that of the controlled Hamiltonian (3.3.4), we have taken a set of N initial angles evenly distributed in $[0, 2\pi]$ for one initial action J and then computed the mean diffusion time for each J in both controlled and uncontrolled cases :

$$\langle T_d \rangle(J) = \frac{1}{N} \sum_{i=1}^{N} T_d(J, \theta_i). \tag{3.3.6}$$

Figure 3.3.7 depicts the the curve of mean diffusion time $\langle T_d \rangle$ versus initial action J. In the numerical computation of $T_d(J, \theta_i)$, the integration is performed till the cut-off time $t = 600\pi$. Therefore for some trajectories the actual diffusion time is certainly above the cut-off time or even goes to infinity. The double frequency control field also works for the regime $1.14 < J < 1.20$ for the reason that the rebuilt invariant torus is a curve which goes beyond $J_0 = \omega_0^{-1/3} = 1.14$ in some areas. Figure 3.3.7 shows that the mean diffusion time for controlled Hamiltonian (3.3.4) is significantly larger than that for Hamiltonian (3.2.1) which clearly shows the effect of the additional microwave field in reducing ionization.

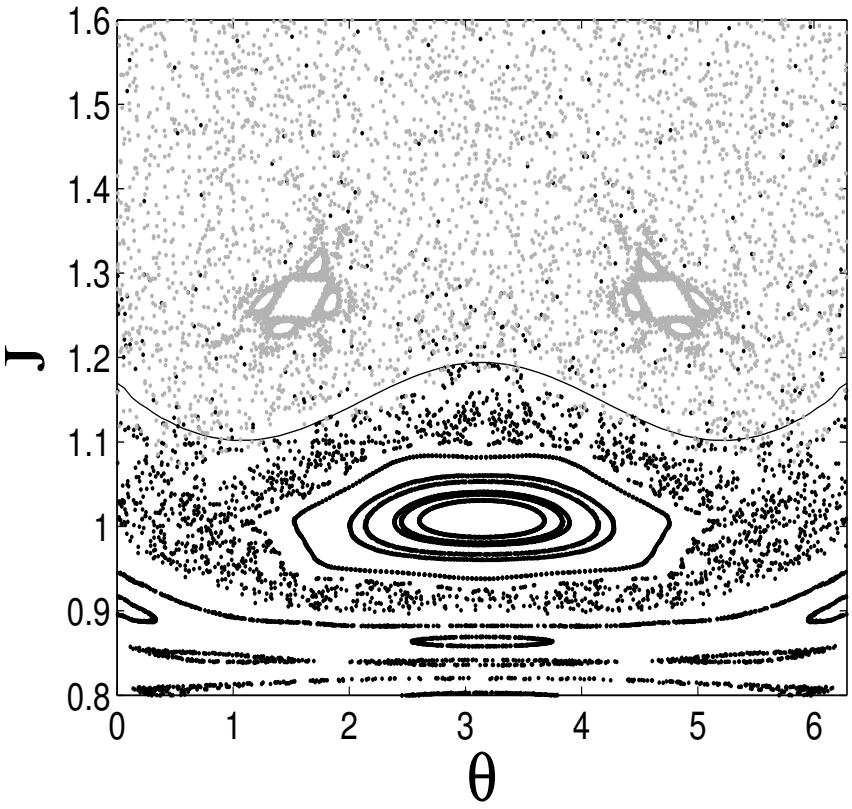

Figure 3.3.5: Poincaré sections of Hamiltonian (3.3.4) for $\lambda = 0.03$ and $\mu = 0.0127$.

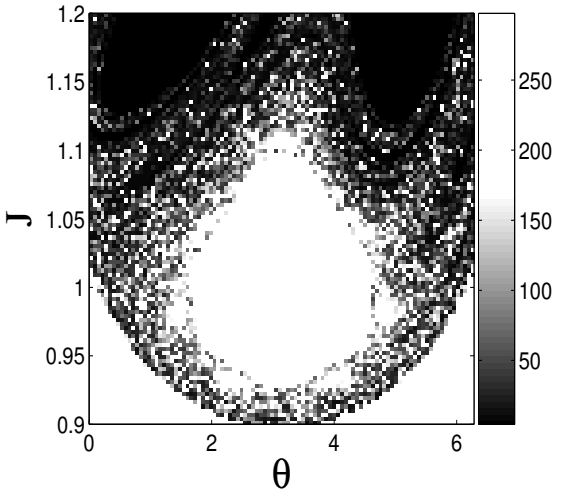

(a)

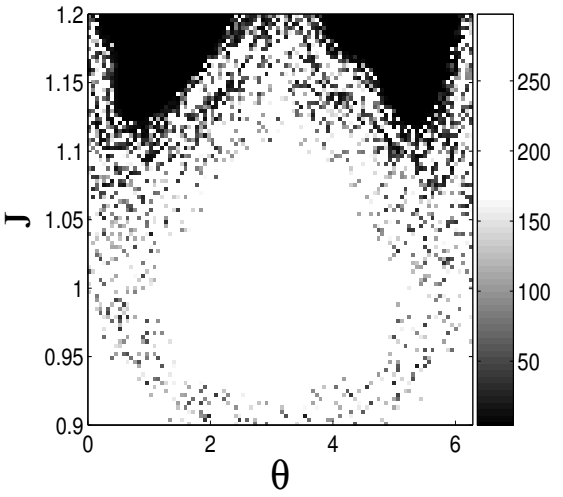

(b)

Figure 3.3.6: Laminar plots of (a) Hamiltonian (3.2.1) and (b) Hamiltonian (3.3.4) for $\lambda = 0.03$ and $\mu = 0.0127$. Cut-off time is 600π and diffusion threshold is $J_{th} = 1.30$.

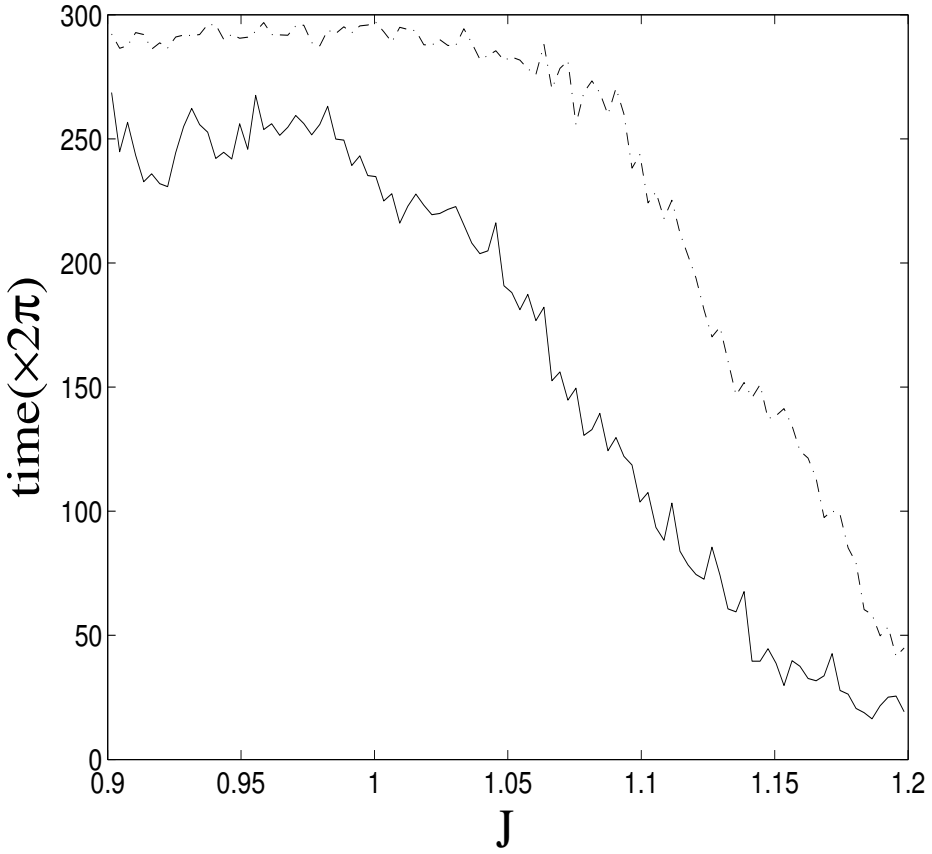

Figure 3.3.7: Mean diffusion time $\langle T_d \rangle$ versus initial action J with amplitude of external field $\lambda = 0.03$. Solid lines are for Hamiltonian (3.2.1). Dash-dotted lines are for Hamiltonian (3.3.4) for $\mu = 0.0127$. Cut-off time is 600π and diffusion threshold is $J_{th} = 1.30$.

3.4 Conclusion

In this chapter we implemented a local control method on the ionization of one-dimensional hydrogen atom model in a linearly polarized (LP) microwave field in order to reduce ionization. After simplifying the originally complicated control function numerically, we obtained an extremely simple control term which is in the same form as the external LP microwave field but with smaller amplitude. Adding the small control field to the perturbed Hamiltonian leads to a reduction of ionization. We have done the calculations in a regime where the quantum and classical methods agree, and our classical computations show efficient suppression of ionization. This work exhibits a heuristic way of controlling ionization in higher dimensions.

CHAPTER IV

LINEAR STABILITY ANALYSIS FOR PERIODIC ORBITS WITH HIGH EFFICIENCY

Chaotic behavior can exist in many simple Hamiltonian systems with deterministic properties. Kolmogorov [67], Arnold [2] and Moser [84] (KAM) introduced a theorem regarding periodic orbits or tori that are lying in phase space and governing these chaotic systems. The variation of either initial conditions or parameters of the systems can make the type of these orbits change drastically. In this chapter, we review some important concepts regarding periodic orbits analysis that we will use in the following chapters to investigate multiphoton ionization or dissociation phenomena.

4.1 "Residue"

In this section, we make a brief introduction on a quantity namely "residue", which was first presented by Greene [47] and further analyzed in depth by Mackay [76], Cary and Hanson [16] and Bachelard *et al* [4] to describe the linear stability properties of these orbits.

4.1.1 Definition

For a d-dimensional flow depending on a set of parameters $\boldsymbol{\beta}$, according to Hamilton's equations of motion, we have

$$\frac{d\boldsymbol{x}}{dt} = \mathbb{J}_d \nabla_{\boldsymbol{x}} H(\boldsymbol{x}, t; \boldsymbol{\beta}), \tag{4.1.1}$$

where $\boldsymbol{x} = \begin{pmatrix} \boldsymbol{p} \\ \boldsymbol{q} \end{pmatrix} = \begin{pmatrix} x_1 \\ x_2 \\ \vdots \\ x_d \end{pmatrix}$ is a vector of the flow, H is the Hamiltonian of this flow and $\mathbb{J}_d = \begin{pmatrix} 0 & \mathbb{I}_d \\ -\mathbb{I}_d & 0 \end{pmatrix}$. Here $\begin{pmatrix} \boldsymbol{p} \\ \boldsymbol{q} \end{pmatrix}$ are canonically conjugate variables and $\mathbb{I}_d$ is the d-dimensional identity matrix. With the objective of characterizing the periodic orbits that reflect the linear stability of the Hamiltonian systems, in general, one should consider the tangent flow matrix $\mathcal{J}^t_{\boldsymbol{\beta}}$ described by

$$\frac{d}{dt}\mathcal{J}^t_{\boldsymbol{\beta}} = \mathbb{J}_d \nabla^2 H(\boldsymbol{x}, t; \boldsymbol{\beta}) \mathcal{J}^t_{\boldsymbol{\beta}}. \tag{4.1.2}$$

In particular, the Hamiltonian of one-dimensional perturbed hydrogen atom in terms of action-angle variables (J, θ) is a two-dimensional flow plus an additional dimension for time, and hence Eqn. (4.1.2) reads

$$\frac{d}{dt}\mathcal{J}^t_{\boldsymbol{\beta}} = \mathbb{J} \nabla^2 H(J, \theta, t; \boldsymbol{\beta}) \mathcal{J}^t_{\boldsymbol{\beta}}, \tag{4.1.3}$$

where $\mathbb{J} = \begin{pmatrix} 0 & 1 \\ -1 & 0 \end{pmatrix}$, $\nabla^2 H$ is the two-dimensional Hessian matrix whose elements are second derivatives of H with respect to its action-angle variables J and θ, and the initial condition is $\mathcal{J}^0_{\boldsymbol{\beta}} = \mathbb{I}_2$ (the two-dimensional identity matrix). Eqn. (4.1.3) can be written as

$$\begin{pmatrix} \dot{\mathcal{J}}_{11} & \dot{\mathcal{J}}_{12} \\ \dot{\mathcal{J}}_{21} & \dot{\mathcal{J}}_{22} \end{pmatrix} = \begin{pmatrix} 0 & 1 \\ -1 & 0 \end{pmatrix} \begin{pmatrix} \frac{\partial^2 H}{\partial \theta^2} & \frac{\partial^2 H}{\partial \theta \partial J} \\ \frac{\partial^2 H}{\partial J \partial \theta} & \frac{\partial^2 H}{\partial J^2} \end{pmatrix} \begin{pmatrix} \mathcal{J}_{11} & \mathcal{J}_{12} \\ \mathcal{J}_{21} & \mathcal{J}_{22} \end{pmatrix},$$

which can further be expressed as four differential equations

$$\begin{bmatrix} \dot{\mathcal{J}}_{11} = \mathcal{J}_{11}\frac{\partial^2 H}{\partial J \partial \theta} + \mathcal{J}_{21}\frac{\partial^2 H}{\partial J^2} \\ \dot{\mathcal{J}}_{12} = \mathcal{J}_{12}\frac{\partial^2 H}{\partial J \partial \theta} + \mathcal{J}_{22}\frac{\partial^2 H}{\partial J^2} \\ \dot{\mathcal{J}}_{21} = -\mathcal{J}_{11}\frac{\partial^2 H}{\partial \theta^2} - \mathcal{J}_{21}\frac{\partial^2 H}{\partial \theta \partial J} \\ \dot{\mathcal{J}}_{22} = -\mathcal{J}_{12}\frac{\partial^2 H}{\partial \theta^2} - \mathcal{J}_{22}\frac{\partial^2 H}{\partial \theta \partial J} \end{bmatrix}. \tag{4.1.4}$$

The initial condition for matrix $\mathcal{J}^t_{\boldsymbol{\beta}}$ is

$$\mathcal{J}^0_{\boldsymbol{\beta}} = \begin{pmatrix} \mathcal{J}^0_{11} & \mathcal{J}^0_{12} \\ \mathcal{J}^0_{21} & \mathcal{J}^0_{22} \end{pmatrix} = \begin{pmatrix} 1 & 0 \\ 0 & 1 \end{pmatrix}.$$

In Eqn. (4.1.3), the matrix $\mathcal{J}^t_{\boldsymbol{\beta}}$ is of great importance because for a considered periodic orbit with period T, the spectrum of the monodromy matrix $\mathcal{J}^T_{\boldsymbol{\beta}}$ determine the linear stability properties. Here one should notice that the determinant of $\mathcal{J}^T_{\boldsymbol{\beta}}$ is equal to 1 because the flow is volume preserving. Therefore the numerical solution to Eqn. (4.1.4) is key to study the linear stability of the dynamical system. Since the two eigenvalues of matrix $\mathcal{J}^T_{\boldsymbol{\beta}}$ are dependent on its trace only, a quantity called "residue" was concisely defined by Greene to describe the state of periodic orbits [47, 76] as

$$R = \frac{2 - \mathrm{tr}\mathcal{J}^T_{\boldsymbol{\beta}}}{4}. \tag{4.1.5}$$

4.1.2 Analysis based on residue

With the definition of residue (4.1.5), the two eigenvalues of matrix $\mathcal{J}^T_{\boldsymbol{\beta}}$ are given by

$$\lambda(\boldsymbol{\beta}) = 1 - 2R \pm 2\sqrt{R(R-1)}. \tag{4.1.6}$$

For $0 < R < 1$, the two eigenvalues are complex and can be rewritten as $(\mathrm{e}^{i\omega(\boldsymbol{\beta})}, \mathrm{e}^{-i\omega(\boldsymbol{\beta})})$. In this case, tangent space orbits rotate about the origin for many repetitions steadily and the periodic orbits are hence stable and called elliptical periodic orbits. For $R > 1$ or $R < 0$, the two eigenvalues are real and can be expressed in the form $(\lambda(\boldsymbol{\beta}), 1/\lambda(\boldsymbol{\beta}))$ with $\lambda(\boldsymbol{\beta}) \in \mathbb{R}^*$. Under this condition, tangent space orbits are in hyperbolic shape and tend to escape from the system. Therefore the periodic orbits are unstable then called hyperbolic periodic orbits. For $R = 1$ or $R = 0$, the periodic orbits are called parabolic and higher order expansions are responsible for the stability of these periodic orbits. More detailed mathematical analyses are shown in Refs. [47, 76]. Some concrete examples can be found in Refs. [4, 16]. In Chapter V, we show our work based on residue analysis to investigate the ionization probability of hydrogen atoms driven by a linearly polarized bichromatic microwave field.

4.2 Monitoring periodic orbits with the Newton-Raphson multi-shooting algorithm

In many chaotic systems, the periodic orbits governing the dynamics are varied slowly and continuously in phase space along with the small change of parameters. In order to follow the stability properties of a certain periodic orbit, one should monitor the orbit which deforms with the continuous variation of parameters. In order to efficiently monitor the periodic orbits which are crucial to some multiphoton phenomena, we want to employ a modified Newton-Raphson multi-shooting algorithm as elaborated in Ref. [30]. In this section, we give a brief introduction to this algorithm based on Ref. [30].

4.2.1 Fixed points

The d-dimensional mappings can be expressed as

$$\boldsymbol{x}' = \boldsymbol{f}(\boldsymbol{x}),$$

where both $\boldsymbol{x} = \begin{pmatrix} x_1 \\ x_2 \\ \vdots \\ x_d \end{pmatrix}$ and $\boldsymbol{x}' = \begin{pmatrix} x'_1 \\ x'_2 \\ \vdots \\ x'_d \end{pmatrix}$ are vectors. In order to search for fixed points, one solves $\boldsymbol{F}(\boldsymbol{x}^*) = \boldsymbol{x}^* - \boldsymbol{f}(\boldsymbol{x}^*) = 0$ using Newton-Raphson method with an initial guess for $\boldsymbol{x_0}$. Provided that $\mathbb{I}_d - \frac{\partial \boldsymbol{f}}{\partial \boldsymbol{x}}$ is invertible, the Newton-Raphson iteration for a search of fixed points is given by

$$\boldsymbol{x}_1 = \boldsymbol{x_0} - \left(\mathbb{I}_d - \frac{\partial \boldsymbol{f}}{\partial \boldsymbol{x}}\right)^{-1} (\boldsymbol{x_0} - \boldsymbol{f}(\boldsymbol{x_0})), \tag{4.2.1}$$

where $\mathbb{I}_d$ is the d-dimensional identity matrix and $\frac{\partial \boldsymbol{f}}{\partial \boldsymbol{x}}$ is a $d \times d$ matrix of variations whose elements are

$$\left(\frac{\partial \boldsymbol{f}}{\partial \boldsymbol{x}}\right)_{ij} = \frac{\partial f_i}{\partial x_j}.$$

4.2.2 Multipoint cycle orbit

Here, we briefly recall the basic equations for the determination of multipoint cycle orbit by the Newton-Raphson multi-shooting method following Ref. [30, 87].

For d-dimensional multipoint cycle orbit, we assume that the periodic orbit has n points on the Poincaré section. In order to search for n-point orbits, one uses Newton-Raphson method to solve

$$\mathrm{F}(\boldsymbol{x}^{(1)}, \boldsymbol{x}^{(2)}, \ldots, \boldsymbol{x}^{(n)}) = \begin{pmatrix} \boldsymbol{x}^{(1)} - \boldsymbol{f}(\boldsymbol{x}^{(n)}) \\ \boldsymbol{x}^{(2)} - \boldsymbol{f}(\boldsymbol{x}^{(1)}) \\ \vdots \\ \boldsymbol{x}^{(n)} - \boldsymbol{f}(\boldsymbol{x}^{(n-1)}) \end{pmatrix} = 0, \tag{4.2.2}$$

where $\boldsymbol{x}^{(k)} = \begin{pmatrix} x_1^{(k)} \\ x_2^{(k)} \\ \vdots \\ x_d^{(k)} \end{pmatrix}$. Apparently in Eqn. (4.2.2) the dimension of the vector is dn. The equation for New-Raphson iteration for n-point orbits search reads

$$\mathrm{x}_1 = \mathrm{x}_0 - \mathcal{M}^{-1}\mathrm{G}, \tag{4.2.3}$$

where x_0 is an initial guess for $[(d+1)n]$ dimensional vector $\begin{pmatrix} \boldsymbol{x}^{(1)} \\ \boldsymbol{x}^{(2)} \\ \vdots \\ \boldsymbol{x}^{(n)} \\ \boldsymbol{T}_0 \end{pmatrix}$, where $\boldsymbol{T}_0 = \begin{pmatrix} T_0^{(1)} \\ T_0^{(2)} \\ \vdots \\ T_0^{(n)} \end{pmatrix}$ is the initial time for each point. $\mathrm{G} = \begin{pmatrix} \mathrm{F} \\ 0 \\ \vdots \\ 0 \end{pmatrix}$ is a $[(d+1)n]$ dimensional

vector. $\mathcal{M}$ is a $[(d+1)n \times (d+1)n]$ matrix which reads

$$\mathcal{M} = \begin{pmatrix} \mathcal{K} & \mathcal{V} \\ \mathcal{A} & 0 \end{pmatrix}.$$

Here $\mathcal{K}$ is a $[dn \times dn]$ matrix given by

$$\mathcal{K} = \begin{pmatrix} \mathbb{I}_d & 0 & \dots & 0 & -\frac{\partial \boldsymbol{f}(\boldsymbol{x}^{(n)})}{\partial \boldsymbol{x}} \\ -\frac{\partial \boldsymbol{f}(\boldsymbol{x}^{(1)})}{\partial \boldsymbol{x}} & \mathbb{I}_d & \ddots & \ddots & 0 \\ 0 & -\frac{\partial \boldsymbol{f}(\boldsymbol{x}^{(2)})}{\partial \boldsymbol{x}} & \ddots & \ddots & \vdots \\ \vdots & \ddots & \ddots & \ddots & 0 \\ 0 & \dots & 0 & -\frac{\partial \boldsymbol{f}(\boldsymbol{x}^{(n-1)})}{\partial \boldsymbol{x}} & \mathbb{I}_d \end{pmatrix}, \tag{4.2.4}$$

where $\mathbb{I}_d$ is the d-dimensional identity matrix and $\frac{\partial \boldsymbol{f}(\boldsymbol{x}^{(m)})}{\partial \boldsymbol{x}}$ is the monodromy matrix $\mathcal{J}_{\boldsymbol{\beta}}^{(m)}$ for mth point. Here $1 \leq m \leq n$ and m is an integer. $\mathcal{V}$ is a $[dn \times n]$ matrix which is

$$\mathcal{V} = \begin{pmatrix} v^{(1)} & & 0 \\ & \ddots & \\ 0 & & v^{(n)} \end{pmatrix},$$

where $v^{(m)} = \dot{x}^{(m)}$ is a d-dimensional velocity vector (column vector) for each point. $\mathcal{A}$ is an $[n \times dn]$ matrix given by

$$\mathcal{A} = \begin{pmatrix} a & & 0 \\ & \ddots & \\ 0 & & a \end{pmatrix},$$

where a is a d-dimensional vector (row vector) normal to Poincaré section. It should be pointed out that the crucial information regarding the dynamics in matrix $\mathcal{M}$ is in fact included in matrix $\mathcal{K}$. However, matrix $\mathcal{K}$ is not invertible while matrix $\mathcal{M}$ is in general. The invertibility of matrix $\mathcal{M}$ is required for the iteration equation (4.2.3). The initial guess can be made in Poincaré section with accuracy such that the "guess" is almost guaranteed to be a good "guess". With the Newton-Raphson multi-shooting

algorithm, we can monitor the considered periodic orbits with variation of parameters $\boldsymbol{\beta}$ very efficiently and investigate the role that the orbits play in the dynamics.

CHAPTER V

PERIODIC ORBIT BIFURCATIONS AS AN IONIZATION MECHANISM: THE BICHROMATICALLY DRIVEN HYDROGEN ATOM

With permission from IOP Publishing Ltd, this chapter is modified from the papers originally published as:

S. Huang, C. Chandre and T. Uzer, "Periodic orbit bifurcations as an ionization mechanism: The bichromatically driven hydrogen atom", J. Phys. B: At. Mol. Opt. Phys. **41**, 035604 (2008). http://stacks.iop.org/JPhysB/41/035604

and

S. Huang, C. Chandre and T. Uzer, "How periodic orbit bifurcations drive multiphoton ionization", J. Phys. B: At. Mol. Opt. Phys. **40**, F181 (2007). http://dx.doi.org/10.1088/0953-4075/40/11/F02

The homepage of Journal of Physics B is http://www.iop.org/journals/JPhysB

5.1 Introduction

Among systems at the atomic level, one-electron systems are the most fundamental and have proven to be a source of numerous surprising discoveries [9] : The multiphoton ionization of hydrogen in a strong microwave field [7] is such a simple system with surprisingly complex dynamics. With the development of theory of chaos, its stochastic and diffusional nature was elucidated [80], and intense research activity in the last three decades has resulted in a rather complete understanding of this problem [17, 60, 65]. In the recent years, the attention has shifted from understanding the physical process to manipulating or controlling it [93, 104]. In this context control

refers to tailoring the physical behavior of dynamical systems (which generically show chaotic dynamics) using "knobs" (i.e., suitable external parameters). Identifying such knobs and understanding the mechanism by which they affect the dynamics is the ultimate goal of such research.

Bichromatic pulses [36, 63] are natural tools in atomic control research because they offer practical control parameters such as polarization, amplitudes and phases [6, 14, 29, 51, 54, 57, 66, 89, 94, 106, 107]. It has even been shown that it is possible to use the direction of transport in a ratchet by varying the phase lag in the bichromatic pulse [15]. In this chapter we consider the ionization behavior of a one-dimensional hydrogen atom driven by a strong bichromatic linearly polarized electric field which is modeled by the following one-dimensional Hamiltonian ($x > 0$) in atomic units

$$H = \frac{p^2}{2} - \frac{1}{x} + F_h x \sin(h\omega t) + F_l x \sin(l\omega t + \phi), \tag{5.1.1}$$

where the indices l and h refer to the low and high frequency modes with frequencies $l\omega$ and $h\omega$, respectively. These two modes are frequency locked (and denoted h:l), i.e. l and h are integers. The experimental results as well as the quantum calculations results on ionization probability obtained in Refs. [66,106] for two cases, mode lockings 3:1 and 3:2, show two very distinct regimes as the phase lag ϕ is varied : For 3:1, the ionization probability shows a plateau in phase located at a rather high value of ionization probability, and for 3:2, the ionization probability shows no such plateau but rather a small value of ionization probability.

In this chapter, we want to show that these experimental observations are qualitatively and quantitatively captured using a periodic orbit analysis, which reveals the classical bifurcations responsible for ionization. Our analysis also allows the prediction of ionization at other values of parameters without resorting to large numerical simulations.

This chapter is organized as follows: First, in Sec. 5.2, we summarize the residue analysis of periodic orbits [4] in the bichromatically driven hydrogen atom. In Sec. 5.3

and Sec. 5.4, we consider two cases, the 3:1 mode locking and 3:2 one, respectively. These two cases show drastically different ionization behavior which we explain through bifurcations of selected periodic orbits. In these two cases, we described the bifurcations (if any) in the system. We also compute the bifurcation surface which is defined by the set of parameters where a change of linear stability (associated with a period doubling or halving) has occurred in the chaotic sea. In Sec. 5.5 we discuss the generalities of residue curve behavior for other mode lockings.

5.2 Residue analysis of periodic orbits

First, we map Hamiltonian (5.1.1) into action-angle variables (of the unperturbed system $F_h = F_l = 0$) such that the principal quantum number n is reflected by action J. The relationship between J and n reads

$$J = (t_0\omega)^{1/3} n,$$

where $t_0 = 2.4188843243 \times 10^{-17} s$ (atomic time unit) and $\omega = 2\pi f = 12\pi$ GHz in both cases. The action-angle variables [72] are denoted (J, θ) and obtained through the canonical change of coordinates $x = 2J^2 \sin^2\varphi$, $p = J^{-1}\cot\varphi$ with $\theta = 2\varphi - \sin 2\varphi$.

We assume $\omega = 1$ without loss of generality (after a rescaling $H' = \omega^{-2/3}H$, $t' = \omega t$, $x' = \omega^{2/3}x$, $p' = \omega^{-1/3}p$ and consequently $\phi' = \phi$ and $F' = \omega^{-4/3}F$). The Hamiltonian (5.1.1) becomes [17]

$$\begin{aligned} H &= -\frac{1}{2J^2} + 2J^2[F_h \sin(ht) \\ &\quad + F_l \sin(lt + \phi)] \left(a_0/2 + \sum_{k=1}^{\infty} a_k \cos k\theta \right), \end{aligned} \tag{5.2.1}$$

where $a_n = [J_n(n) - J_{n-1}(n)]/n$ and J_n's are Bessel functions of the first kind. Note that for a given mode locking h:l, there are three variables (J, θ, t) and three parameters (F_h, F_l, ϕ). We denote this Hamiltonian $H(J, \theta, t; F_h, F_l, \phi)$. In general, for a given set of parameter values, the phase space as depicted on a Poincaré section (a

stroboscopic plot with period 2π, see Fig. 5.3.1), is composed of a mixture of regular structures surrounded by a chaotic sea. More precisely, the lower part of phase space (J small) is composed of rotational invariant tori (which persist from the integrable case $F_h = F_l = 0$ as asserted by KAM theorem). The upper part is formed by regular islands surrounded by an unbounded chaotic sea. The ionizing trajectories are the ones in the chaotic sea which are unbounded (J, or equivalently n, becomes progressively large). At the center of the regular islands, there are elliptic (stable) periodic orbits which organize the regular motion around them. These periodic orbits result partly from the break-up of resonant tori into a pair of elliptic/hyperbolic orbits (according to Birkhoff's theorem). Other periodic orbits result from the bifurcation of these orbits.

The general idea which is applied here is to follow a finite set of periodic orbits (both elliptic or hyperbolic) which have been identified as important. The criteria of choice combine several factors: the size of the island, the period and the location. For each periodic orbit of this set, we compute its location (J, θ) and its linear stability property as given by the residue (which is to be defined below). As the three parameters are varied, we follow the locations and residues of these orbits instead of computing the Poincaré section for each value of parameters. This allows us to form a clear idea of what is going on in phase space and to predict ionization thresholds.

In what follows, we perform two kinds of computations : First, we compute the residue curves which are obtained as functions of the relative phase ϕ for fixed values of the amplitudes (F_h, F_l). Second, we compute bifurcation surfaces which are defined as the set of parameters (F_h, F_l, ϕ) where a change of linear stability has occurred.

In order to start monitoring the stability of a family of periodic orbits, we first consider a specific periodic orbit, denoted $\mathcal{O}(0)$, of Hamiltonian (5.2.1) for $\phi = 0$ which is our reference case. Numerically it is determined using a modified Newton-Raphson multi-shooting algorithm as described in Ref. [30]. The initial condition for launching

the iterative algorithm can be taken from a Poincaré section, for instance. As ϕ is continuously varied, the orbit $\mathcal{O}(0)$ deforms continuously into $\mathcal{O}(\phi)$, whose period is denoted $T(\phi)$. In addition to its location, we also monitor its linear stability properties given by the integration of the reduced tangent flow as introduced in Sec. 4.1.1

$$\frac{d\mathcal{J}_\phi^t}{dt} = \mathbb{J}\nabla^2 H(J,\theta,t;\phi)\mathcal{J}_\phi^t,$$

where $\mathbb{J} = \begin{pmatrix} 0 & 1 \\ -1 & 0 \end{pmatrix}$ and $\nabla^2 H$ is the two-dimensional Hessian matrix. The initial condition is $\mathcal{J}_\phi^0 = \mathbb{I}_2$ (the two-dimensional identity matrix). The two eigenvalues of the monodromy matrix $\mathcal{J}_\phi^{T(\phi)}$ which make a pair $(\lambda(\phi), 1/\lambda(\phi))$ determine the stability properties. The linear stability properties are described by a concise form using Greene's residue R [47,76]

$$R(\phi) = \frac{2 - \mathrm{tr}\mathcal{J}_\phi^{T(\phi)}}{4}.$$

If $R(\phi) \in]0,1[$, the periodic orbit is elliptic and the spectrum is $(\mathrm{e}^{i\omega(\phi)}, \mathrm{e}^{-i\omega(\phi)})$ (stable, except for some particular cases); if $R(\phi) < 0$ or $R(\phi) > 1$ it is hyperbolic and the spectrum is $(\lambda(\phi), 1/\lambda(\phi))$ with $\lambda(\phi) \in \mathbb{R}^*$ (unstable); and if $R(\phi) = 0$ and $R(\phi) = 1$, it is parabolic. Generically, periodic orbits and their linear stabilities are robust against small changes of parameters, except at specific values where bifurcations occur [16]. These rare events affect the dynamical behavior drastically. They can be associated with an enhancement as well as a reduction of stability depending on the type of bifurcations, as shown in Refs. [4,16]. We identify the bifurcations (if any) of a set of short periodic orbits, i.e., the type and the value of the parameter ϕ_c where they bifurcate. This provides a way to foretell if a relatively high ionization rate should be expected or not. The importance of considering two associated Birkhoff periodic orbits (i.e. periodic orbits with the same action but different angles in the integrable case, one elliptic and one hyperbolic), was emphasized in Ref. [4]. The main reason is that it allows one to discard some specific bifurcations (like collisions or exchanges of

stability) and draw appropriate conclusions concerning the enhancement or reduction of stability.

In the following sections, we analyze the short-time dynamics through residues of selected periodic orbits. We compute residue curves $\phi \mapsto R(\phi, F_h, F_l)$ for fixed values of the amplitudes F_h and F_l, and bifurcation surfaces associated with a given periodic orbit defined as the set of parameters such that $R(\phi, F_h, F_l) = 1$. We correlate these results with ionization probabilities obtained experimentally and also by quantum simulations through an empirical formula.

5.3 3:1 mode locking

For this mode locking, we consider $F_h = 24\ \mathrm{Vcm}^{-1}$ and $F_l = 53.4\ \mathrm{Vcm}^{-1}$ as in Ref. [66]. These values correspond to the dimensionless values $F_h = 24v_0(t_0\omega)^{-4/3}/d_0 = 0.5278$ and $F_l = 53.4v_0(t_0\omega)^{-4/3}/d_0 = 1.1743$, where $v_0 = 0.036749326$ and $d_0 = 1.88972613 \times 10^8$ are both conversion factors, $t_0 = 2.4188843243 \times 10^{-17}s$ (atomic time unit). These values are referred as Case (I) in what follows.

5.3.1 Poincaré section

Figure 5.3.1 shows a Poincaré section of Hamiltonian (5.2.1) for Case (I) at $\phi = 0$. The phase space is divided into two main parts : a lower regular containing many invariant tori, and a upper chaotic sea where trajectories escape rapidly to unbounded actions J (ionized trajectories). We notice two main islands in the chaotic sea. At the centers of these islands sit elliptic periodic orbits with period 2π (indicated by full circles). In addition, there is also a period 2 island in between these two main islands (associated with an elliptic and hyperbolic periodic orbits with period 4π). In the region of phase space around $J_i \approx 0.49$ (indicated by a straight line) where the initial states $n = 51$ are prepared [66], any regular structures like the main islands and smaller ones are associated with trappings and hence reduce the ionization rate.

Figure 5.3.2 shows a Poincaré section of Hamiltonian (5.2.1) for Case (I) at $\phi =$

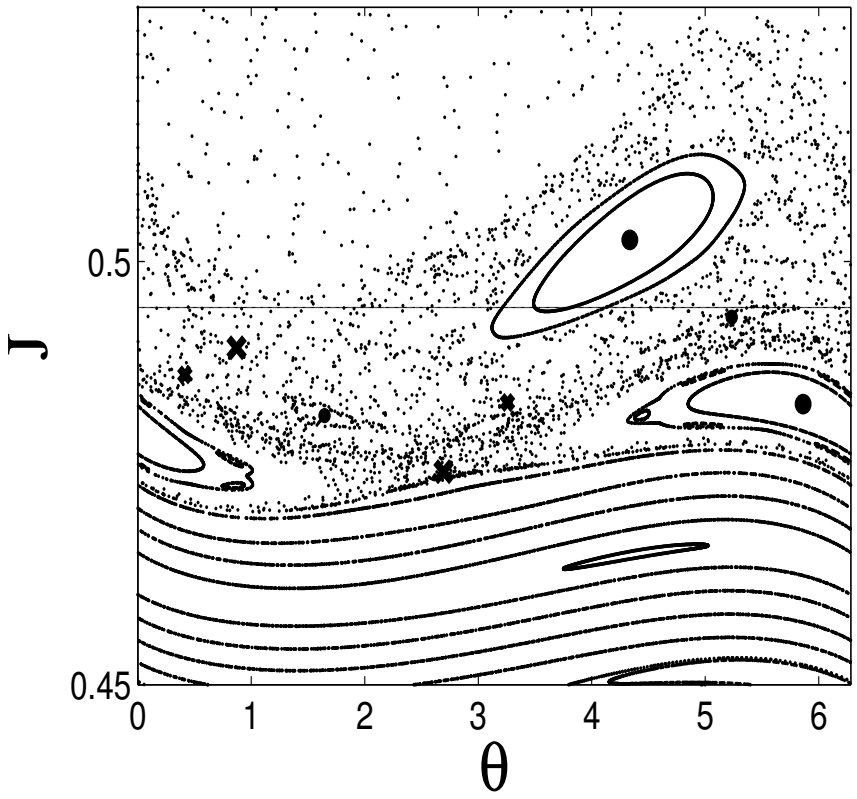

Figure 5.3.1: Poincaré section of Hamiltonian (5.2.1) for Case (I) at $\phi = 0$. Full big circles (or big crosses, respectively) indicate the two elliptic (resp. hyperbolic) periodic orbits with period 2π we consider. Full small circles (or small crosses, respectively) indicate the two elliptic (resp. hyperbolic) periodic orbits with period 4π we consider. The horizontal line corresponds to the principal quantum number $n = 51$.

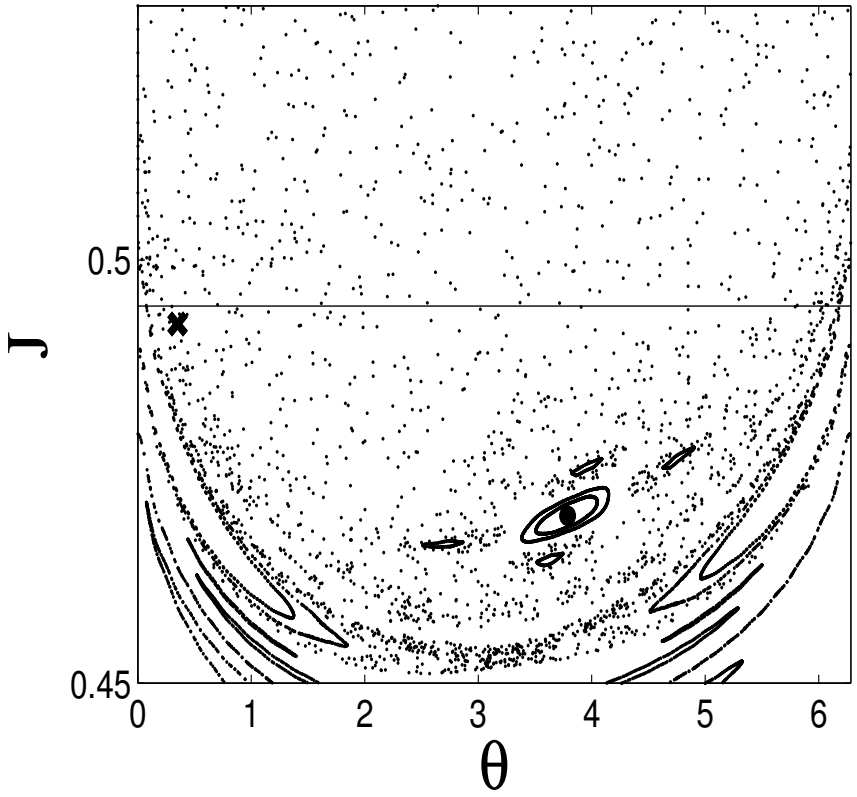

Figure 5.3.2: Poincaré section of Hamiltonian (5.2.1) for Case (I) at $\phi = \pi/3$. Full circle (respectively cross) indicates the elliptic (resp. hyperbolic) periodic orbit with period 2π we consider. The horizontal line corresponds to the principal quantum number $n = 51$.

$\pi/3$. Apparently the upper elliptic periodic orbit of period 2π in Fig. 5.3.1 has disappeared in chaotic sea. This case is associated with a higher ionization probability. Therefore, the loss of stability of the main periodic orbit near J_i plays a major role in the ionization process.

The residue method will monitor the location and stability of elliptic periodic orbits as well as their associated hyperbolic periodic orbits [4] as a function of the parameters of the system.

For Case (I), Figure 5.3.3 shows the positions of the upper elliptic and hyperbolic periodic orbits of period 2π on the Poincaré section as functions of ϕ. We notice that the action J is changing weakly as ϕ is varied. In contrast, its angle θ is very sensitive to this parameter.

5.3.2 Residue curve

We follow the residue for each of the elliptic and hyperbolic periodic orbits mentioned above as the parameter ϕ varies for Case (I). Figure 5.3.4 shows the residue curves of these orbits.

In Fig. 5.3.4, we monitor the upper elliptic periodic orbit (period 2π) of Fig. 5.3.1 from $\phi = 0$. This periodic orbit remains elliptic ($R(\phi) \in]0, 1[$) until $\phi_c \approx 0.49$ where a bifurcation occurs. At this critical point, the orbit turns parabolic. Increasing ϕ further, it turns and remains hyperbolic ($R(\phi) > 1$) until $2\pi/3 - \phi_c$ where another bifurcation appears, making the orbit elliptic again. This bifurcation process is of the period doubling kind at ϕ_c and a period halving at $2\pi/3 - \phi_c$ (by symmetry).

The bifurcation diagram for Case (I) is shown in Fig. 5.3.5. The computation of $\log|\lambda_\pm(\phi)|$ (where $\lambda_\pm(\phi)$ are the two eigenvalues of the monodromy matrix $\mathcal{J}_\phi^{T(\phi)}$ associated with the upper elliptic periodic orbit) gives $\log|\lambda_\pm(\phi)| = 0$ before the bifurcation and $\log|\lambda_\pm(\phi)| \propto \pm\sqrt{\phi - \phi_c}$ right after the bifurcation.

Figure 5.3.6 shows a projection of the upper elliptic periodic orbit undergoing the

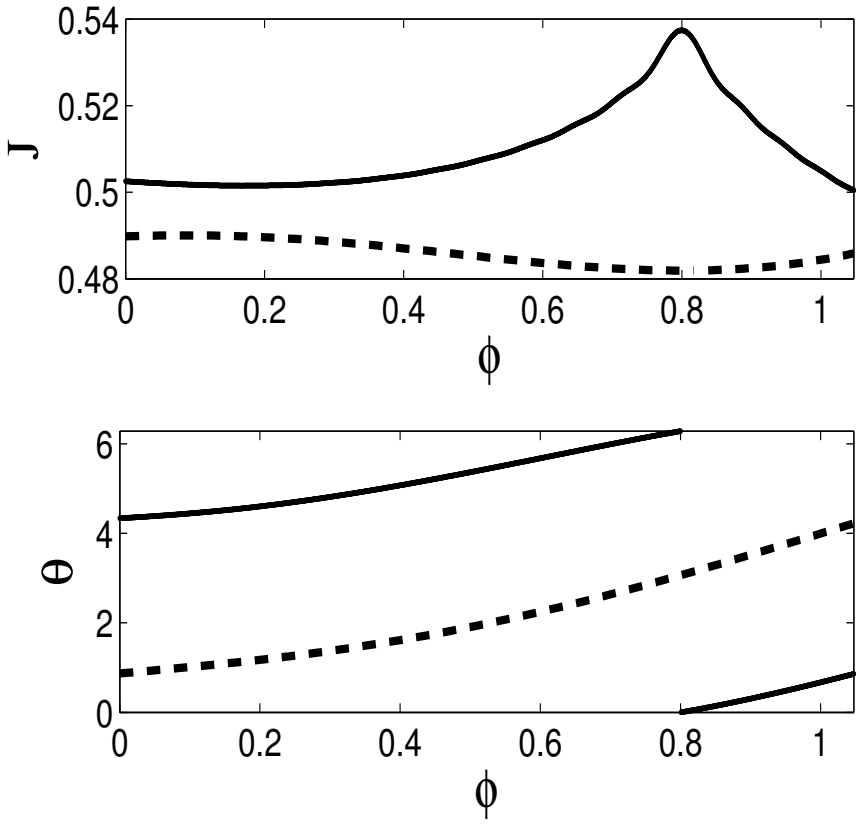

Figure 5.3.3: The positions of the upper elliptic and hyperbolic periodic orbits with period 2π on the Poincaré section as functions of ϕ for Case (I). The solid curves and the dashed ones correspond to the upper elliptic and hyperbolic periodic orbits of Fig. 5.3.1 respectively.

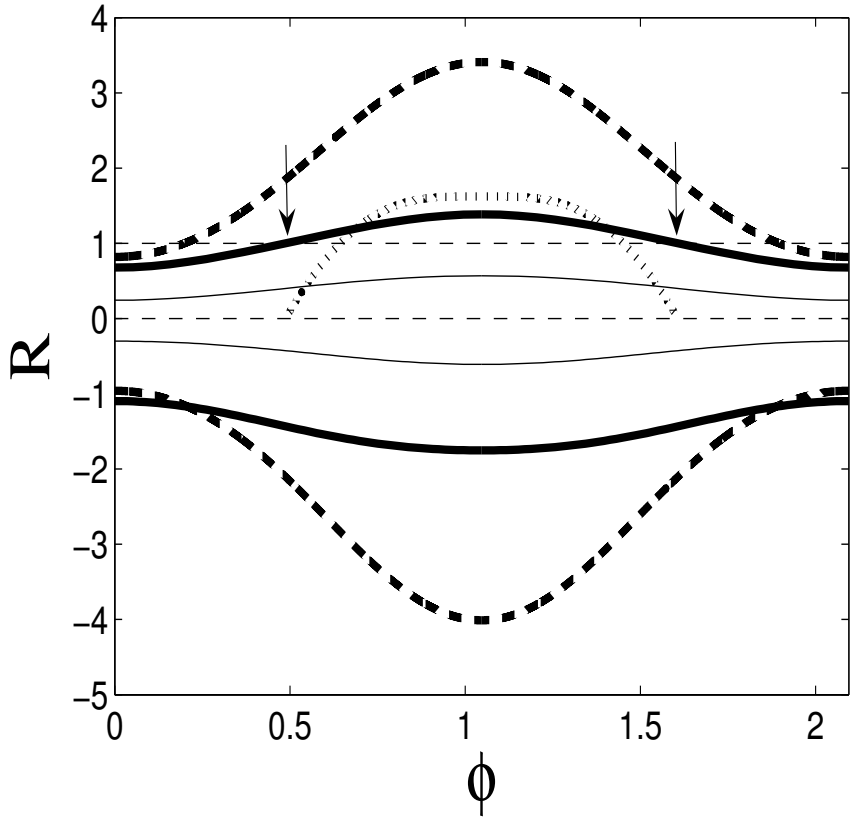

Figure 5.3.4: Residue curves for the four periodic orbits with period 2π (solid curves) and the two periodic orbits with period 4π (dashed bold curves), indicated by crosses and circles on Fig. 5.3.1 for Case (I). The solid bold curves are for the upper set of elliptic/hyperbolic orbits of period 2π. Small arrows indicate where bifurcations happen. The dotted bold curve between two arrows is associated with the residues of the elliptic periodic orbit with period 4π born of the period doubling bifurcation.

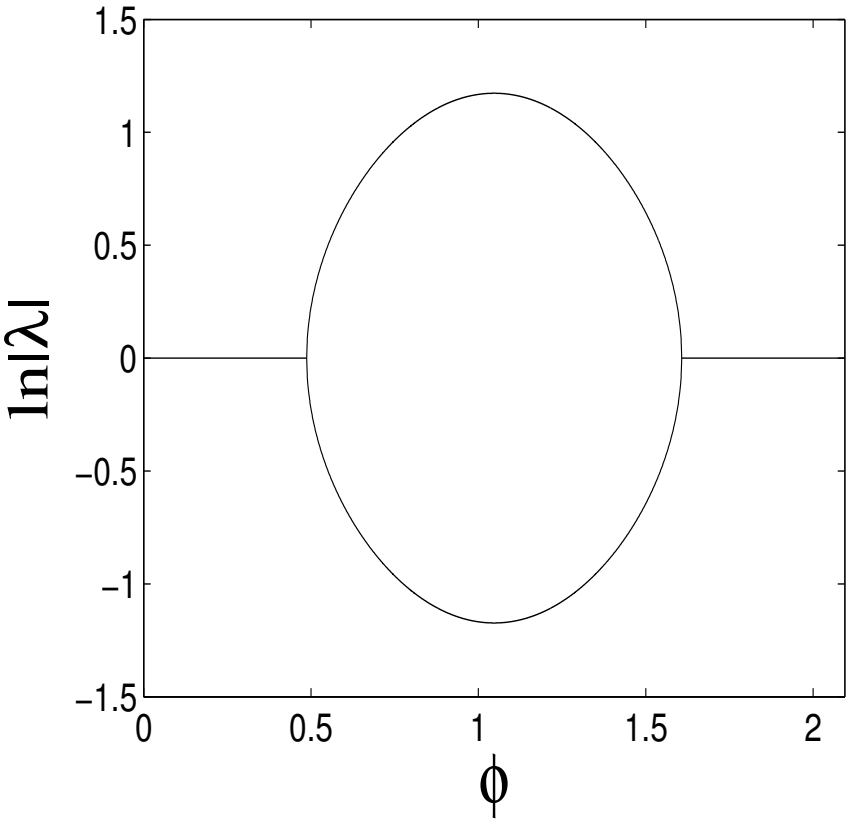

Figure 5.3.5: Bifurcation diagram for Case (I) showing the bifurcations indicated by arrows in Fig. 5.3.4.

period doubling bifurcation in $x-p$ representation where we note the doubling of the number of branches.

Note that while the upper elliptic periodic orbit undergoes a bifurcation as ϕ is varied, the other three periodic orbits with period 2π retain the stability properties they had at $\phi = 0$.

In the parameter range $\phi \in]\phi_c, 2\pi/3 - \phi_c[$, the upper part of phase space does exhibit more chaos as it can be shown on the Poincaré section for $\phi = \pi/3$ (see Fig. 5.3.2).

Since the initial atomic beam is taken in the region with principal quantum number $n = 51$ which corresponds to action $J_i \approx 0.495$, the ionization rate is expected to be higher in the regime where there are no big islands in the chaotic sea, i.e. for $\phi \in]\phi_c, 2\pi/3 - \phi_c[$. On a finer scale, one has to take into account the smaller regular structures that are present in the chaotic sea, like for instance the period-2 island on the Poincaré section (period 4π). A similar period doubling and halving occur at $\phi_{c,1} \approx 0.199$ and $2\pi/3 - \phi_{c,1} \approx 1.895$ respectively, as can be seen on Fig. 5.3.4 (upper bold dashed curve). We notice that the residue curve for the period 4π orbit is higher than the upper solid curve (for the period 2π orbit) and the phase region between period doubling ($\phi_{c,1}$) and period halving ($2\pi/3 - \phi_{c,1}$) is much wider than the one based on the period 2π. This observation indicates that for longer pulse duration for which longer periodic orbits have to be taken into account, the period 4π orbit obtained by a repetition of the period 2π orbit is more important (as a limiting factor) for ionization than the orbit with primary period 4π. As a by-product, the bifurcation at $\phi_{c,1}$ does not affect significantly the leading ionization behavior based on period 2π. Another important periodic orbit with period 4π is the one born of the period doubling bifurcation of the upper periodic orbit at ϕ_c. This orbit is close to the newly hyperbolic periodic orbit and is at first elliptic, as seen on Fig. 5.3.4. It is expected that the associated elliptic islands slow down ionization. This orbit

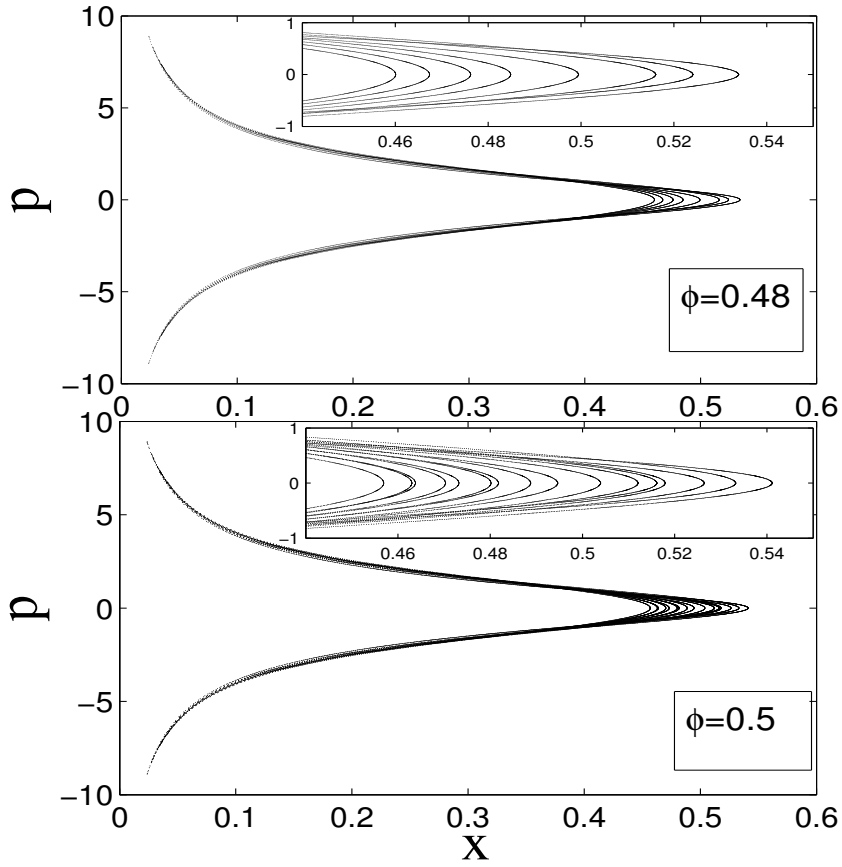

Figure 5.3.6: Upper elliptic periodic orbit (period 2π) of Case (I) undergoing the periodic doubling bifurcation in $x - p$ representation. The insets shows the doubled number of branches indicating periodic doubling bifurcation.

experiences a period doubling bifurcation at $\phi_{c,2} \approx 0.643$ and halving bifurcation at $2\pi/3 - \phi_{c,2} \approx 1.451$. In summary, the shortest periodic orbits (period 2π) always play the most dominant role on ionizations rates, although with larger pulse durations longer periodic orbits might be taken into account for a more detailed analysis.

For values of ϕ around $\pi/3$, a plateau is expected in the ionization probability versus ϕ. The reason is that a strongly hyperbolic orbit only influences the ionization time and not the value of the ionization probability. Of course, this is true provided that the duration of the maximum pulse envelope is large enough. In the experiment, this is approximately 15 times the period of the shortest periodic orbits considered. Roughly speaking, this means that in the chaotic region all the orbits ionize (i.e., escape to a value of the action $J_{\text{ion}} \gtrsim 1.26$) regardless of the hyperbolicity degree. In Ref. [66], experimental results as well as one-dimensional quantum calculations show this plateau. From quantum calculations, $\phi_c \approx 0.5$ was obtained in Ref. [66] which is in very good agreement with the parameter value $\phi_c \approx 0.49$ at which the bifurcation of the upper elliptic periodic orbit (period 2π) occurs. If the duration of the experiment or simulations is longer (two or three times longer), then higher-order regular structures (like the regular island of period 4π in the Poincaré section and the elliptic periodic orbit with period 4π born of bifurcations) will play a role and we expect a similar, but smaller, plateau for $\phi \in]\phi_{c,2}, 2\pi/3 - \phi_{c,2}[$.

The periodic orbit analysis above elucidates whether or not there is a significant ionization probability for specific parameter values, and also where plateaus are expected to occur. This qualitative agreement highlights the important role played by these orbits. Furthermore, we can obtain quantitative agreement concerning the shape of the ionization curve versus phase lag ϕ by using the residue curves. Here we devise an empirical formula for relative ionization probability in the following way : First, the values of ϕ giving the highest ionization would be the ones associated with the highest variations of the residues (in absolute value) with respect to the minimum

ionization. Second, if the periodic orbit is too far (in action) from the considered action J_i then it will not influence the dynamics so there should be a penalizing term depending on its position with respect to the chosen rescaled action. The relative ionization probability formula reads :

$$P_{\text{ion}}(\phi) = A + B \sum_{m=1}^{M} \frac{\exp |R_m(\phi) - R_m(\phi_0)|}{\exp |\overline{J_m(\phi)} - J_i|}, \tag{5.3.1}$$

where the sum is taken over the M different periodic orbits considered and $\overline{J_m(\phi)} = \int_0^{2\pi} J(\theta) d\theta / 2\pi$ is the action of the periodic orbit m. The parameters A and B in Eqn. (5.3.1) are merely a translation and a dilatation of the curve in order to match the mean value and the amplitude of variations of P_{ion} obtained in Ref. [66]. This formula takes into account the value of the residues at ϕ_0, where the minimum ionization takes place for each case. The aim is to set up a baseline for each of the periodic orbits (which is taken here at the value of the parameter where the ionization is minimal). Specifically for Case (I) $\phi_0 = 0$ [66]. In general, Eqn. (5.3.1) can exhibit values which are greater than 1, which are not relevant. In order to remedy to this problem, we truncate P_{ion} at the value where a bifurcation occurs in accordance with the previous discussion on the relevance of the degree of hyperbolicity. Therefore in the range where $R_n(\phi)$ is larger than one, P_{ion} is constant (taken as the value of the residue at ϕ_c where the bifurcation occurs).

Figure 5.3.7 depicts P_{ion} given by Eqn. (5.3.1) versus parameter ϕ as well as the data taken from Ref. [66] for Case (I). Only the shortest periodic orbits with period 2π are considered as relevant. We notice that the empirical formula reproduces accurately the results obtained from quantum calculations. If we take into account the period 4π orbits for longer pulse duration, then a second plateau appears for $\phi \in]\phi_{c,2}, 2\pi/3 - \phi_{c,2}[$ together with an increase at $\phi_{c,1}$ and a decrease at $2\pi/3 - \phi_{c,1}$.

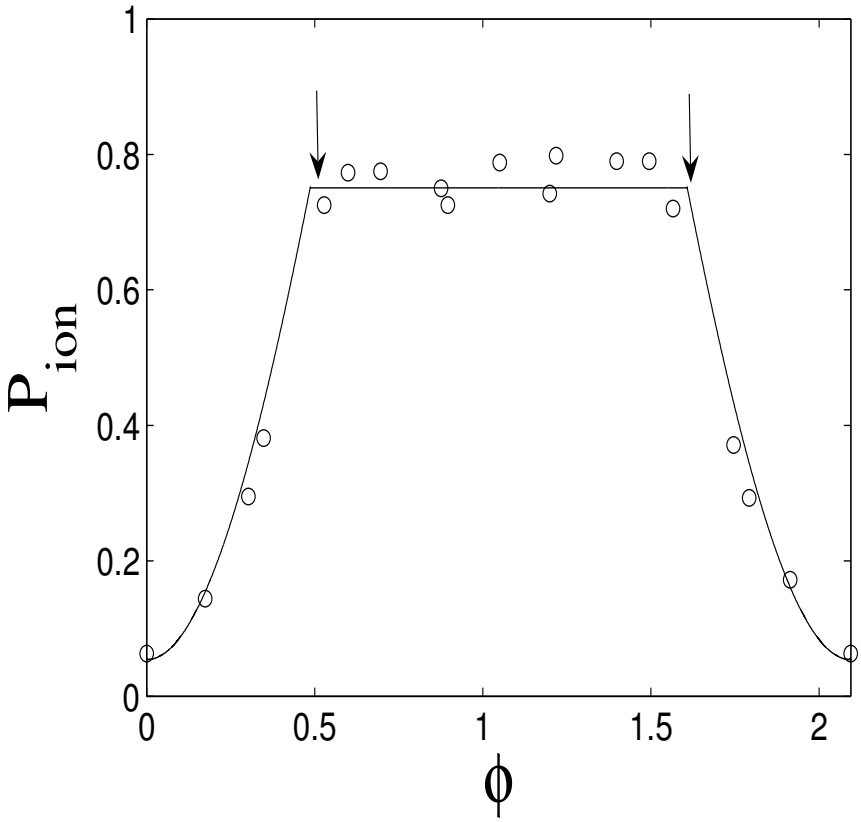

Figure 5.3.7: Normalized ionization probability *vs* ϕ based on Eqn. (5.3.1) for Case (I) with $A = -2.52$ and $B = 0.65$. Circles represent the data obtained by one-dimensional quantum calculations, taken from Ref. [66]. Only periodic orbits with period 2π are considered.

Table 1: Ionization thresholds obtained for $F_h = 6\ \mathrm{Vcm}^{-1}$, experimentally in Ref. [106] and by the residue method (see Fig. 5.3.4). The 1f case corresponds to $F_h = 0$.

$F_l(\ \mathrm{Vcm}^{-1})$	$\phi = 0$	$\phi = \pi/3$	1f
[106]	107	85	96
residue	109.6	81.4	94.8

5.3.3 Bifurcation surface

The residue method is also carried out to predict the behavior of the system as all three parameters (the two amplitudes F_h and F_l and the phase lag ϕ) are varied. In Fig. 5.3.8, we represent the set of parameters where the upper elliptic periodic orbit (with period 2π) of Fig. 5.3.1 is in fact parabolic (i.e., the set of parameters where the system undergoes a major bifurcation). The equation of this surface in parameter space is $R(\phi, F_h, F_l) = 1$. The boundaries of the plateaus in parameter ϕ of Fig. 5.3.7 obtained by fixing the two values for F_h and F_l are on this surface. When F_h approaches zero, this surface is less dependent on parameter ϕ. Table 1 reports some values based on our analysis which are in good agreement with experimental results from Ref. [106].

Of course, the surface of Fig. 5.3.8 could also have been obtained from tedious numerical simulations of a large number of classical trajectories for each value of the parameters (ϕ, F_h, F_l). This integration needs to be performed for a sufficiently long time in order to decide if a given trajectory leads to ionization or not. In contrast, only one orbit for a short time (typically the period of the field) is needed for the residue analysis. Furthermore, using residues, this surface can be constructed locally without any need to consider all possible values of the parameters.

Remark : In Table 1, we actually compare the onset of the plateau for one-dimensional hydrogen model to 10% onset ionization thresholds for three-dimensional experimental results. Since all one-dimensional classical simulation curves have roughly

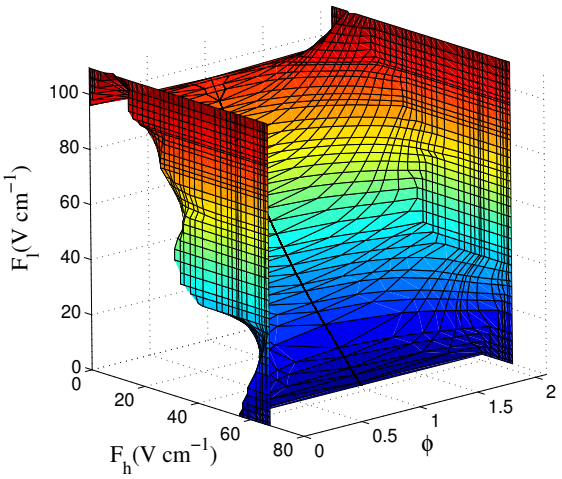

(a)

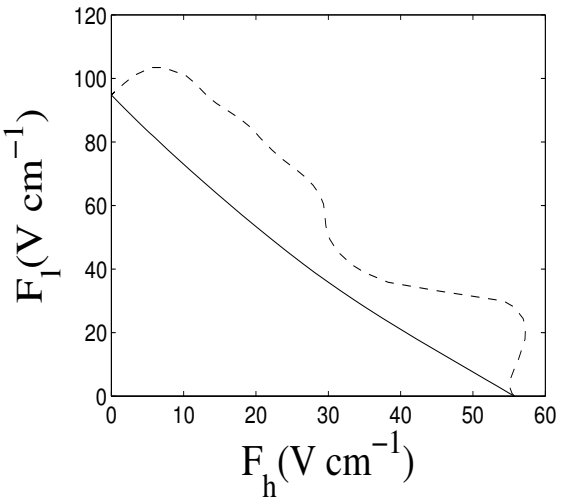

(b)

Figure 5.3.8: (a) Bifurcation surface in parameter space (ϕ, F_h, F_l) for h:l=3:1. (b) The continuous curve is a section of the bifurcation surface (a) at $\phi = \pi/3$, whereas the dashed one is for $\phi = 1.95$.

identical shape between 10% ionization (onset of ionization) and 95% ionization (onset of plateau) and meanwhile there is a fixed shift (15V/cm) between the one-dimensional and three-dimensional onset of ionization [106], this comparison is justified and very heuristic.

5.4 3:2 mode locking

In what follows, we study in detail one set of values for the amplitudes of the fields $F_h = 25$ Vcm^{-1} and $F_l = 33.5$ Vcm^{-1} which correspond to $F_h = 0.5498$ and $F_l = 0.7367$ in dimensionless units. This case will be referred as Case (II).

5.4.1 Poincaré section

Figure 5.4.1 shows a Poincaré section of Hamiltonian (5.2.1) for Case (II) at $\phi = 0$. Similar to Case (I), there are two primary islands in the chaotic sea where two elliptic periodic orbits with period 2π sit at the centers, and the two associated hyperbolic orbits are in the chaotic sea. In addition, there are also two associated hyperbolic periodic orbits with period 4π as indicated by small crosses. One should notice that the (rescaled) principal quantum number considered in Ref. [66] lies in between these two islands (see the continuous horizontal line). We monitor the stability of this set of periodic orbits as we have performed for Case (I).

5.4.2 Residue curve

Figure 5.4.2 shows the four residue curves of period 2π orbits and the two residue curves of period 4π orbits. For short periodic orbits (period 2π), the elliptic periodic orbits remain elliptic and the hyperbolic ones remain hyperbolic for all values of ϕ. No bifurcation occurs except in a small range of phase (see inset of Fig. 5.4.2) where no significant stability change is observed. Consequently, the ionization probability is expected to be approximately independent of ϕ and to be lower than Case (I) since for these values of amplitudes, the chaotic region is smaller. This is consistent with

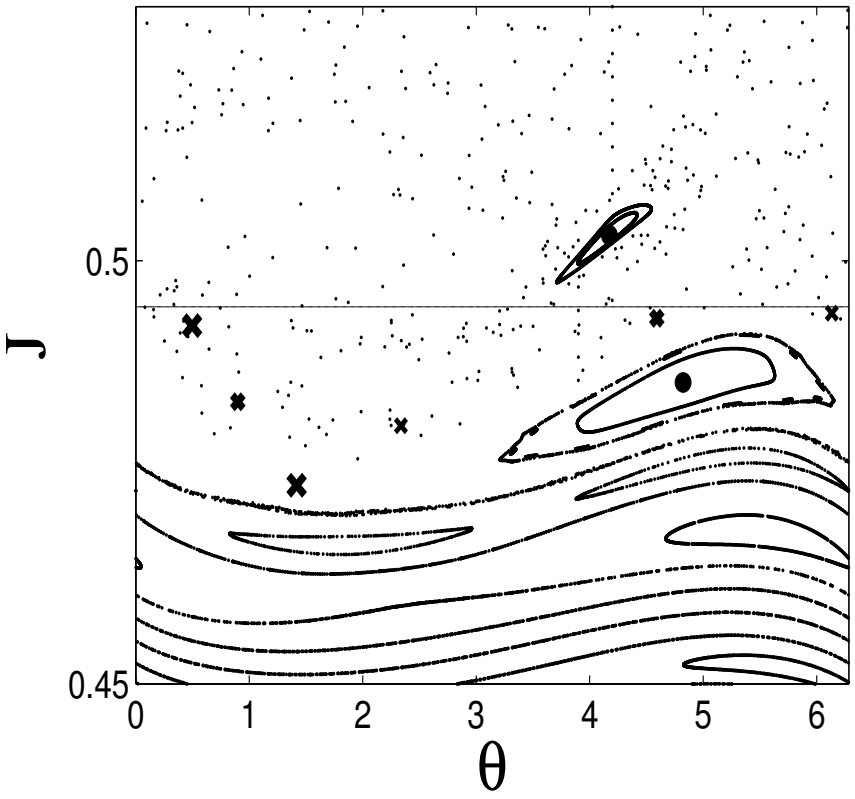

Figure 5.4.1: Poincaré section of Hamiltonian (5.2.1) for Case (II) at $\phi = 0$. Full circles (respectively crosses) indicate the two elliptic (resp. hyperbolic) periodic orbits with period 2π we consider. Small crosses indicate the two hyperbolic periodic orbits with period 4π we consider. The horizontal line corresponds to the principal quantum number $n = 51$.

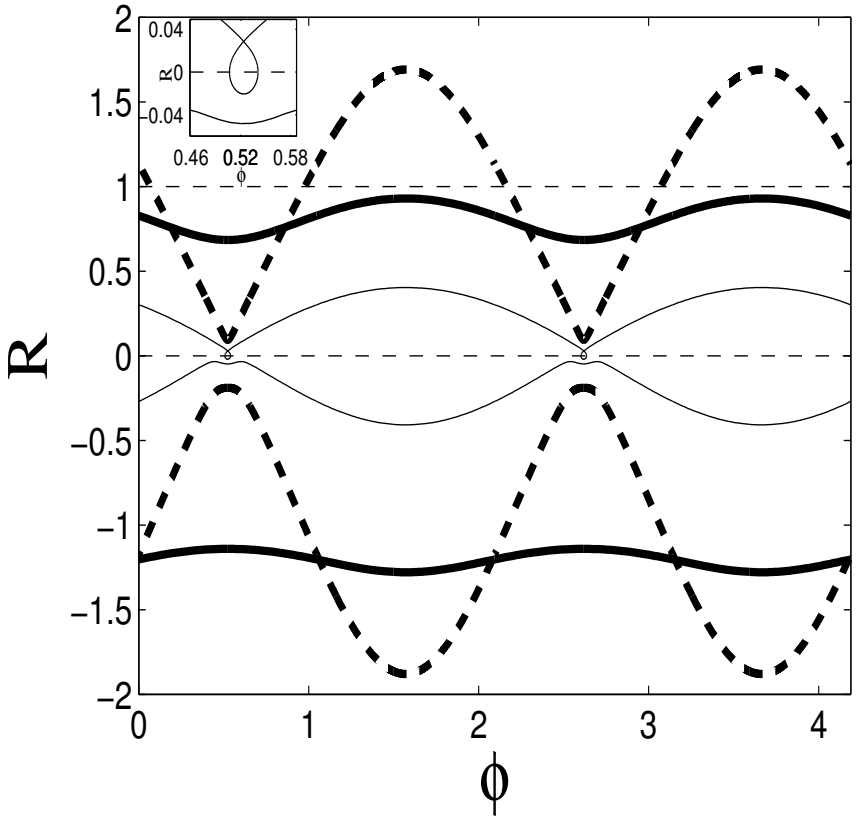

Figure 5.4.2: Residue curves for the four periodic orbits with period 2π indicated by crosses and circles on Fig. 5.4.1 and the two periodic orbits indicated by small crosses with period 4π for Case (II). The bold solid curves are for the upper set of elliptic/hyperbolic orbits with period 2π. The thin solid curves are for the lower set of elliptic/hyperbolic orbits with period 2π. The dashed curves are for the two initially hyperbolic periodic orbits with period 4π. The inset shows irregular behavior of residue at $\phi \simeq \pi/6$. The same behavior also occurs at $\phi \simeq 5\pi/6$ for that residue curve.

the experimental and quantum calculations of Ref. [66]. The experimental results show a nearly flat curve for the ionization probability versus ϕ, whereas the quantum calculations show significant variations for this probability but no sharp increase and decrease as in Case (I).

When the duration of pulse is longer we should take into account the effect of longer periodic orbits whose residues are shown by bold dashed curves in Fig. 5.4.2 with period 4π in this particular case. Apparently the upper period 4π orbit experiences period halving bifurcations at $\phi \approx 0.07$ and $\phi \approx 2.164$; and period doubling bifurcations at $\phi \approx 0.977$ and $\phi \approx 3.072$.

Figure 5.4.3 depicts $P_{\rm ion}$ given by Eqn. (5.3.1) versus the parameter ϕ as well as the data taken from Ref. [66] for Case (II). Only periodic orbits with period 2π are considered. In Eqn. (5.3.1) we again take $\phi_0 = 0$ since the ionization is minimal at $\phi = 0$ for Case (II) [66]. We notice that it captures some essential features of the ionization curve, like the two unequal-sized peaks and the specific shape of both peaks (one more peaked, the other one, more round). This feature results from the asymmetry property of bichromatic microwave amplitude [100]. For this case, the bichromatic microwave field at $\phi = \pi/6 \pm \triangle\phi$ has exactly the same amplitude but opposite direction as at $\phi = \pi/2 \pm \triangle\phi$, where $0 < \triangle\phi < \pi/6$. Replacing "+" in front of the bichromatic field by "-" in Eqn. (5.1.1) leads to a Hamiltonian for the other direction. Because of this symmetry property of bichromatic field, the ionization probability along the other direction can be obtained from Fig. 5.4.3 by a horizontal translation of $\pi/3$. The total ionization rate should be the sum of the rates for both directions, which shows equally high peaks for total ionization rate in ϕ. For longer pulse duration, we should consider longer periodic orbits like those with period 4π. Again we should take the baseline (minimal ionization point) at $\phi = 0$. Since in Fig. 5.4.2 the residue value of elliptic periodic orbit with period 4π (upper dashed curve) at minimal ionization point ($\phi = 0$) is already greater than

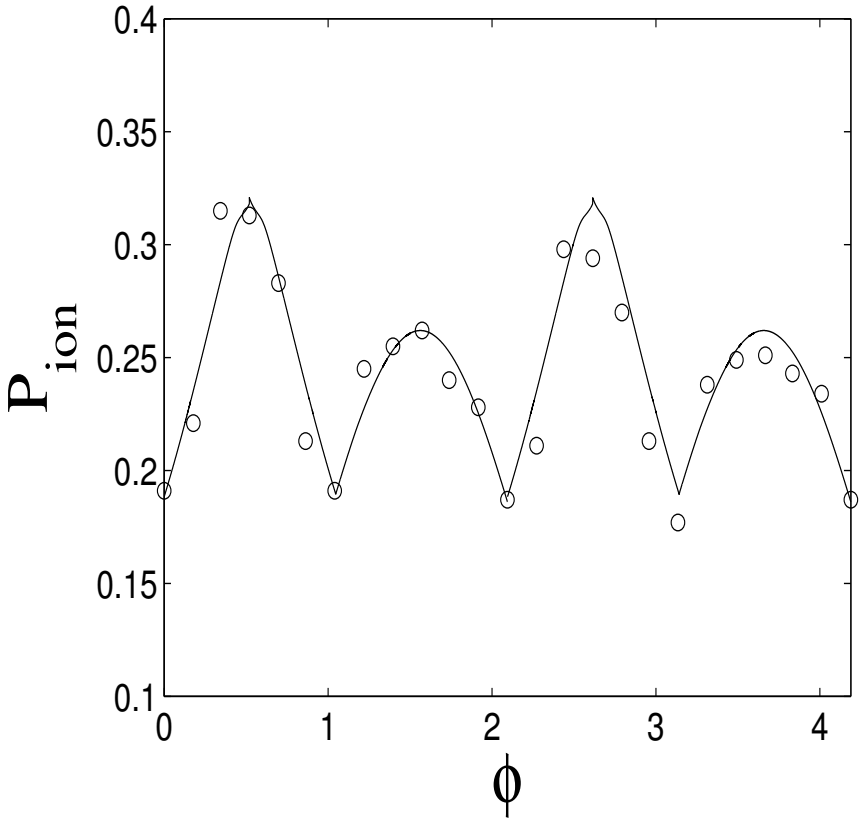

Figure 5.4.3: Normalized ionization probability *vs* ϕ based on Eqn. (5.3.1) for Case (II) with $A = -0.485$ and $B = 0.17$. Circles represent the data obtained by one-dimensional quantum calculations, taken from Ref. [66]. Only periodic orbits with period 2π are considered.

1, the ionization rate should be high and roughly identical on the whole ϕ space. This indicates that when pulse duration gets longer, the ionization rate for any ϕ goes higher and suggests ionization rate for any ϕ will reach a roughly constant upper limit if the time duration is sufficiently long. This property is obviously true because when the system is exposed to external microwave field for a longer time, more electrons will gain sufficient energy to escape. However, as mentioned in Sec. 5.3, the shortest periodic orbits (period 2π) always play the most dominant role on ionizations rates, while the longer periodic orbits might be taken into account heuristically for a finer analysis when the pulse duration gets a lot longer. Finally, our analysis also indicates the asymmetric ionization property does not exist for 3:1 mode locking case, in agreement with Ref. [100].

5.5 Generalization to h:l mode locking

In order to generalize this approach, we also investigate h:l=2:1, denoted Case (III), and 5:1, denoted Case (IV) mode locking.

5.5.1 Residue curves

For Case (III), we take $F_h = 24$ Vcm^{-1}, $F_l = 53.4$ Vcm^{-1} and the high frequency of 12 GHz. Figure 5.5.1 shows Poincaré section at $\phi = 0$. It indicates the relevant periodic orbits to consider in the residue analysis. Figure 5.5.2 shows the residue curves based on the two periodic orbits with period 2π in the chaotic sea of Fig. 5.5.1. No bifurcations take place for these orbits. Figure 5.5.3 depicts relative ionization rate with respect to ϕ based on Eqn. (5.3.1). For this case we take $\phi_0 = 0$ in Eqn. (5.3.1) since the minimal ionization point is at $\phi = 0$ according to the maximum field rule (see next section). Based on our approach, the asymmetric ionization property along a single direction (unequal-sized peaks) does appear for the $2:1$ mode locking, in agreement with Ref. [100].

For Case (IV), we take $F_h = 24$ Vcm^{-1}, $F_l = 53.4$ Vcm^{-1} and the high frequency

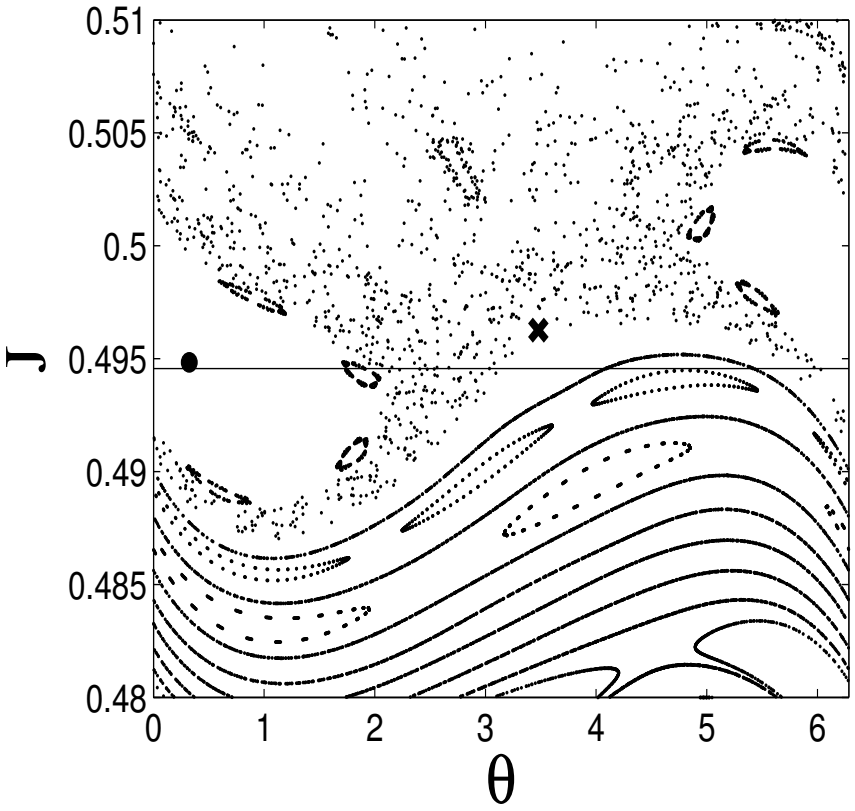

Figure 5.5.1: Poincaré section of Hamiltonian (5.2.1) for Case (III) at $\phi = 0$. Full circle (respectively cross) indicates the elliptic (resp. hyperbolic) periodic orbit with period 2π we consider. The horizontal line corresponds to the principal quantum number $n = 51$.

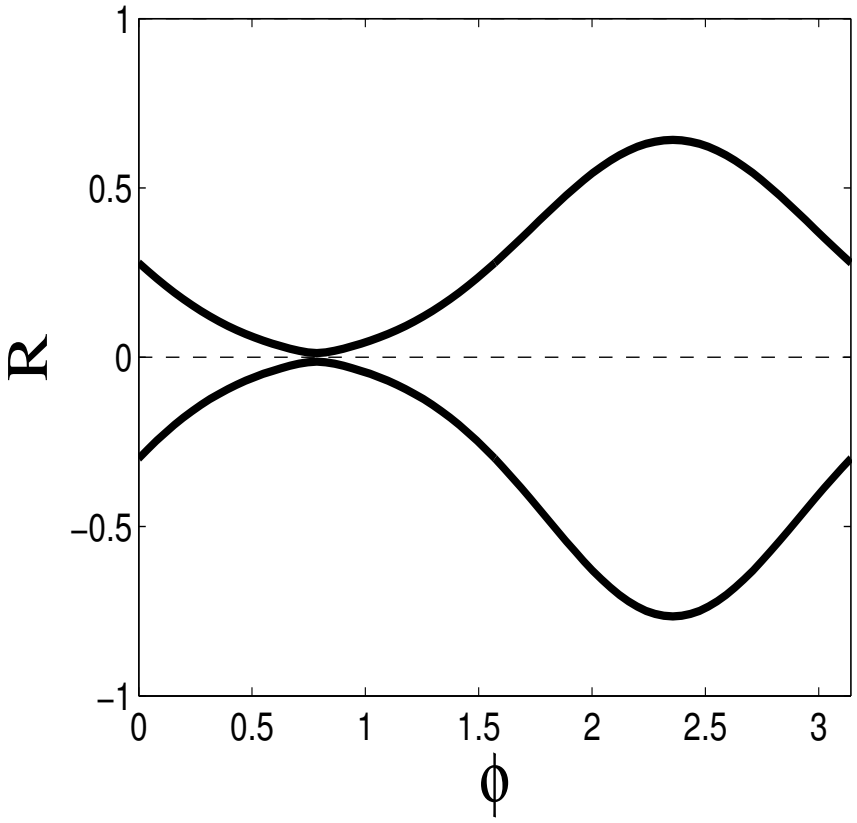

Figure 5.5.2: Residue curves for the two periodic orbits with period 2π indicated by cross and circle on Fig. 5.5.1 for Case (III).

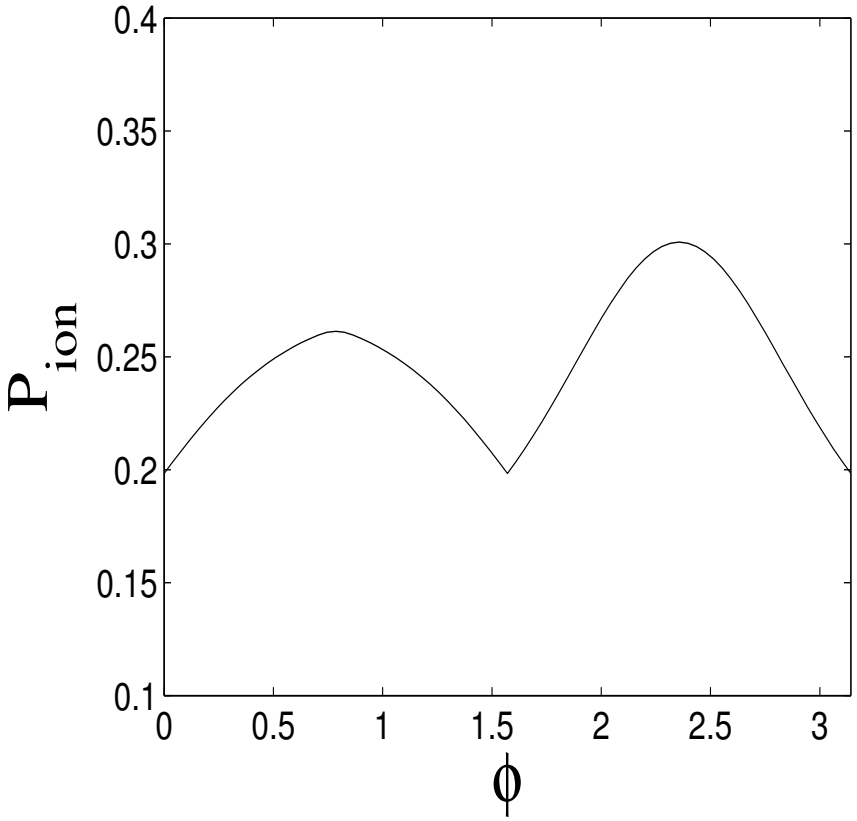

Figure 5.5.3: Relative ionization probability *vs* ϕ at principal quantum number $n = 51$ based on Eqn. (5.3.1) for Case (III) with $A = 0$ and $B = 0.1$. The absolute ionization rate may differ according to the pulse duration.

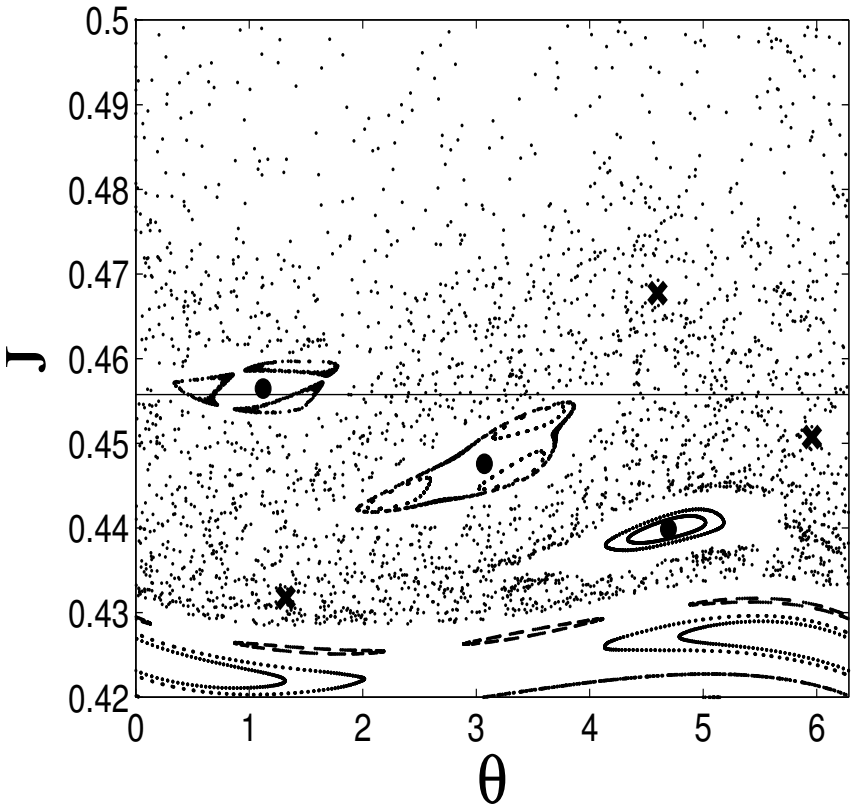

Figure 5.5.4: Poincaré section of Hamiltonian (5.2.1) for Case (IV) at $\phi = 0$. Full circles (respectively crosses) indicate the elliptic (resp. hyperbolic) periodic orbits with period 2π we consider. The horizontal line corresponds to the principal quantum number $n = 47$.

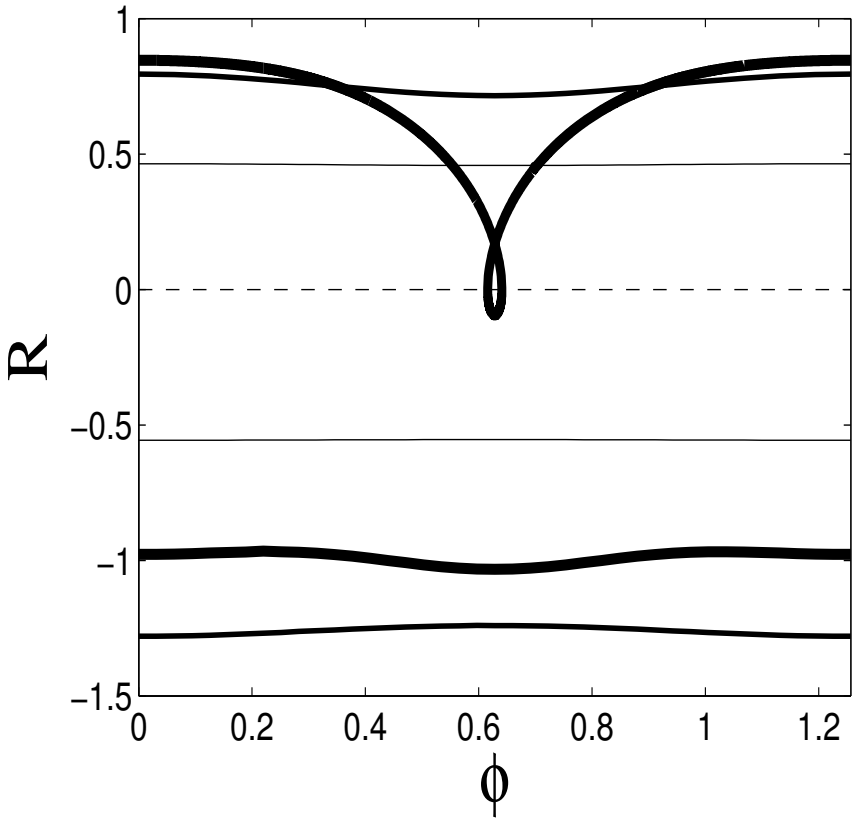

Figure 5.5.5: Residue curves of the six periodic orbits with period 2π indicated by crosses and circles on Fig. 5.5.4 for Case (IV).

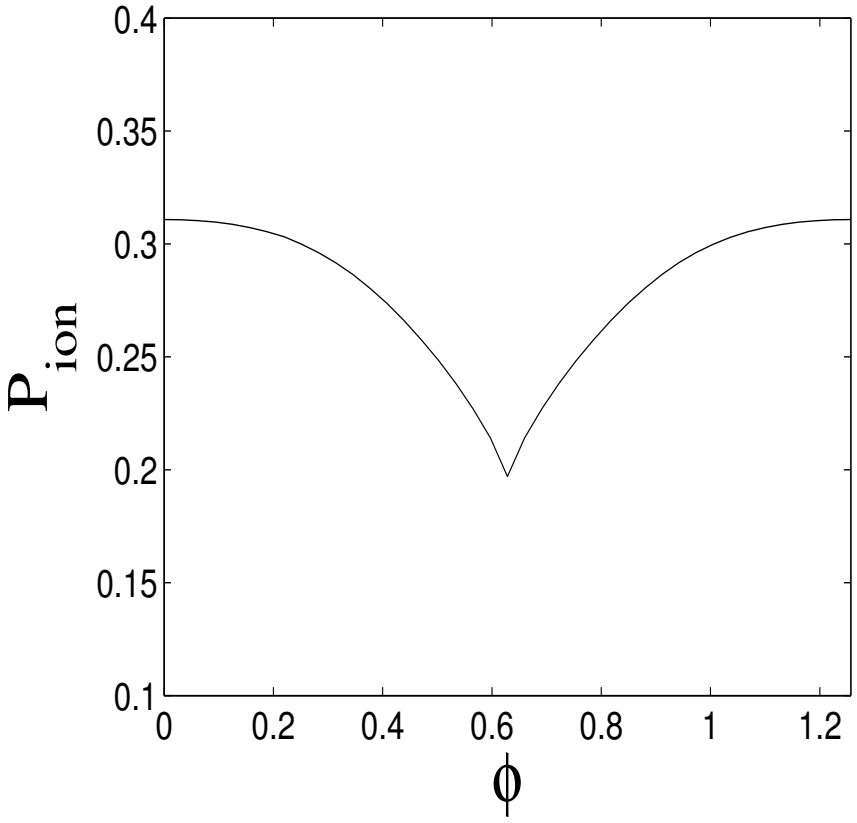

Figure 5.5.6: Relative ionization probability *vs* ϕ at principal quantum number $n = 47$ based on Eqn. (5.3.1) according to Fig. 5.5.5 for Case (IV) with $A = -0.2$ and $B = 0.1$. The absolute ionization rate may differ according to the pulse duration.

is 30 GHz. Figure 5.5.4 shows a Poincaré section at $\phi = 0$, and Fig. 5.5.5 shows the residue curves based on the six periodic orbits of period 2π in the chaotic sea of Fig. 5.5.4. We notice that the residue based on the upper elliptic periodic orbit has similar behavior to the one of the lower elliptic periodic orbit for Case (II) as shown in the inset of Fig. 5.4.2. The two residue curves (two thin lines) in Fig. 5.5.5 from the two lower periodic orbits in Fig. 5.5.4 are almost constant and therefore have little influence on ionization probability. Figure 5.5.6 depicts relative ionization rate with respect to ϕ based on Eqn. (5.3.1) according to Fig. 5.5.5 (The lowest two periodic orbits are not considered since their corresponding residue curves are almost constant). For this case we take $\phi_0 = \pi/5$ in Eqn. (5.3.1) since the minimal ionization point is at $\phi = \pi/5$ according to the maximum field rule. This asymmetry in the ionization property does not exist for the 5:1 mode locking.

Generally speaking, with Hamiltonian (5.2.1) plus empirical formula (5.3.1), we can obtain the directional ionization for Case (II) and Case (III) for the model that the electrons ionize along both directions. For Case (I) and Case (IV), the directional ionization does not appear due to the symmetry property [100] of the bichromatic pulse.

5.5.2 Comparison with the maximum field rule

A traditional way of explaining ionization probability behavior is the maximum field rule (peak field amplitude rule) formulated in Ref. [99, 106]. The relative ionization probability *vs* ϕ based on the maximum field rule can be written in the form

$$P_{\text{ion}}(\phi) = C + D\max_{t\in[0,2\pi]}|F_h \sin(ht) + F_l \sin(lt + \phi)|. \tag{5.5.1}$$

The parameters C and D in Eqn. (5.5.1) are merely a translation and a dilatation of the curve in order to make the curves from the maximum field rule comparable to those based on bifurcation analysis. Figure 5.5.7 shows relative ionization probability based on Eqn. (5.5.1) for four different cases. Compared with our periodic orbit bifurcation

analysis in finite pulse duration, apparently the maximum field rule does not result in quantitative agreement with the quantum simulation results of Ref. [66] for either Case (I) or (II). In Case (III), the maximum field rule does not produce the two unequal-sized peaks as our bifurcation analysis does. Only in Case (IV) do the results based on the maximum field rule agree with our bifurcation analysis because there is neither bifurcation nor asymmetric ionization property for this case. Insets of Fig. 5.5.7 show one cycle ($t \in [0, 2\pi]$) bichromatic field $\epsilon(t) = F_h \sin(ht) + F_l \sin(lt + \phi)$ with typical parameters as used for our previous analyses in dimensionless units for different ϕ values. Arrows indicate the ϕ values for which the bichromatic fields are drawn. Generally for Case (I) the positive component of the bichromatic field is the same as the negative component for any ϕ in each full cycle (directional symmetry), whereas this directional symmetry does not appear for Case (III) [100] except for some specific ϕ values like $\phi = 0, \frac{\pi}{2}, \pi$. Similarly, for Case (II) this directional symmetry generally does not appear except for some specific ϕ values like $\phi = 0, \frac{\pi}{3}, \frac{2\pi}{3}, \pi, \frac{4\pi}{3}$, whereas for Case (IV), this directional symmetry does appear for any ϕ values. Although the maximum field rule can be used to determine qualitative features like the minimal ionization point with respect to ϕ, the quantitative agreement is not as satisfactory as the one given by a method which relies on analyzing the chaotic dynamics like the one used in this article based on periodic orbit bifurcation analysis to depict relative ionization.

5.6 Conclusion

In this chapter we carried out investigations on bichromatic microwave-driven multiphoton ionization through classical tools and identified useful "knobs" as control parameters such as amplitudes and phase of the external bichromatic microwave field. The role that the periodic orbits play in this system was illustrated through linear stability analysis. Our analyses based on classical nonlinear dynamics are in quantitative

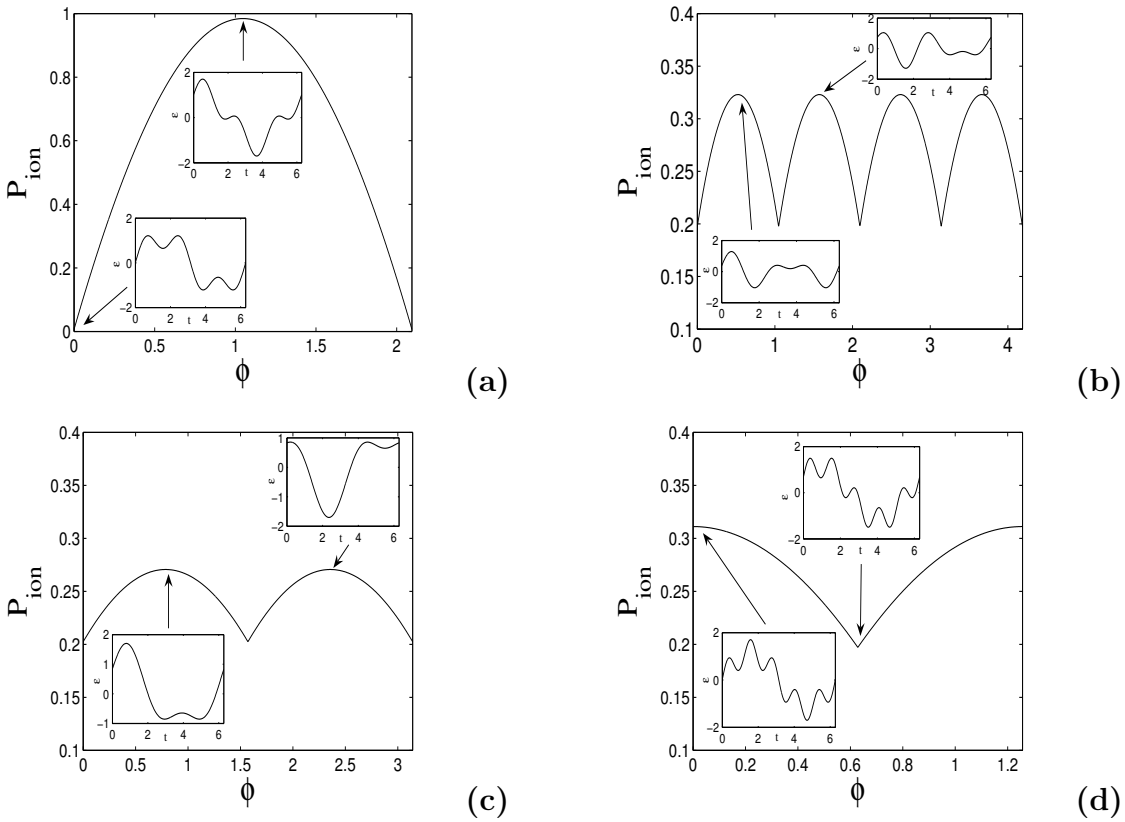

Figure 5.5.7: Relative ionization probability based on the maximum field rule, on Eqn. (5.5.1), for (a) Case (I) with $C = -2.42$ and $D = 2$. Insets show the bichromatic field for $\phi = 0$ (bottom panel) and $\phi = \pi/3$ (top panel).(b) Case (II) with $C = -2.25$ and $D = 2$. Insets show the bichromatic field for $\phi = \pi/6$ (bottom panel) and $\phi = \pi/2$ (top panel). (c) Case (III) with $C = -0.24$ and $D = 0.3$. Insets show the bichromatic field for $\phi = \pi/4$ (bottom panel) and $\phi = 3\pi/4$ (top panel). and (d) Case (IV) with $C = -0.625$ and $D = 0.55$. Insets show the bichromatic field for $\phi = 0$ (bottom panel) and $\phi = \pi/5$ (top panel). Arrows indicate the ϕ values for which the bichromatic fields are drawn.

agreement with quantum simulations and qualitative agreement with experimental results. The high efficiency of numerical computation in our analysis is an additional advantage.

CHAPTER VI

PERIODIC ORBIT ANALYSIS OF THE DISSOCIATION OF DRIVEN DIATOMIC MORSE MOLECULES

6.1 Introduction

The dissociation behavior of molecules driven by bichromatic fields with commensurate frequencies has emerged as a rich research subject, especially for the control of molecular processes [45, 46, 102, 103]. The interplay of the two radiation fields opens up many new dissociation pathways. It is well known that the relative phase between the two fields can affect these pathways drastically, which makes the relative phase a useful means to control the outcome of the reaction [6, 21]. The relative phase is a very convenient control parameter since it does not require additional energy input from the fields (as opposed to their amplitudes). However, the mechanisms by which the relative phase controls the dissociation behavior are less well-known.

The two-color laser-driven dissociation of molecules is of great interest to researchers, mainly because these seemingly simple systems display complex dynamics and behavior that single-component laser field cannot exhibit [6, 21, 29, 43, 46, 52, 74, 103, 108]. In the past three decades, the literature on theoretical studies of laser-driven dissociation of molecules has been extensive [5, 6, 21, 27–29, 31, 34, 43, 44, 49, 50, 52, 53, 74, 82, 86, 108, 109, 111]. In Ref. [29] the dissociation probability of a diatomic Morse molecule exposed to a two-color laser field has been investigated for various parameters using direct simulations of classical mechanical equations.

In this chapter, we report how dissociation probability as obtained in Ref. [29] by direct numerical simulations can be predicted qualitatively using a linear stability analysis of a small set of periodic orbits. Our main result is that for most values of the

parameters the features of the dissociation probability can be reproduced using two short periodic orbits (with the period equal to the one of the field), and in particular by the identification of the main bifurcations which will have a drastic effect on the dissociation probability. In this way, our approach allows the qualitative prediction of the dynamics with significant time savings as parameters are varied. Theoretically, the necessary time is of the same order as the period of the considered orbit which is also the period of the laser field. Our findings echo similarly the ones obtained in the microwave ionization of Rydberg atoms in a strong bichromatic field, for which a qualitative agreement has been reached with experimental data (and a quantitative agreement with quantum simulations) based on a specific bifurcation of just a few periodic orbits [56].

The Hamiltonian of a diatomic Morse [83] molecule exposed to a strong bichromatic field in atomic units reads [29]

$$\begin{aligned} H(r,p,\tau) = \frac{p^2}{2m} + D(1-\mathrm{e}^{-\alpha(r-r_e)})^2 \\ +(r-r_e)[A_1\sin(\Omega_1\tau) + A_2\sin(\Omega_2\tau+\phi)], \end{aligned} \tag{6.1.1}$$

where the parameters are m (the reduced mass), D (the dissociation energy) and r_e (the equilibrium distance). Here we take the envelop of the pulses constant since the pulse duration effect has very minor impact on this system, as suggested in Ref. [29]. Dimensionless variables are $\tilde{r} = \alpha(r-r_e)$, $\tilde{p} = p/\sqrt{2Dm}$, $t = \alpha\sqrt{2D/m}\tau$, $F_i = A_i/(2D\alpha)$, $\omega_i = \Omega_i/\sqrt{2D\alpha^2/m}$ as given by Ref. [49] . The Hamiltonian (6.1.1) expressed in these new coordinates is

$$\begin{aligned} \tilde{H}(\tilde{r},\tilde{p},t) &= \frac{\tilde{p}^2}{2} + \frac{1}{2}\left(1-\mathrm{e}^{-\tilde{r}}\right)^2 \\ &\quad +\tilde{r}\left(F_1\sin\omega_1 t + F_2\sin(\omega_2 t+\phi)\right), \end{aligned} \tag{6.1.2}$$

where $\tilde{r}$ and $\tilde{p}$ are canonically conjugate.

In what follows, we consider hydrogen fluoride (HF) molecule for which $m = 1732$, $D = 0.2101$, $r_e = 1.75$ and $\alpha = 1.22$ in atomic units. In order to compare our

results with direct numerical simulations [29] later, we want to use the same field parameters as Ref. [29] used. Therefore, we consider a field with two commensurate frequencies such that $\omega_1 = \omega_2/3 = 0.28$, which corresponds to the fast laser frequency $\frac{\Omega_2}{2\pi c} = 3476\text{cm}^{-1}$ [29]. A normalized dimensionless amplitude $F_i = 1$ equals a laser intensity of 320TW/cm^2 [29]. We notice that Hamiltonian (6.1.2) is time-periodic with period $2\pi/\omega_1$.

In Sec. 6.2, we briefly recall the method which monitors the position and the residue of periodic orbits. In Sec. 6.3, we analyze the dynamics using short a selection of periodic orbits, as parameters are varied. We relate a linear stability measure (the residue of a given periodic orbit) to the dissociation probability. Good agreement is found for most of the values of the parameters. However, a discrepancy for small phases is observed and discussed at the end.

6.2 Residue method

The general idea of the method is to follow a set of periodic orbits as parameters are varied in order to determine qualitative properties of the dynamics. As it was shown in the bichromatic microwave driven multiphton ionization problem, short periodic orbits play the role of organizing centers of the dynamics. Higher order periodic orbits give more refined details of the dynamics, especially the ones on longer time scales. In principle, for atomic and molecular systems where short pulses are considered, only short periodic orbits should influence the dynamics. We determine the location of a periodic orbit (given by its number of intersections with the Poincaré surface of section) using a modified Newton-Raphson multi-shooting algorithm [30], as we did for the bichromatic microwave driven multiphton ionization problem. We also take the same residue analysis as we described in Sec. 5.2.

For a given periodic orbit, we follow its location in phase space and residue as parameters are varied. In this case, there are three parameters, two amplitudes F_1

and F_2, and a phase lag ϕ. We compute $R(F_1, F_2, \phi)$ and identify the points in parameter space where bifurcations occur. The bifurcations we are interested in are when a periodic orbit is likely to change its linear stability, which occurs in particular for $R(F_1, F_2, \phi) = 0$ or $R(F_1, F_2, \phi) = 1$. In general such bifurcations (based on a linear stability analysis) will also play an important role in the nearby phase space region (by continuity in phase space).

6.3 Dissociation probability

6.3.1 Identification of fundamental periodic orbits

In Fig. 6.3.1, we represent a Poincaré section (stroboscopic plot of phase space with period $2\pi/\omega_1$) of Hamiltonian (6.1.2) for amplitudes $F_1 = 0.18$, $F_2 = 0.02$ and phase $\phi = 0$. We notice that an elliptic island is present at the entrance of the dissociation channel. At the center of this island sits an elliptic periodic orbit with one intersection with the Poincaré surface of section (i.e. with period $2\pi/\omega_1$). Standard Hamiltonian dynamics show that the trajectories that are likely to dissociate can get trapped around the resonant island for a while before finding a way to escape. Therefore, this particular periodic orbit plays a crucial role on the dissociation probability. This periodic orbit, named $\mathcal{O}_e$, is the main focus of this problem: We investigate its role on dissociation as parameter are varied. Due to a symmetry ($\phi \mapsto \pi - \phi$) the fundamental domain of variations of ϕ is $[0, \pi[$. We also restrict the amplitudes to $(F_1, F_2) \in [0, 0.22] \times [0, 0.06]$.

We anticipate two mechanisms which may influence dissociation: one is the location of this orbit, and the other is the change of its stability. In Fig. 6.3.2, we represented the position of $\mathcal{O}_e$ or more precisely its action and angle as defined by [49]

$$\begin{aligned} I &= 2\left(1 - \sqrt{1-E}\right), \\ \tan\theta &= -\frac{\tilde{p}\sqrt{1-E}}{1 - \mathrm{e}^{-\tilde{r}} - E}, \end{aligned} \tag{6.3.1}$$

where $E(\tilde{r}, \tilde{p}) = \tilde{p}^2 + (1 - \mathrm{e}^{-\tilde{r}})^2$, for a typical set of parameters $F_1 = 0.18$ and $F_2 = 0.02$,

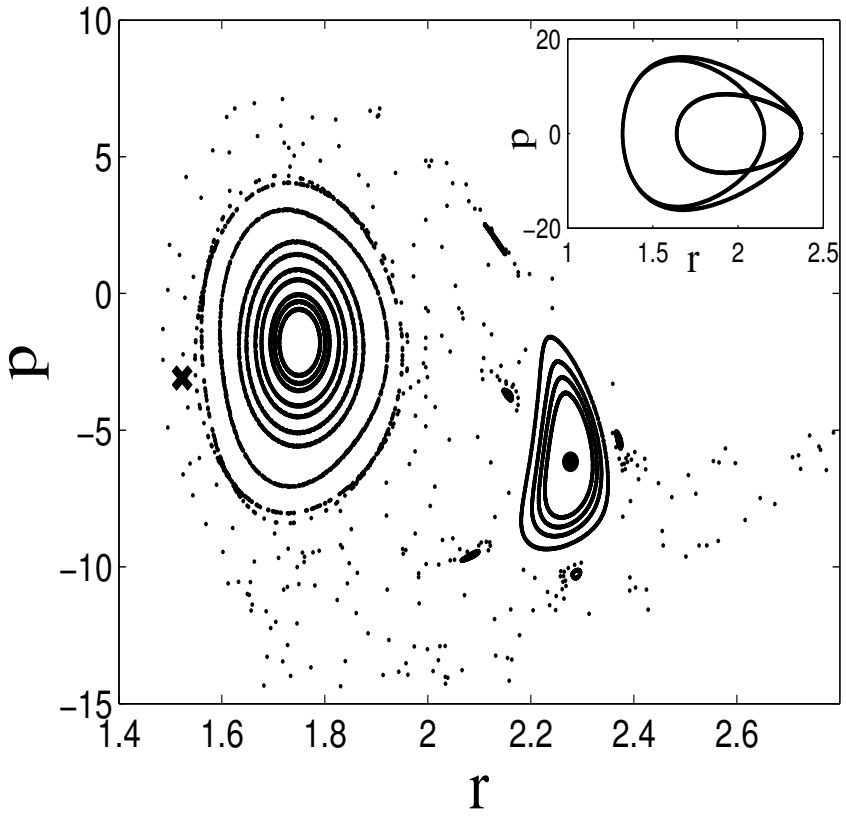

Figure 6.3.1: Stroboscopic plot of phase space of Hamiltonian (6.1.1) for $F_1 = 0.18$, $F_2 = 0.02$ and $\phi = 0$. The dot and the cross indicate the elliptic periodic orbit $\mathcal{O}_e$ and its associated hyperbolic one, respectively. The inset depicts a projection of $\mathcal{O}_e$ in the (r, p) plane.

while ϕ is varied. As can be seen in Fig. 6.3.2, the action of $\mathcal{O}_e$ does not vary a lot with the change of relative phase, whereas the angle does vary more rapidly and irregularly. Considering that in this case the increase of the relative phase in $[0, \pi[$ leads to a monotonic increase of dissociation probability [29], we have come to the conclusion that the position of the specific periodic orbit does not appear to have a significant relationship to dissociation probability.

The second mechanism based on a bifurcation has a more drastic influence on dissociation. In order to monitor this bifurcation properly, we also need to follow the associated hyperbolic orbit. We have to make sure that the hyperbolic orbit stays hyperbolic while the elliptic one turns hyperbolic (in order to discard a stability exchange which would not affect significantly the dissociation probability). A typical residue plot (the residue as a function of ϕ) is represented on Fig. 6.3.3 for $F_1 = 0.18$ and $F_2 = 0.02$. At $\phi = 0.75$, the residue crosses one and a bifurcation (which is a period doubling as shown in Fig. 6.3.4) occurs. This increase of hyperbolicity is associated with more chaos and hence more likely to dissociate. This is in agreement with direct simulations as obtained in Ref. [29].

We should point out that the computation of Ref. [29] was done for initial conditions in the ground level ($E = 0.045$), which is lower than the set of periodic orbits we consider ($E = 0.29$) in Fig. 6.3.1. This justifies the importance of the chosen periodic orbits for dissociating trajectories. For other values of parameters we consider, the energy level of the periodic orbit $\mathcal{O}_e$ is always well above $E = 0.045$.

6.3.2 Residue contour plots in parameter space

For fixed values of ϕ, we vary the amplitudes F_1 and F_2 and track the residue value of the elliptic periodic orbit $\mathcal{O}_e$. We depict the contour plots of these residues in Fig. 6.3.5 in the (F_1, F_2) plane for $\phi = 0$, $\pi/6$, $\pi/2$ and π. This figure should be compared to Fig. 2 of Ref. [29].

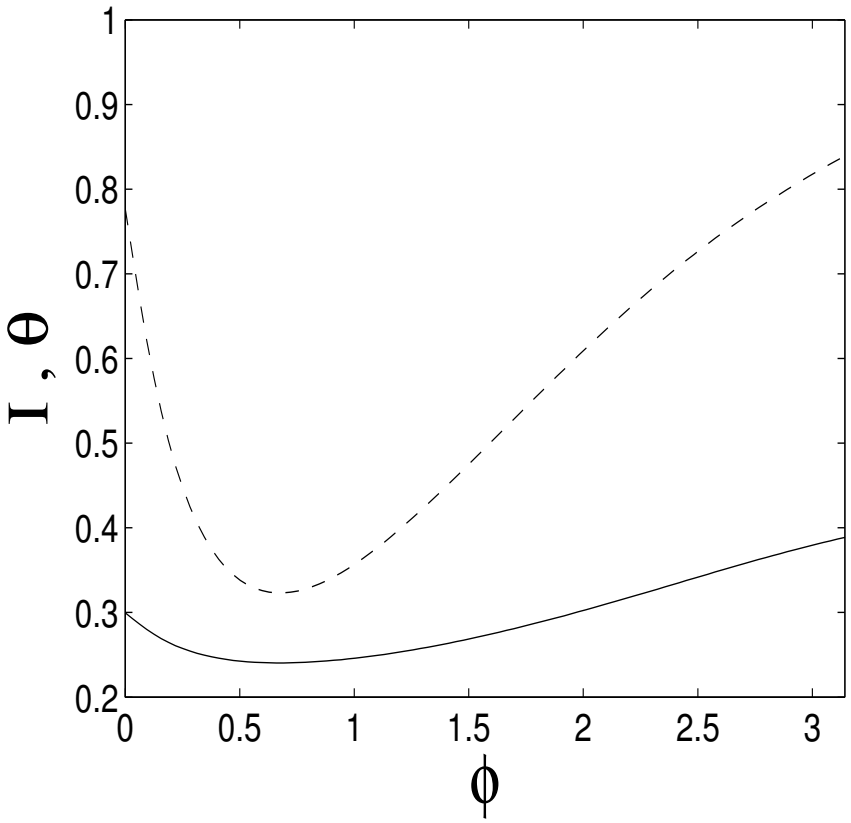

Figure 6.3.2: Action(solid) and angle(dashed) curves for $F_1 = 0.18$ and $F_2 = 0.02$.

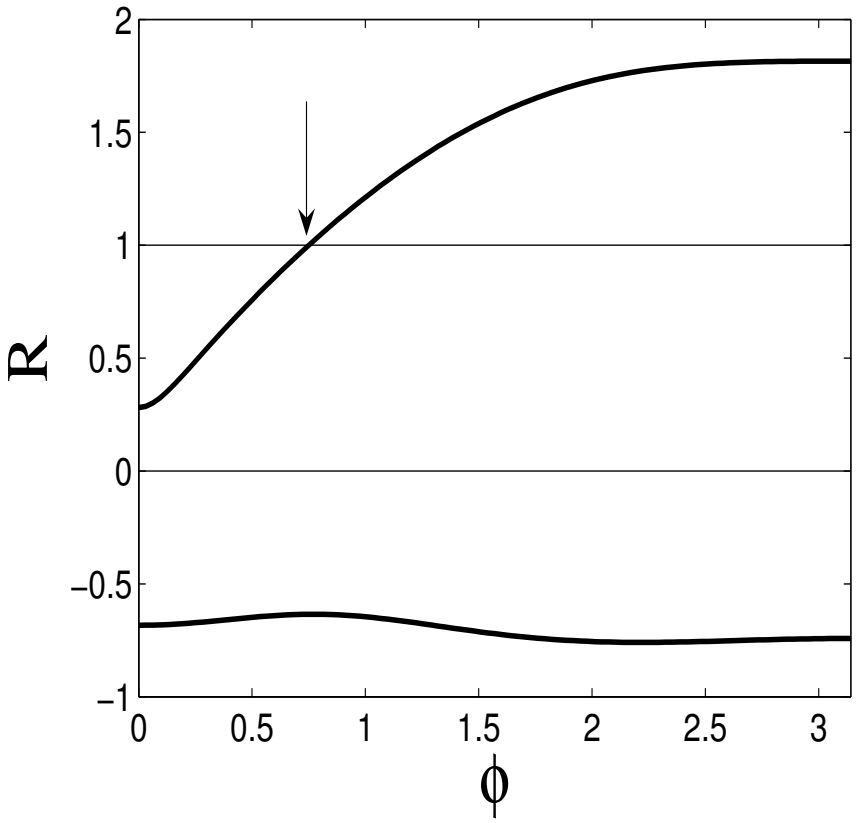

Figure 6.3.3: Residue curves (bold solid) for the considered set of periodic orbits for $F_1 = 0.18$ and $F_2 = 0.02$. The arrow indicates where the bifurcation happens.

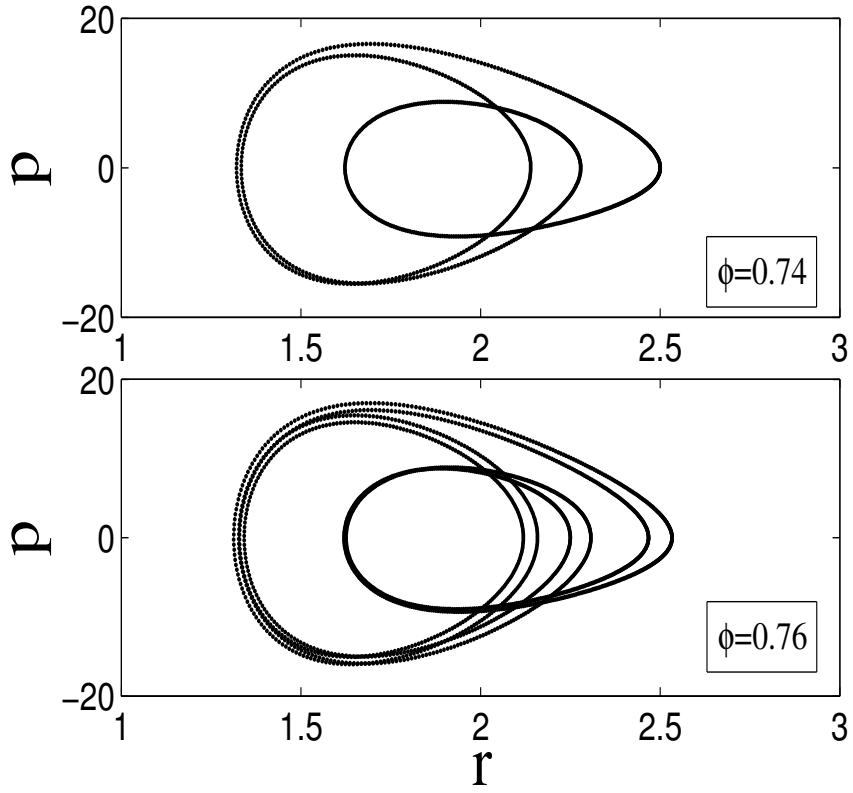

Figure 6.3.4: The considered elliptic periodic orbit undergoes the periodic doubling bifurcation around $\phi = 0.75$ for $F_1 = 0.18$ and $F_2 = 0.02$. This figure shows a projection of the considered elliptic periodic orbit right before (upper panel) and right after (lower panel) of this bifurcation.

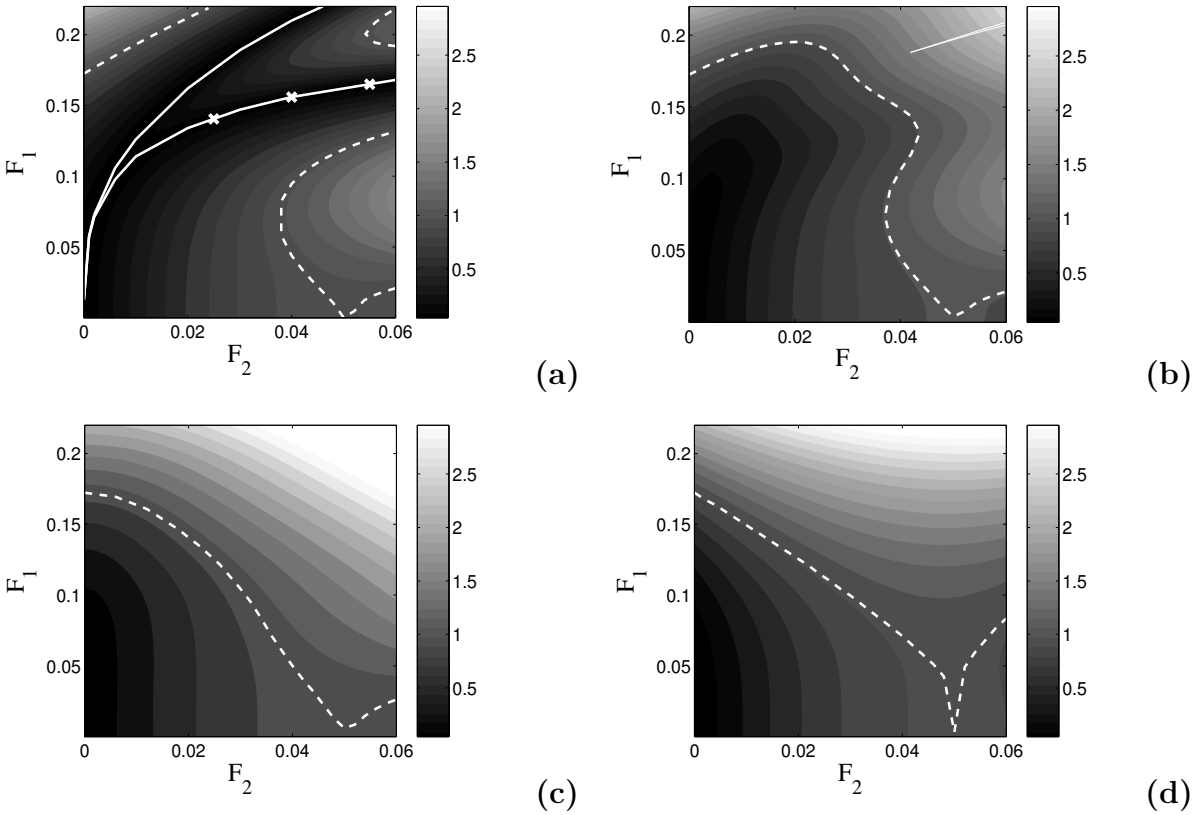

Figure 6.3.5: F_1-F_2 plane contour plot of residue value that originates from the elliptic periodic orbit in Fig. 3.3.1 for (a) $\phi = 0$, (b) $\phi = \pi/6$, (c) $\phi = \pi/2$ and (d)$\phi = \pi$. White dashed curves indicate $R = 1$, where bifurcations happen . Two white solid curves in (a) indicate $R = 0$, between which a loop structure appears. The extremely tiny area enclosed by two thin white curves around the up-right corner in (b) indicates where $\mathcal{O}_h$ turns to elliptic and then turns back to hyperbolic.

We have plotted the curves $R(F_1, F_2) = 1$ through which the periodic orbit $\mathcal{O}_e$ changes its stability. The corresponding bifurcation from elliptic to hyperbolic linear stability indicates a possible increase in dissociation probability due to an increase of hyperbolicity in this region. Since the trajectories are no longer trapped when $\mathcal{O}_e$ is hyperbolic, it is expected that the dissociation probability increases. This is in good agreement with Ref. [29] where we notice that for ϕ=$\pi/6$, $\pi/2$ and π, there is a qualitative agreement in the shape of the dissociation probability. In particular, the following features are reproduced : the non-monotonicity for $\phi = \pi/6$ as F_2 is increased (with a fixed value of F_1), and the monotonicity for $\phi = \pi/2$ and π with a sharper downward bifurcation curve (dashed line) for $\phi = \pi$ as F_2 is increased in the region $F_2 \in [0, 0.05]$. Our analysis also confirms that the stabilization effect decreases when ϕ is increased (from 0 to π). For $\phi = 0$ case, the contour plot shows agreement with direct simulations for most regions in the (F_1, F_2) plane once more, and the property that it reproduces the two upper-right bumps observed in the dissociation probability contour plot. These are interpreted as remnants of the ellipticity of the bifurcated $\mathcal{O}_e$. We notice that the corresponding hyperbolic periodic orbit $\mathcal{O}_h$ remains hyperbolic ($R < 0$) for most values of the parameters. However, for $\phi \in [\pi/6, \pi]$, there is a tiny region around the upper-right corner of the (F_1, F_2) plane where the $\mathcal{O}_h$ turns to elliptic and then turns back to hyperbolic, as it is shown on (F_1, F_2) plane contour plot of Fig. 6.3.5 (b). In general, this bifurcation does not affect the dissociation probability because, due to its location, this periodic orbit does not play an important role compared to the periodic orbit $\mathcal{O}_e$ which has already bifurcated ($R > 1$) for these values of parameters (see Figs. 6.3.5 (c) and (d)). However, for low values of ϕ and high values of the amplitudes F_i, the orbit $\mathcal{O}_e$ is still elliptic and $\mathcal{O}_h$ undergoes a bifurcation, as shown in Figs. 6.3.7 which we discuss in the following section. This region corresponds to the disagreement observed for $\phi = 0$ on Fig. 6.3.5 with the direct simulations of Ref. [29].

6.3.3 Low values of ϕ : Influence of loop structure of $\mathcal{O}_h$ orbit

For $\phi = 0$, we observe two branches on Fig. 6.3.5 (a) where the residues of $\mathcal{O}_e$ vanish. Along these lines we expect from a linear stability analysis that there is locally a constant degree of chaos in the system, and hence a dissociation probability. However this is not what is seen in direct simulations since the dissociation probability increases along these lines as F_1 is increased. This feature is represented using laminar plots which represent contour plots of the number of return times on the Poincaré section before dissociation (defined as trajectories for which E becomes greater than $E_{th} = 2$). The maximum integration time is $200\pi/\omega_1 \approx 2244$. Figures 6.3.6 show laminar plots for amplitudes on the line as marked by "x" in Fig. 6.3.5 (a). In these laminar plots, it takes longer time for trajectories launched from the whiter region to have $E \geq E_{th}$, which shows clearly that dissociation is increasing as F_1 is increased. Figure 6.3.6 clearly displays that dissociation for the case $(c) > (b) > (a)$.

In order to gain further insight into the parameter region where this discrepancy occurs, we describe here the associated bifurcation. In Fig. 6.3.7 and Fig. 6.3.8 the residue as a function of F_1 is plotted for both $\mathcal{O}_e$ and $\mathcal{O}_h$ with fixed F_2 and ϕ. We see clearly that there is a loop around $R = 0$, indicating that the $\mathcal{O}_h$ undergoes a bifurcation at $R = 0$ which involves three periodic orbits of the same period, two hyperbolic ones and an elliptic one. When ϕ is equal to 0, the upper loop in hyperbolic residue curve will merge with the small part of elliptic residue curve right above it, as shown in Fig. 6.3.7(b), and meanwhile the loop size reaches its maximum size. Clearly a smaller ϕ leads to a bigger size loop area, as shown in Fig. 6.3.7(a). With fixed ϕ and smaller F_2, the loop area will drift towards the direction of less F_1 with smaller size, as shown in Fig. 6.3.8. The following picture emerges : Without a loop in the residue curve, the system has two periodic orbits with the period of the field, $\mathcal{O}_e$ and $\mathcal{O}_h$. In the region of parameters where there is a loop in the residues, the system has four of these periodic orbits, two elliptic ones (which are close to

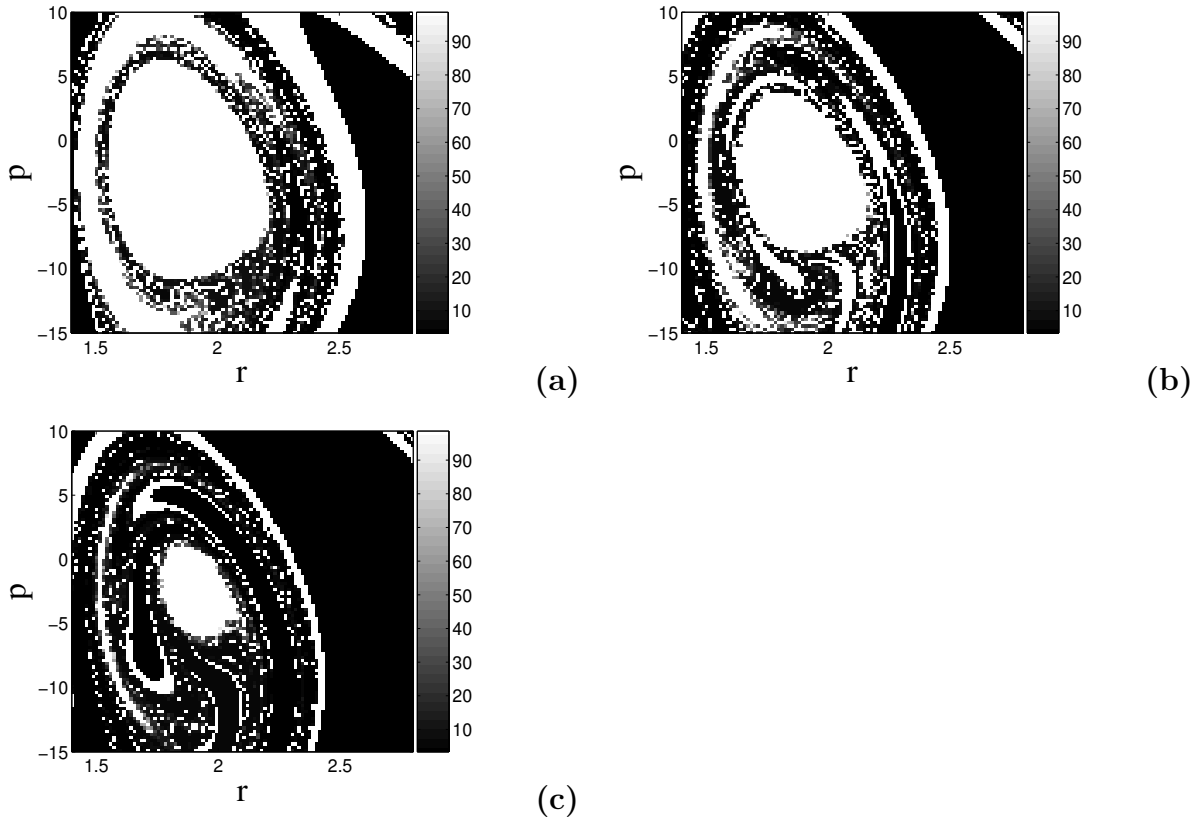

Figure 6.3.6: Laminar plots with $\phi = 0$ for (a) $F_1 = 0.1405$, $F_2 = 0.025$, (b) $F_1 = 0.1559$, $F_2 = 0.04$ and (c) $F_1 = 0.165$, and $F_2 = 0.055$. The cutoff time is $\frac{200\pi}{\omega_1} \approx 2244$ and diffusion threshold is $E_{th} = 2$.

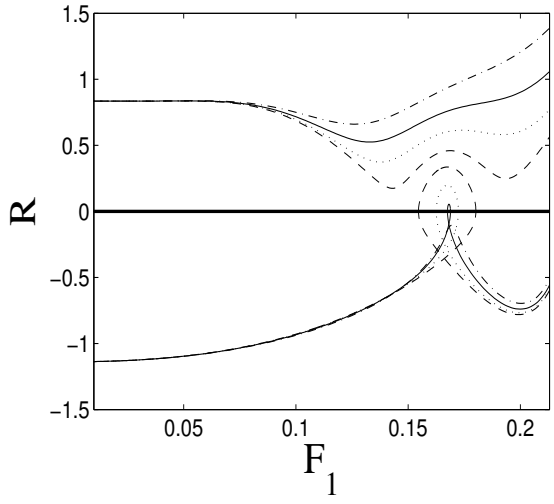

(a)

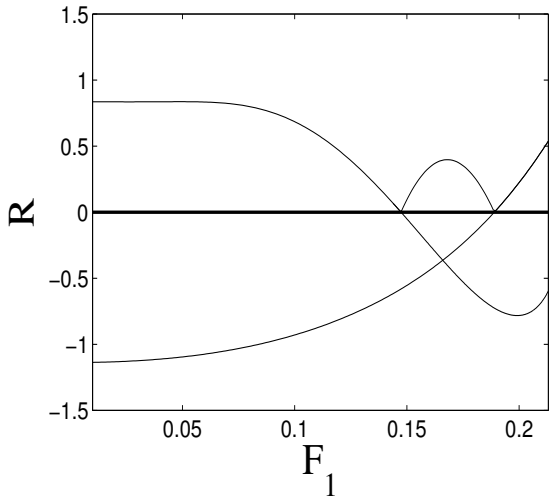

(b)

Figure 6.3.7: Residue versus F_1 for both elliptic and hyperbolic periodic orbits at $F_2 = 0.03$ for (a) several different ϕs (Dash-dotted, solid, dotted and dashed curves correspond to $\phi = \pi/6, 0.35, 0.2$ and 0.06 respectively.) and (b) $\phi = 0$.

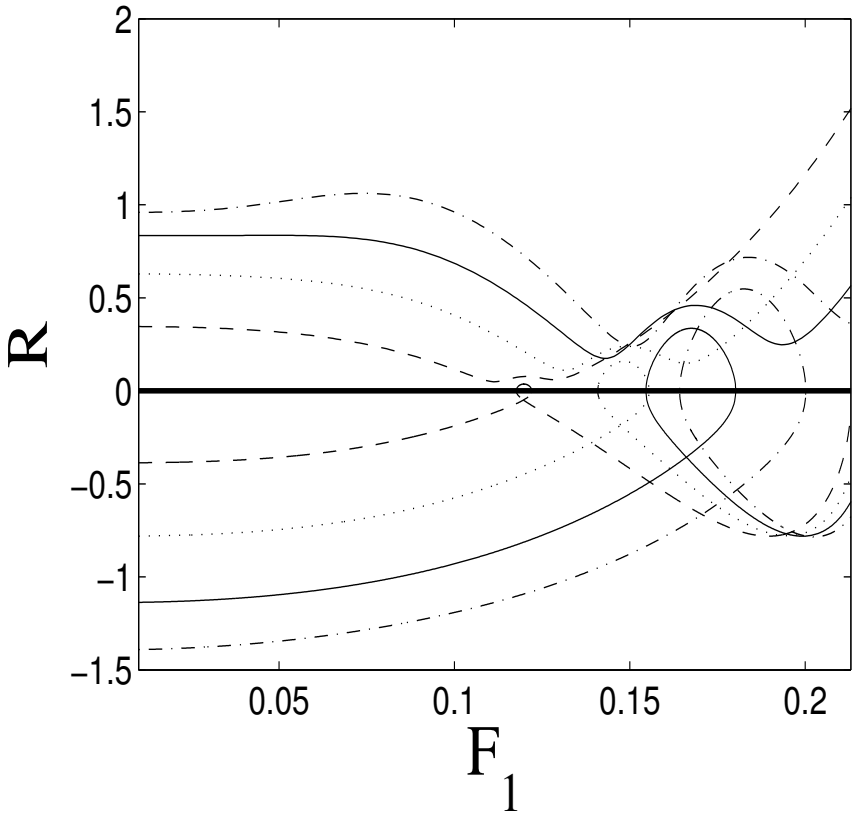

Figure 6.3.8: Residue versus F_1 for fixed $\phi = 0.06$ (Dash-dotted, solid, dotted and dashed curves correspond to $F_2 = 0.04, 0.03, 0.02$ and 0.01 respectively).

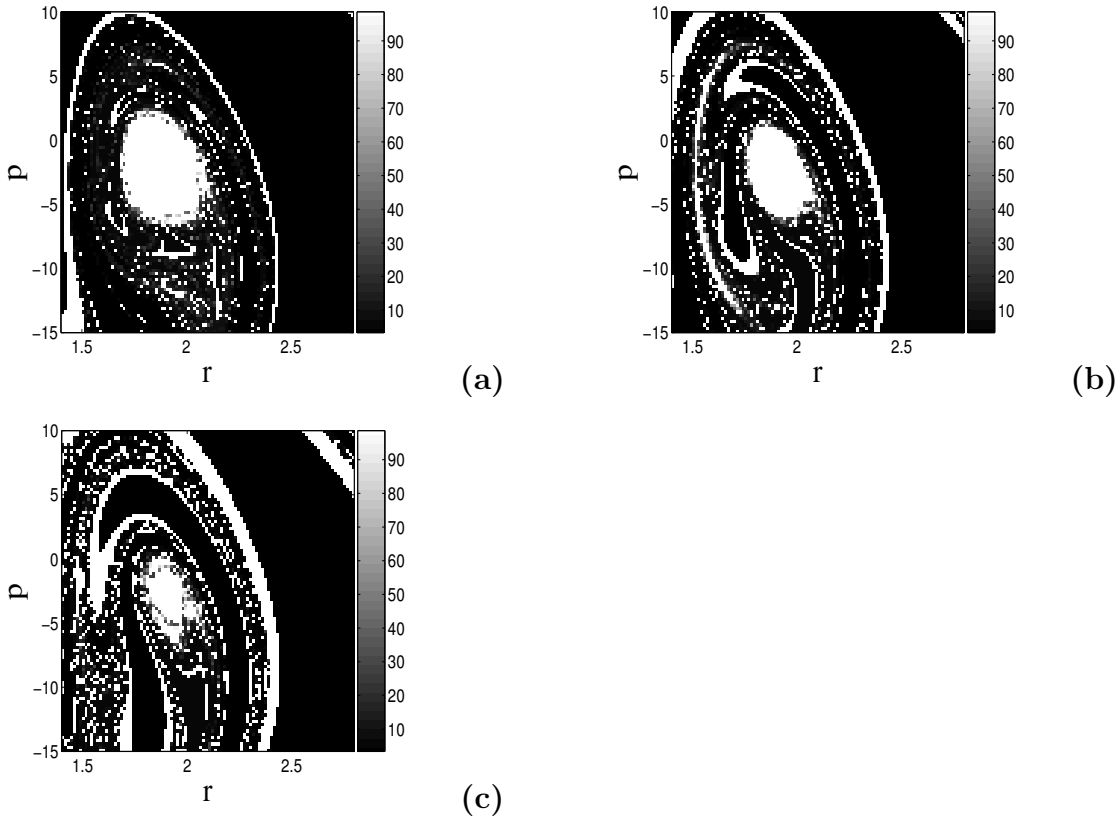

Figure 6.3.9: Laminar plots with $\phi = 0$ for (a) $F_1 = 0.19$, $F_2 = 0.055$, (b) $F_1 = 0.165$, $F_2 = 0.055$ and (c) $F_1 = 0.14$, and $F_2 = 0.055$. The cutoff time is $\frac{200\pi}{\omega_1} \approx 2244$ and diffusion threshold is $E_{th} = 2$.

each other or even coincides at $\phi = 0$) and two hyperbolic ones. This additional hyperbolicity increases chaos locally and hence increases dissociation. However, these two thin branch areas only appear when ϕ is low (approximately $0 < \phi < \pi/6$) and amplitudes F_i are high. Therefore for most parameters this loop structure will not appear and our analyses show striking agreement with direct simulation of our residue analysis Ref. [29]. Figures 6.3.9 show three laminar plots at $\phi = 0$ for fixed $F_2 = 0.055$. Figure 6.3.9 (b) corresponds to the rightmost "x" in Fig. 6.3.5 (a). We can see that the three pictures in Figs. 6.3.9 show almost the same high dissociation probability due to high F_2.

6.4 Conclusion

We have analyzed the dynamics of the dissociation of a model diatomic molecule driven by a bichromatic field in terms of periodic orbit bifurcations. Following the linear stability of a few selected periodic orbits, we can reproduce the dissociation probability qualitatively in parameter space (two field amplitudes and one relative phase). For relatively low ϕ and high amplitudes F_i, the original hyperbolic periodic orbit $\mathcal{O}_h$ undergoes a particular bifurcation, which leads to two branch lines on F_1-F_2 residue plane. Along these two branch lines, there is a discrepancy between the prediction based on the residues and direct simulations. The role of additional periodic orbits is underlined regardless of whether the discrepancy originates from bifurcated orbits (and the resulted increase of hyperbolicity) or from higher-order periodic ones.

CHAPTER VII

GENERAL CONCLUSIONS

In this thesis, we have presented our classical-mechanical analyses on multiphoton ionization of hydrogen atom in the regime where classical and quantum simulations agree.

We applied a local control method to one-dimensional hydrogen atom exposed to linearly polarized microwave field to obtain a control term which might consist of additional microwave fields. The modification of this control term leads to a microwave field with frequency twice the one of initial driving field. Using Poincaré sections and laminar plots, we have demonstrated that adding the complete or modified control term to the original non-integrable hydrogen Hamiltonian can shut off or significantly reduce ionization.

Using the stability analysis of periodic orbits, we investigated multiphoton ionization probability of hydrogen atom driven by a bichromatic microwave field. Our results show good agreement with previous experimental or quantum studies for the variation of parameters. These parameters are useful tools to control this system. Compared with the traditional and empirical peak amplitude rule, our analysis can achieve more accurate results. Moreover, our computation based on short periodic orbits is a lot more efficient than traditional simulations such as Monte Carlo method.

We extended the stability analysis of periodic orbits to the bichromatic laser driven diatomic molecule problem. Our results show good qualitative agreement with direct simulations of classical mechanics on most parameter space, again with great time savings.

Generally, our work has demonstrated several reliable classical approaches for

some complex atomic and molecular systems in the quantum-classical correspondence regime. We believe our research will help find new ways of controlling or manipulating more complex dynamical systems ranging from atoms to plasmas.

Some future research topics may be the extension of our classical analysis for multi-dimensional hydrogen atom problems, non-hydrogenic Rydberg atoms and more complicated molecule systems such as polyatomic molecule problems. Other work that remains to be done includes the application of these classical tools for Rydberg atoms exposed to circularly/elliptically polarized microwave fields. Our work reported in the thesis shows the promise of broader applications on these problems, although they are beyond the scope of this thesis.

REFERENCES

[1] Ammosov, M. V., Delone, N. B., and Krainov, V. P., "Tunnel ionization of complex atoms and atomic ions in an alternating electromagnetic field," *Sov. Phys. JETP*, vol. **64**, p. 1191, 1986.

[2] Arnold, V. I., "Proof of a theorem of A. N. Kolmogorov on the invariance of quasi-periodic motions under small perturbations of the Hamiltonian," *Russ. Math. Surv.*, vol. **18**, p. 9, 1963.

[3] Arnold, V. I., *Methematical Methods of Classical Mechanics*. New York: Springer-Verlag, 1989.

[4] Bachelard, R., Chandre, C., and Leoncini, X., "Reducing or enhancing chaos using periodic orbits," *Chaos*, vol. **16**, p. 023104, 2006.

[5] Bandrauk, A. D., Sedik, E.-W. S., and Matta, C. F., "Effect of absolute laser phase on reaction paths in laser-induced chemical reactions," *J. Chem. Phys.*, vol. **121**, p. 7764, 2004.

[6] Batista, V. S. and Brumer, P., "Coherent control in the presence of intrinsic decoherence: Proton transfer in large molecular systems," *Phys. Rev. Lett.*, vol. **89**, p. 143201, 2002.

[7] Bayfield, J. E. and Koch, P. M., "Multiphoton ionization of highly excited hydrogen atoms," *Phys. Rev. Lett.*, vol. **33**, p. 258, 1974.

[8] Berry, M. V., "The Bakerian Lecture, 1987: Quantum Chaology," *Proc. R. Soc. Lond. A*, vol. **413**, p. 183, 1987.

[9] Blümel, R. and Reinhardt, W. P., *Chaos in Atomic Physics*. Cambridge, UK: Cambridge University Press, 1997.

[10] Blümel, R. and Smilansky, U., "Localization of floquet states in the rf excitation of Rydberg atoms," *Phys. Rev. Lett.*, vol. **58**, p. 2531, 1987.

[11] Blümel, R. and Smilansky, U., "Ionization of excited hydrogen atoms by microwave fields: A test case for quantum chaos," *Phys. Scr.*, vol. **40**, p. 386, 1989.

[12] Bohr, N., "On the constitution of atoms and molecules," *Phil. Mag.*, vol. **26**, pp. 1, 476, 857, 1913.

[13] Braiman, Y., Lindner, J. F., and Ditto, W. L., "Taming spatiotemporal chaos with disorder," *Nature*, vol. **378**, p. 465, 1995.

[14] Buchleitner, A., Delande, D., and Gay, J.-C., "Microwave ionization of three-dimensional hydrogen atoms in a realistic numerical experiment," *J. Opt. Soc. Am. B*, vol. **12**, p. 505, 1995.

[15] Carlo, G. G., Benenti, G., Casati, G., and Shepelyansky, D. L., "Quantum ratchets in dissipative chaotic systems," *Phys. Rev. Lett.*, vol. **94**, p. 164101, 2005.

[16] Cary, J. R. and Hanson, J. D., "Stochasticity reduction," *Phys. Fluids*, vol. **29**, p. 2464, 1986.

[17] Casati, G., Chirikov, B. V., Guarneri, I., and Shepelyansky, D. L., "Relevance of classical chaos in quantum mechanics: The hydrogen atom in a monochromatic field," *Phys. Rep.*, vol. **154**, p. 77, 1987.

[18] Casati, G., Chirikov, B. V., Shepelyansky, D. L., and Guarneri, I., "New photoelectric ionization peak in the hydrogen atom," *Phys. Rev. Lett.*, vol. **57**, p. 823, 1986.

[19] Casati, G., Guarneri, I., and Shepelyansky, D. L., "Hydrogen atom in monochromatic field: chaos and dynamical photonic localization," *IEEE J. Quantum Electron.*, vol. **24**, p. 1420, 1988.

[20] Chandre, C., Vittot, M., Ciraolo, G., Ghendrih, P., and Lima, R., "Control of stochasticity in magnetic field lines," *Nucl. Fusion*, vol. **46**, p. 33, 2006.

[21] Charron, E., Giusti-Suzor, A., and Mies, F. H., "Fragment angular distribution in one- and two-color photodissociation by strong laser fields," *Phys. Rev. A*, vol. **49**, p. R641, 1994.

[22] Chen, G. and Dong, X., *From Chaos to Order : Methodologies, Perspectives and Applications*. Singapore: World Scientific, 1998.

[23] Chirikov, B. V., "A universal instability of many-dimensional oscillator systems," *Phys. Rep.*, vol. **52**, p. 263, 1979.

[24] Ciraolo, G., Chandre, C., Lima, R., Vittot, M., Pettini, M., Figarella, C., and Ghendrih, P., "Controlling chaotic transport in a Hamiltonian model of interest to magnetized plasmas," *J. Phys. A*, vol. **37**, p. 3589, 2004.

[25] Ciraolo, G., Chandre, C., Lima, R., Vittot, M., Pettini, M., and Ghendrih, P., "Tailoring phase space: A way to control Hamiltonian chaos," *Europhys. Lett.*, vol. **69**, p. 879, 2005.

[26] Connerade, J.-P., *Highly Excited Atoms*. Cambridge, UK: Cambridge University Press, 1998.

[27] Constantoudis, V. and Nicolaides, C. A., "Regular and chaotic multiphoton dissociation," *Phys. Rev. A*, vol. **55**, p. 1325, 1997.

[28] Constantoudis, V. and Nicolaides, C. A., "Nonhyperbolic escape and changes in phase-space stability structures in laser-induced multiphoton dissociation of a diatomic molecule," *Phys. Rev. E*, vol. **64**, p. 056211, 2001.

[29] Constantoudis, V. and Nicolaides, C. A., "Stabilization and relative phase effects in a dichromatically driven diatomic Morse molecule: Interpretation based on nonlinear classical dynamics," *J. Chem. Phys.*, vol. **122**, p. 084118, 2005.

[30] Cvitanović, P., Artuso, R., Mainieri, R., Tanner, G., and Vattay, G., *Chaos: Classical and Quantum*. Copenhagen, `ChaosBook.org`: Niels Bohr Institute, 2005.

[31] Dardi, P. C. and Gray, S. K., "Classical and quantum mechanical studies of HF in an intense laser field," *J. Chem. Phys.*, vol. **77**, p. 1345, 1982.

[32] Delande, D., *Chaos in atomic and molecular physics, in: M. J. Giannoni, A. Voros, J. Zinn-Justin(Eds), Chaos and Quantum Physics, Les Houches, Session LII, 1989*. Amsterdam: Elsevier, 1991.

[33] Delone, N. B., Krainov, V. P., and Shepelyansky, D. L., "Highly-excited atoms in the electromagnetic field," *Sov. Phys. Usp.*, vol. **26**, p. 551, 1983.

[34] Dimitriou, K. I., Constantoudis, V., Mercouris, T., Komninos, Y., and Nicolaides, C. A., "Quantum and classical dynamics of a diatomic molecule in laser fields with frequency in the region producing maximum dissociation," *Phys. Rev. A*, vol. **76**, p. 033406, 2007.

[35] Ditto, W. L., Rauseo, S. N., and Spano, M. L., "Experimental control of chaos," *Phys. Rev. Lett.*, vol. **65**, p. 3211, 1990.

[36] Ehlotzky, F., "Atomic phenomena in bichromatic laser fields," *Phys. Rep.*, vol. **345**, p. 175, 2001.

[37] Faisal, F. H. M., "Multiple absorption of laser photons by atoms," *J. Phys. B*, vol. **6**, p. L89, 1973.

[38] Farrelly, D. and Uzer, T., "Resonance overlap structure in the microwave ionization of the hydrogen atom," *Phys. Rev. A*, vol. **38**, p. 5902, 1988.

[39] Farrelly, D. and Uzer, T., "Ionization mechanism of Rydberg atoms in a circularly polarized microwave field," *Phys. Rev. Lett.*, vol. **74**, p. 1720, 1995.

[40] Gallagher, T. F., *Rydberg Atoms*. Cambridge, UK: Cambridge University Press, 1994.

[41] Galvez, E. J., Sauer, B. E., Moorman, L., Koch, P. M., and Richards, D., "Microwave ionization of H atoms: Breakdown of classical dynamics for high frequencies," *Phys. Rev. Lett.*, vol. **61**, p. 2011, 1988.

[42] Gauthier, D. J., "Resource Letter : CC-1 : Controlling chaos," *Am. J. Phys.*, vol. **71**, p. 750, 2003.

[43] Goggin, M. E. and Milonni, P. W., "Driven morse oscillator: Classical chaos and quantum theory for two-frequency excitation," *Phys. Rev. A*, vol. **38**, p. 5174, 1988.

[44] Goggin, M. E. and Milonni, P. W., "Driven Morse oscillator: Classical chaos, quantum theory, and photodissociation," *Phys. Rev. A*, vol. **37**, p. 796, 1988.

[45] Gong, J. and Brumer, P., "Quantum chaos meets coherent control," *Ann. Rev. Phys. Chem.*, vol. **56**, p. 1, 2005.

[46] Gordon, R. J., Zhu, L., and Seideman, T., "Coherent control of chemical reactions," *Acc. Chem. Res.*, vol. **32**, p. 1007, 1999.

[47] Greene, J. M., "A method for determining a stochastic transition," *J. Math. Phys.*, vol. **20**, p. 1183, 1979.

[48] Griffiths, J. A. and Farrelly, D., "Ionization of Rydberg atoms by circularly and elliptically polarized microwave fields," *Phys. Rev. A*, vol. **45**, p. R2678, 1992.

[49] Gu, Y. and Yuan, J.-M., "Classical dynamics and resonance structures in laser-induced dissociation of a morse oscillator," *Phys. Rev. A*, vol. **36**, p. 3788, 1987.

[50] Guldberg, A. and Billing, G. D., "Laser-induced dissociation of hydrogen fluoride," *Chem. Phys. Lett.*, vol. **186**, p. 229, 1991.

[51] Haffmans, A., Blümel, R., Koch, P. M., and Sirko, L., "Prediction of a new peak in two-frequency microwave "ionization" of excited hydrogen atoms," *Phys. Rev. Lett.*, vol. **73**, p. 248, 1994.

[52] He, F., Ruiz, C., and Becker, A., "Control of electron excitation and localization in the dissociation of h_2^+ and its isotopes using two sequential ultrashort laser pulses," *Phys. Rev. Lett.*, vol. **99**, p. 083002, 2007.

[53] Heather, R. and Metiu, H., "Multiphoton dissociation of a diatomic molecule: Laser intensity, frequency, and pulse shape dependence of the fragment momentum distribution," *J. Chem. Phys.*, vol. **88**, p. 5496, 1988.

[54] Howard, J. E., "Theory of two-frequency microwave ionization of hydrogen atoms," *Phys. Lett. A*, vol. **156**, p. 286, 1991.

[55] Howard, J. E., "Stochastic ionization of hydrogen atoms in a circularly polarized microwave field," *Phys. Rev. A*, vol. **46**, p. 364, 1992.

[56] Huang, S., Chandre, C., and Uzer, T., "How periodic orbit bifurcations drive multiphoton ionization," *J. Phys. B*, vol. **40**, p. F181, 2007.

[57] Ivanov, M., Corkum, P. B., Zuo, T., and Bandrauk, A. D., "Routes to control of intense-field atomic polarizability," *Phys. Rev. Lett.*, vol. **74**, p. 2933, 1995.

[58] Jensen, R. V., "Stochastic ionization of surface-state electrons," *Phys. Rev. Lett.*, vol. **49**, p. 1365, 1982.

[59] Jensen, R. V., "Stochastic ionization of surface-state electrons: Classical theory," *Phys. Rev. A*, vol. **30**, p. 386, 1984.

[60] Jensen, R. V., Susskind, S. M., and Sanders, M. M., "Chaotic ionization of highly excited hydrogen atoms: Comparison of classical and quantum theory with experiment," *Phys. Rep.*, vol. **201**, p. 1, 1991.

[61] Kadanoff, L. P., *From Order to Chaos : Essays : Critical, Chaotic and Otherwise*. Singapore: World Scientific, 1998.

[62] Keldysh, L. V., "Ionization in the field of a strong electromagnetic wave," *Sov. Phys. JETP*, vol. **20**, p. 1307, 1965.

[63] Ko, L., Noel, M. W., Lambert, J., and Gallagher, T. F., "Two-mode multiphoton transitions," *J. Phys. B*, vol. **32**, p. 3469, 1999.

[64] Koch, P. M., *The Ubiquity of Chaos (Edited by S. Krasner), Chapter 8: Microwave Excitation and Ionization of Excited Hydrogen Atoms*. Washington DC: American Association for the Advancement of Science, 1990.

[65] Koch, P. M. and van Leeuwen, K. A. H., "The importance of resonances in microwave "ionization" of excited hydrogen atoms," *Phys. Rep.*, vol. **255**, p. 289, 1995.

[66] Koch, P. M., Zelazny, S. A., and Sirko, L., "Dependence on relative phase for bichromatically driven atoms," *J. Phys. B*, vol. **36**, p. 4755, 2003.

[67] Kolmogorov, A. N., "On the conservation of quasi-periodic motions for a small change in the Hamiltonian function," *Dokl. Akad. Nauk. SSSR*, vol. **98**, p. 527, 1954.

[68] Krug, A. and Buchleitner, A., "Universal ionization threshold for strongly driven Rydberg states," *Phys. Rev. A*, vol. **72**, p. 061402(R), 2005.

[69] Landau, L. D. and Lifshitz, E. M., *Quantum Mechanics: Non-relativistic Theory*. Oxford, UK: Pergamon, 3rd ed., 1977.

[70] Leopold, J. G. and Percival, I. C., "Microwave ionization and excitation of Rydberg atoms," *Phys. Rev. Lett.*, vol. **41**, p. 944, 1978.

[71] Leopold, J. G. and Percival, I. C., "Ionisation of highly excited atoms by electric fields. III. Microwave ionisation and excitation," *J. Phys. B*, vol. **12**, p. 709, 1979.

[72] Leopold, J. G. and Richards, D., "The effect of a resonant electric field on a one-dimensional classical hydrogen atom," *J. Phys. B*, vol. **18**, p. 3369, 1985.

[73] Leopold, J. G. and Richards, D., "Quasi-resonances for high-frequency perturbations," *J. Phys. B*, vol. **22**, p. 1931, 1989.

[74] Levesque, J., Chelkowski, S., and Bandrauk, A. D., "Isotopic effects in the laser control of dissociative ionization at high intensities: Role of permanent dipole moments," *J. Phys. Chem. A*, vol. **107**, p. 3457, 2003.

[75] Lichtenberg, A. J. and Lieberman, M. A., *Regular and Stochastic Motion*. New York: Springer-Verlag, Applied Mathematial Sciences, 1983.

[76] MacKay, R. S., "Greene's residue criterion," *Nonlinearity*, vol. **5**, p. 161, 1992.

[77] MacKay, R. S. and Meiss, J. D., "Relation between quantum and classical thresholds for multiphoton ionization of excited atoms," *Phys. Rev. A*, vol. **37**, p. 4702, 1988.

[78] Maeda, H. and Gallagher, T. F., "Quantum suppression of microwave ionization of Rydberg atoms at high scaled frequency," *Phy. Rev. Lett.*, vol. **93**, p. 193002, 2004.

[79] Maeda, H., Gurian, J. H., Norum, D. V. L., and Gallagher, T. F., "Coherent population transfer in an atom by multiphoton adiabatic rapid passage," *Phy. Rev. Lett.*, vol. **96**, p. 073002, 2006.

[80] Meerson, B. I., Oks, E. A., and Sasorov, P. V., "Stochastic instability of an oscillator and the ionization of highly-excited atoms under the action of electromagnetic radiation," *JETP Lett.*, vol. **29**, p. 72, 1979.

[81] Meerson, B. I., Oks, E. A., and Sasorov, P. V., "A highly excited atom in a field of intense resonant electromagnetic radiation. I. Classical motion," *J. Phys. B*, vol. **15**, p. 3599, 1982.

[82] Mercouris, T. and Nicolaides, C. A., "He in dichromatic weak or strong ac fields of $\lambda_1 = 248$ nm and $\lambda_2 = (1/m)248$ nm $m = 2, 3, 4$," *Phys. Rev. A*, vol. **63**, p. 013411, 2001.

[83] Morse, P. M., "Diatomic molecules according to the wave mechanics. ii. Vibrational levels," *Phys. Rev.*, vol. **34**, p. 57, 1929.

[84] Moser, J., "On invariant curves of area-preserving mappings of an annulus," *Nachr. Akad. Wiss. Goett, Math. Phys. Kl. IIa*, vol. **1**, p. 1, 1962.

[85] Mostowski, J. and Sanchez-Mondragon, J. J., "Interaction of highly excited hydrogen atoms with a resonant oscillating field," *Opt. Commun.*, vol. **29**, p. 293, 1979.

[86] Nicolaides, C. A., Mercouris, T., and Petsalakis, I. D., "Above and below threshold multiphoton dissociation of volcanic ground states. Application to BeH^{2+}," *Chem. Phys. Lett.*, vol. **212**, p. 685, 1993.

[87] Paškauskas, R., "Chaotic Scattering in Rydberg Atoms, Trapping in Molecules," *Ph.D thesis, http://etd.gatech.edu/theses/available/etd-11142007-101551/*, 2007.

[88] Perotti, L., "Ionization of Rydberg alkali-metal atoms in quasistatic electric fields: A classical view of the n^{-5} scaling of the threshold field," *Phys. Rev. A*, vol. **73**, p. 053405, 2006.

[89] Petrosyan, D. and Lambropoulos, P., "Phase control of photoabsorption in optically dense media," *Phys. Rev. Lett.*, vol. **85**, p. 1843, 2000.

[90] Petrov, V., Gaspar, V., Masere, J., and Showalter, K., "Controlling chaos in the Belousov-Zhabotinsky reaction," *Nature*, vol. **361**, p. 240, 1993.

[91] Poincaré, H., *Les méthodes Nouvelles de la Mécanique Celeste.* Paris: Gauthier-Villars, 1892.

[92] Prosen, T. and Shepelyansky, D. L., "Microwave control of transport through a chaotic mesoscopic dot," *Eur. Phys. J. B*, vol. **46**, p. 515, 2005.

[93] Rabitz, H., de Vivie-Riedle, R., Motzkus, M., and Kompa, K., "Whither the future of controlling quantum phenomena?," *Science*, vol. **288**, p. 824, 2000.

[94] Rangan, C., Bloch, A. M., Monroe, C., and Bucksbaum, P. H., "Control of trapped-ion quantum states with optical pulses," *Phys. Rev. Lett.*, vol. **92**, p. 113004, 2004.

[95] Reichl, L. E., *The Transition to Chaos in Conservative Classical Systems: Quantum Manifestations.* New York: Springer-Verlag, 1992.

[96] Reiss, H. R., "Effect of an intense electromagnetic field on a weakly bound system," *Phys. Rev. A*, vol. **22**, p. 1786, 1980.

[97] Richards, D., "Ionisation of excited one-dimensional hydrogen atoms by low-frequency fields," *J. Phys. B*, vol. **20**, p. 2171, 1987.

[98] Sacha, K. and Zakrzewski, J., "Resonances overlap criterion for H atom ionization by circularly polarized microwave fields," *Phys. Rev. A*, vol. **55**, p. 568, 1997.

[99] Sauer, B. E., Yoakum, S., Moorman, L., Koch, P. M., Richards, D., and Dando, P. A., "Dynamic tunneling ionization of excited hydrogen atoms: A precise experiment versus theories," *Phys. Rev. Lett.*, vol. **68**, p. 468, 1992.

[100] Schafer, K. J. and Kulander, K. C., "Phase-dependent effects in multiphoton ionization induced by a laser field and its second harmonic," *Phys. Rev. A*, vol. **45**, p. 8026, 1992.

[101] Schiff, S. J., Jerger, K., Duong, D. H., Chang, T., Spano, M. L., and Ditto, W. L., "Controlling chaos in the brain," *Nature*, vol. **370**, p. 615, 1994.

[102] Schwieters, C. D. and Rabitz, H., "Optimal control of nonlinear classical systems with application to unimolecular dissociation reactions and chaotic potentials," *Phys. Rev. A*, vol. **44**, p. 5224, 1991.

[103] Shapiro, M. and Brumer, P., "Coherent control of molecular dynamics," *Rep. Prog. Phys.*, vol. **66**, p. 859, 2003.

[104] Shapiro, M. and Brumer, P., "Quantum control of bound and continuum state dynamics," *Phys. Rep.*, vol. **425**, p. 195, 2006.

[105] Shchekinova, E., Chandre, C., and Uzer, T., "Phase space structures and ionization dynamics of hydrogen atom in elliptically polarized microwaves," *Phys. Rev. A*, vol. **74**, p. 043417, 2006.

[106] Sirko, L. and Koch, P. M., "Control of common resonances in bichromatically driven hydrogen atoms," *Phys. Rev. Lett.*, vol. **89**, p. 274101, 2002.

[107] Sirko, L., Zelazny, S. A., and Koch, P. M., "Use of the relative phase in a bichromatic field pulse to control a quasienergy gap," *Phy. Rev. Lett.*, vol. **87**, p. 043002, 2001.

[108] Stine, J. R. and Noid, D. W., "Classical treatment of the dissociation of hydrogen fluoride with one and two infrared lasers," *Opt. Commun.*, vol. **31**, p. 161, 1979.

[109] Thachuk, M. and Wardlaw, D. M., "Classical analysis of diatomic dissociation dynamics in intense laser fields," *J. Chem. Phys.*, vol. **102**, p. 7462, 1995.

[110] Vittot, M., Chandre, C., Ciraolo, G., and Lima, R., "Localized control for non-resonant Hamiltonian systems," *Nonlinearity*, vol. **18**, p. 423, 2005.

[111] Wu, B. and Liu, W.-K., "Stochastic excitation and dissociation of adsorbate in a laser field," *Physica A*, vol. **205**, p. 470, 1994.